ANALYSIS FOR TAYLOR VORTEX FLOW

by

Rihua Li

Dissertation submitted to the Faculty of the

Virginia Polytechnic Institute and State University

in partial fulfillment of the requirements for the degree of

Doctor of Philosophy

in

Engineering Mechanics

APPROVED:

'h. Herbert, Chairman

H.W. Johnson

L. Meirovitch

D.T. Mook

C.W. Smith

March, 1986

Blacksburg, Virginia

ANALYSIS FOR TAYLOR VORTEX FLOW

by

Rihua Li

Committee Chairman: Thorwald Herbert
Engineering Mechanics

(ABSTRACT)

Taylor vortex flow is one of the basic problems of nonlinear hydrodynamic stability. In contrast with the wide region of wavenumber predicted by the linear theory, experiments show that Taylor vortex flow only appears in a small region containing the critical wavenumber β_{cr}. This phenomenon is called wave selection. In this work, several high-order perturbation methods and a numerical method are established. Both evolution and steady state of the flow caused by single or several disturbances are studied. The existence of multiple steady states for disturbances with small wavenumber is discovered and proved. The stable and unstable steady state solutions and some associated phenomena such as jump phenomenon and hysteresis phenomenon are found and explained. In the small region, the wavenumbers and initial amplitudes of disturbances determine the wavenumber of the flow. But outside this region, only the wavenumbers of the disturbances have effect on the wave selection. These results indicate that unstable solutions play a key role in wave selection. The side-band stability curve produced by the high-order perturbation methods is accurate at low Taylor numbers but incorrect at relatively high Taylor numbers. The relation of the unstable solutions and side-band stability is discussed. Besides, the overshoot and the oscillation phenomena during evolution are studied in detail. Connections between this work and experiments are discussed.

ACKNOWLEDGEMENTS

I would like to express my sincere appreciation to my advisor and committee chairman, Th. Herbert for his guidance and encouragement throughout the course of this work. Sincere appreciation is also extended to professors L.W. Johnson, L. Meirovitch, D.T. Mook, C.W. Smith for their teaching and contribution as committee members. Also thanks are extended to fellow researchers and and research specialist for their help.

This work was sponsored by the National Science Foundation under Contract MEA-8120935 and Army Research Office under Contract DAAG29-82-K-0129.

TABLE OF CONTENTS

CHAPTER 1

INTRODUCTION

1.1 Problem and Previous Work

The instability of the viscous incompressible flow between two concentric rotating cylinders is one of the classic and important problems in the theory of hydrodynamic stability. In most of the studies of this problem, the outer cylinder is fixed. At low rotation speeds the fluid forms a coaxial laminar flow called circular Couette flow. When the rotation speed exceeds a certain critical value, the Couette flow becomes unstable and a new kind of motion occurs. The new flow, now called (axisymmetric) Taylor vortex flow, consists of toroidal vortices spaced equally along the axis of the cylinders as shown in Fig. 1.1. Any two adjacent vortices have opposite directions of circulation. Each vortex is referred to as a cell. The length of two cells, $\tilde{\lambda}$, is defined as the wavelength of the flow. The wavenumber of the flow, $\tilde{\beta}$, is defined as $\tilde{\beta}=2\pi/\tilde{\lambda}$. The parameter characterizing the stability of the flow is the Taylor number, T, which is proportional to the square of the rotation speed, or equivalently the Reynolds number R_e. The definitions of these two parameters will be given in Sect. 2.1. The critical Taylor number was measured and calculated based on the linear theory by G. I. Taylor in 1921-1923. The agreement between the experiment and the theory was excellent. Since Taylor's work, the flow between two concentric cylinders has been studied widely and deeply. As the Taylor number is increased beyond a second critical value, Taylor vortex flow becomes unstable. Traveling azimuthal waves with a definite wave velocity and wavenumber are superimposed on the Taylor vortex flow such that the

boundaries between adjacent cells become wavy. Hence, the flow is called the wavy vortex flow. Experiments show that as the Taylor number is further increased the flow experiences subsequent transitions from wavy vortex flow to quasi-periodic flow, and finally to turbulence (chaos).

A new and comprehensive review of the studies on the instabilities and transition in the flow between concentric rotating cylinders was completed by DiPrima and Swinney [1], in which 122 papers are cited.

Our work is restricted to the transition from Couette flow (basic flow) to Taylor vortex flow (secondary flow) when the outer cylinder is at rest and the two cylinders are assumed to be infinitely long. Our work is concerned with the nonlinear hydrodynamic stability. Therefore, we only briefly describe some previous nonlinear studies on the transition from Couette flow to Taylor vortex flow. These studies can be classified into three categories: experimental work, numerical work and theoretical work.

The experiments conducted by Coles [2], Snyder [3], Burkhalter and Koschmieder [4],[5] are frequently mentioned in literature. Coles showed that the wavenumber of Taylor vortex flow is not unique for a given Taylor number. Snyder showed that the wavenumber obtained from the experiments depends on the initial conditions. He concluded that any method which neglects the time-dependent behavior of the problem can not select the final state from the manifold of solutions of the nonlinear problem. Figure 1.2 shows the results obtained by Burkhalter and Koschmieder. The ratio of the inner cylinder to the outer cylinder is equal to 0.727. The dimensionless wavelength, λ, is defined as $\tilde{\lambda}/d$ where d is the gap of the cylinders. In this experiment, three methods are employed to obtain Taylor vortex flow: 'sudden start', 'quasi-steady variation' and 'slow filling'. In sudden start method, the inner cylinder

is brought from rest to some Taylor number almost instantaneously (less than one second) and the flow changes from Couette flow to Taylor vortex flow in seconds. In the quasi-steady method, the Taylor number is changed very slowly as smooth as possible. In the filling method, the gap is slowly filled with fluid from the bottom while the inner cylinder is rotating at some constant supercritical angular velocity. In Fig. 1.2., we can see that the quasi-steady variation method gives the wavelength almost equal to the critical wavelength. The sudden start method results in shorter wavelengths while the slow filling method produces longer wavelengths. The curve separating the wavelength-Taylor number plane (λ- T plane) into stable and unstable regions is obtained from the linear stability theory. According to the linear theory, an axisymmetric disturbance with wavelength λ dies out in the stable region or grows and thus develops into Taylor vortex flow in the unstable region. The lowest Taylor number on the curve is called the critical Taylor number, T_{cr}, and the corresponding wavelength (or wavenumber) is the critical wavelength, λ_{cr} (or critical wavenumber, β_{cr}). Though the linear theory predicts T_{cr} and λ_{cr} (or β_{cr}) quite successfully, it has at least two drawbacks. First, at high Taylor numbers, the linear theory indicates that the dimensionless wavelength λ could be very big or very small (note that in Fig. 1.2 λ is of log scale). However, all the forementioned experiments showed that the wavelengths appear in a narrow band consisting of the critical wavenumber in spite of the methods used to create the Taylor vortex flow. Hence, the values of λ are close to 2, which means the cross section of cells is almost square. The second drawback resulting from the linear theory is that amplitudes of the flow can not be evaluated. Some experimental work is concerned with the end effects which become important in short cylinders. Benjamin and Mullin [6],[7],[8] discovered in the

short cylinder experiments the hysteresis phenomenon which indicates the multiplicity of the flow. We shall discuss this phenomenon in Sect. 6.2.

Some numerical work has been done. Most of the early studies were focused on the steady state of the flow. Recently, Neitzel [9] performed computations of time-dependent Taylor vortex flow in finite length-cylinders. The objective of his work was to compare the results of the computation with the experimental results by Burkhalter and Koschmieder. The values of the wavelength determined numerically are in good agreement with the wavelengths measured for $1<T/T_{cr}<16$. Very recently, computations of the steady state have been done by Meyer-Spasche and Keller [10]. Unstable steady state solutions were found in some cases.

At present the mathematical tool available for the analytical study of the nonlinear hydrodynamic stability is the perturbation method where an expansion in the amplitude is used. In 1944, based on a heuristic argument, Landau [11] proposed an amplitude equation now referred to as the Landau equation whose modified and generalized form is

$$\frac{1}{A}\frac{dA}{dt} = a_0+a_1A^2+a_2A^4+a_3A^6+\cdots \tag{1.1}$$

where A is the time-dependent amplitude of a disturbance and a_0, a_1, a_2, ... are Landau constants. Note that a_0 is the growth rate of the disturbance predicted by the linear theory. In 1958, Stuart [12] derived the Landau equation from the energy principle for Poiseuille flow between parallel planes and for the flow between rotating cylinders. Since Stuart's work, the Landau equation has been widely accepted and applied to problems of nonlinear hydrodynamic stability. For Taylor vortex flow, Stuart and Watson [13],[14] proposed a formal asymptotic expansion (third order) which was later used by

Davey [15],[16] to compute the amplitude and the torque on the inner cylinder for the Taylor numbers slightly greater than the critical Taylor number. Davey's calculation of the torque was in good agreement with the experimental measurements.

We have mentioned that in experiments Taylor vortices always show up in a much narrower region (see Fig. 1.2) than that predicted by the linear theory. One explanation for such discrepancy is that Taylor vortices are unstable to a side band of axisymmetric disturbances. Hence, such instability of secondary flow is sometimes called side-band instability or Benjamin-Feir instability. To investigate the side-band stability, Echkaus [17], Kogelman and DiPrima [18] developed an approach based on the Landau equation and the concept of wave interaction. Their asymptotic expansions in the amplitude were carried out to the third order. They found that inside the unstable region predicted by the linear theory, there is a subregion where stable Taylor vortex flow can exist. The boundary of this subregion is called the side-band stability curve which is the dashed line shown in Fig. 1.2. However, as compared with the experiment results, the region encompassed by this third order side-band stability curve seems too wide at large Taylor numbers. Nakaya [18] designed a method to compute the side-band stability curve up to the fifth order. The subregion he obtained is somewhat narrower than that from the third order approximation. But his result is subject to doubt as we shall discuss in Chap. 8. Hence, a natural question arises: whether or not the side-band stability curve will become narrower if a higher order asymptotic expansion is used.

The asymptotic expansions in amplitude used by Stuart, Waston and others suffer some shortcomings such that the Landau constants $a_2, a_3, a_4, \cdots$ are not uniquely determined and their results are restricted to the third or fifth

order. Herbert [19],[20] improved the expansion by introducing a new definition of amplitude based on reasonable normalization. In Herbert's procedures, all high order terms in the expansion are uniquely determined. Hence, the calculation can be carried out to arbitrarily high order.

1.2 Objectives

The initial motivation of our work was to apply high order asymptotic expansions developed by Herbert to study

(1) the evolution and the steady state of the amplitude of Taylor vortex flow;

(2) wave selection, more precisely, the effect of the high order terms of the asymptotic expansions on the side-band stability curve.

In the course of this research, we realized the limitations of the perturbation method which described the evolution of a single disturbance (single-mode). Therefore, a new perturbation method called the two-mode method and a (pure) numerical method are developed. Consequently, we use two approaches in our study: perturbation methods and numerical method. These two approaches support, supplement and sometimes correct each other. Good and reliable results are thus obtained. More importantly, some new phenomena such as jump phenomenon and hysteresis phenomenon are discovered and explained.

CHAPTER 2

GOVERNING EQUATIONS AND CONCEPTS OF STABILITY

2.1 Governing Equations

It is natural to employ cylindrical polar coordinates (r,θ,z) to study circular Couette flow and axisymmetric Taylor vortex flow. Note that both flows are independent of the azimuthal angle θ. The velocity components V_r, V_θ, V_z and the pressure P satisfy the reduced Navier-Stokes equations for viscous incompressible fluid

$$\frac{\partial V_r}{\partial t} + V_r\frac{\partial V_r}{\partial r} + V_z\frac{\partial V_r}{\partial z} - \frac{V_\theta^2}{r} = \frac{-1}{\rho}\frac{\partial P}{\partial r} + \nu\left(\frac{\partial^2 V_r}{\partial r^2} + \frac{1}{r}\frac{\partial V_r}{\partial r} + \frac{\partial^2 V_r}{\partial z^2} - \frac{V_r}{r^2}\right) \tag{2.1.1}$$

$$\frac{\partial V_\theta}{\partial t} + V_r\frac{\partial V_\theta}{\partial r} + V_z\frac{\partial V_\theta}{\partial z} + \frac{V_r V_\theta}{r} = \nu\left(\frac{\partial^2 V_\theta}{\partial r^2} + \frac{1}{r}\frac{\partial V_\theta}{\partial r} + \frac{\partial^2 V_\theta}{\partial z^2} - \frac{V_\theta}{r^2}\right) \tag{2.1.2}$$

$$\frac{\partial V_z}{\partial t} + V_r\frac{\partial V_z}{\partial r} + V_z\frac{\partial V_z}{\partial z} = \frac{-1}{\rho}\frac{\partial P}{\partial z} + \nu\left(\frac{\partial^2 V_z}{\partial r^2} + \frac{1}{r}\frac{\partial V_z}{\partial r} + \frac{\partial^2 V_z}{\partial z^2}\right) \tag{2.1.3}$$

and the equation of continuity

$$\frac{\partial V_r}{\partial r} + \frac{V_r}{r} + \frac{\partial V_z}{\partial z} = 0 \tag{2.1.4}$$

with the boundary conditions

$$\begin{aligned} V_r = V_z = 0 \qquad & V_\theta = r_1\Omega_1 \qquad at \quad r = r_1 \\ V_r = V_z = 0 \qquad & V_\theta = r_2\Omega_2 \qquad at \quad r = r_2 \end{aligned} \tag{2.1.5}$$

where r_1 and r_2 are the inner and outer radii, respectively; Ω_1 and Ω_2 are the

angular velocities of the inner and outer cylinders, respectively; ρ is the density; ν is the kinematic viscosity; t is the time.

The simplest solution (basic flow) of (2.1.1)-(2.1.5) is Couette flow

$$V_{b\theta}(r) = Ar + \frac{B}{r}$$

$$P_b = P_b(r) = \int \rho \frac{V_{b\theta}^2}{r} dr + const. \tag{2.1.6}$$

where $A = \Omega_1 \frac{\mu - \eta^2}{1 - \eta^2}$, $B = \Omega_1 r_1^2 \frac{1 - \mu}{1 - \eta^2}$, $\eta = \frac{r_1}{r_2}$, $\mu = \frac{\Omega_2}{\Omega_1}$.

Taylor vortex flow (secondary flow) is also a solution of (2.1.1)-(2.1.5), which results from the unstable disturbed Couette flow. Thus, its velocity components and pressure can be expressed as

$$\begin{Bmatrix} V_r(r,z,t) \\ V_\theta(r,z,t) \\ V_z(r,z,t) \end{Bmatrix} = \begin{Bmatrix} 0 \\ V_{b\theta}(r) \\ 0 \end{Bmatrix} + \begin{Bmatrix} \overline{U}(r,z,t) \\ \overline{V}(r,z,t) \\ \overline{W}(r,z,t) \end{Bmatrix} \tag{2.1.7}$$

$$P = P_b + \overline{P}$$

where $\overline{U}$, $\overline{V}$, $\overline{W}$ are the axisymmetric disturbance velocity components and $\overline{P}$ is the disturbance pressure.

We substitute (2.1.7) into (2.1.1)-(2.1.5), reduce the three momentum equations to two equations by eliminating $\overline{P}$, and nondimensionalize the resulting equations and the boundary conditions. Finally, we obtain

$$DD^*V + \frac{\partial^2 V}{\partial \varsigma^2} - \frac{\partial V}{\partial \tau} - U = \frac{1}{2A'\delta}(UDV + W\frac{\partial V}{\partial \varsigma}) + \frac{1}{2A'}\frac{UV}{1 + x\delta} \tag{2.1.8}$$

$$DD^*DD^*U + DD^*(2\frac{\partial^2 U}{\partial \varsigma^2} - \frac{\partial U}{\partial \tau}) + \frac{\partial^2}{\partial \varsigma^2}(\frac{\partial^2 U}{\partial \varsigma^2} - \frac{\partial U}{\partial \tau}) - 2T\Omega\frac{\partial^2 V}{\partial \varsigma^2}$$

$$= \frac{1}{2A'\delta}[\frac{\partial^2}{\partial \varsigma^2}(UDU + W\frac{\partial U}{\partial \varsigma}) - \frac{\partial}{\partial \varsigma}D(UDW + W\frac{\partial W}{\partial \varsigma})] + \frac{T}{1 + x\delta}\frac{\partial^2}{\partial \varsigma^2}V^2 \tag{2.1.9}$$

$$D^* U + \frac{\partial W}{\partial \varsigma} = 0 \tag{2.1.10}$$

with boundary conditions at $x = 0$ (inner cylinder) and $x = 1$ (outer cylinder)

$$V = U = D^* U = 0 \tag{2.1.11}$$

where

$$d = r_2 - r_1 \qquad \gamma = 1 - \mu = \frac{\Omega_1 - \Omega_2}{\Omega_1} \qquad \delta = \frac{1-\eta}{\eta} = \frac{d}{r_1}$$

$$t = \frac{d^2}{\nu}\tau \qquad z = \varsigma d \qquad r = r_1 + xd = r_1(1 + x\delta) \quad (0 \le x \le 1)$$

$$\frac{\partial}{\partial r} = \frac{1}{d}\frac{\partial}{\partial x} \qquad \frac{\partial}{\partial z} = \frac{1}{d}\frac{\partial}{\partial \varsigma} \qquad \frac{\partial}{\partial t} = \frac{\nu}{d^2}\frac{\partial}{\partial \tau}$$

$$\overline{U} = \frac{\nu}{d}\frac{\Omega_1}{2A\delta}U \qquad \overline{V} = r_1\Omega_1 V \qquad \overline{W} = \frac{\nu}{d}\frac{\Omega_1}{2A\delta}W \qquad \overline{P} = \rho\frac{\nu^2}{d^2}\frac{\Omega_1}{2A\delta}p$$

$$A' = \frac{A}{\Omega_1} = \frac{\mu - \eta^2}{1 - \eta^2} \qquad \Omega = \Omega(x) = \frac{V_{b\theta}}{r\Omega_1} = \frac{1}{\Omega_1}(A + \frac{B}{r^2}) = 1 - \frac{\gamma x}{\eta(1+\eta)}\frac{2 + x\delta}{(1 + x\delta)^2}$$

$$D = \frac{\partial}{\partial x} \qquad D^* = (\frac{\partial}{\partial x} + \frac{\delta}{1 + x\delta})$$

and the Taylor number

$$T = 2(1 - \frac{\mu}{\eta^2})\frac{1-\eta}{1+\eta}\frac{r_1^2 \Omega_1^2 d^2}{\nu^2} \tag{2.1.12}$$

Note that τ, ς, r, U, V, W and p are dimensionless variables, and $\Omega = \Omega(x)$ represents the dimensionless basic flow.

We define the Reynolds number as

$$R_e = \frac{r_1 \Omega_1 d}{\nu} \tag{2.1.13}$$

Hence, the relation between the Taylor number and the Reynolds number is

$$T = 2(1 - \frac{\mu}{\eta^2})\frac{1-\eta}{1+\eta}R_e^2 \tag{2.1.14}$$

We shall only study the case when the outer cylinder is fixed while the inner cylinder is rotating with Ω_1, hence

$$\Omega_2=0 \qquad \mu=0 \qquad \gamma=1 \qquad A=\Omega_1\frac{-\eta^2}{1-\eta^2} \qquad B=\Omega_1\frac{r_1^2}{1-\eta^2}$$

$$A'=\frac{-\eta^2}{1-\eta^2} \qquad \Omega(x)=1-\frac{x}{\eta(1+\eta)}\frac{2+x\delta}{(1+x\delta)^2}$$

$$T=\frac{2\eta^2}{1-\eta^2}\frac{\Omega_1^2 d^4}{\nu^2}$$

$$R=\frac{r_1\Omega_1 d}{\nu} \qquad T=\frac{2(1-\eta)}{1+\eta}R_c^2 \tag{2.1.15}$$

Since $z=\varsigma d$, the dimensional wavenumber $\tilde{\beta}$ and wavelength $\tilde{\lambda}$ are expressed as

$$\tilde{\beta}=\frac{\beta}{d} \qquad \tilde{\lambda}=\frac{2\pi}{\tilde{\beta}}=\frac{2\pi}{\beta}d=\lambda d \tag{2.1.16}$$

where β and λ are dimensionless wavenumber and wavelength, respectively. If $\beta=\pi$, then $\tilde{\lambda}=2d$, that is, the cross sections of cells are squares.

2.2 Linear Stability

The fact that Taylor vortex flow is axisymmetric and periodic in the axial direction suggests that small axisymmetric disturbances destabilize Couette flow. Furthermore, these axisymmetric disturbances can be decomposed into periodic functions of z (modes). Following the standard procedure of linear stability analysis, we consider the infinitesimal axisymmetric disturbances which are so small that all the nonlinear terms in (2.1.8)-(2.1.11) can be neglected. Thus, we obtain the following linearized disturbance equations

$$DD^* V + \frac{\partial^2 V}{\partial \varsigma^2} - \frac{\partial V}{\partial \tau} - U = 0 \tag{2.2.1}$$

$$DD^* DD^* U + DD^* (2\frac{\partial^2 U}{\partial \varsigma^2} - \frac{\partial U}{\partial \tau}) + \frac{\partial^2}{\partial \varsigma^2}(\frac{\partial^2 U}{\partial \varsigma^2} - \frac{\partial U}{\partial \tau}) - 2T\Omega \frac{\partial^2 V}{\partial \varsigma^2} = 0 \tag{2.2.2}$$

$$D^* U + \frac{\partial W}{\partial \varsigma} = 0 \tag{2.2.3}$$

with boundary conditions at $x = 0$ and $x = 1$

$$V = U = D^* U = 0 \tag{2.2.4}$$

We apply the normal mode method, in which modes are handled separately because each of them satisfies (2.2.1)-(2.2.4). The solution is assumed as

$$\begin{Bmatrix} U(x,\varsigma,\tau) \\ V(x,\varsigma,\tau) \end{Bmatrix} = \begin{Bmatrix} U_{10}(x) \\ V_{10}(x) \end{Bmatrix} e^{(a_0 \tau - i\beta\varsigma)} \tag{2.2.5}$$

where a_0 is called the linear temporal growth rate and β is the dimensionless wavenumber. Couette flow is considered unstable as long as one of the axisymmetric periodic disturbances (modes) has a positive a_0.

Substituting (2.2.5) into (2.2.1)-(2.2.4) leads to

$$[DD^* - (\beta^2 + a_0)]V_{10} - U_{10} = 0 \tag{2.2.6}$$

$$[DD^*DD^* - (2\beta^2 + a_0)DD^* + \beta^2(\beta^2 + a_0)]U_{10} + 2T\Omega\beta^2 V_{10} = 0 \tag{2.2.7}$$

$$D^* U_{10} - i\beta W_{10} = 0 \tag{2.2.8}$$

with boundary conditions at $x = 0$ and $x = 1$

$$U_{10}(x) = V_{10}(x) = D^* U_{10}(x) = 0 \tag{2.2.9}$$

which are a set of linear ordinary differential equations with independent variable x. The independent variables r and ς have been replaced by the parameters, a_0 and β, respectively.

There are three parameters a_0, β, and T in (2.2.6)-(2.2.9). Two basic problems considered in the linear stability are

(1) find the neutral curve, that is, the relation between β and T when $a_0 = 0$;

(2) determine whether Couette flow is stable or unstable for given β and T, that is, find a_0.

Problem (2) is obviously an eigenvalue problem. Problem (1) can also be treated as an eigenvalue problem since the neutral curve is obtained pointwise by solving for T at different given values of β. Nowadays, by use of computers, both problems are solved very quickly and accurately.

Since we are interested in the nonlinear theory, we shall not discuss the details of the linear theory, which can be found in the book by Chandrasekhar [22] or the book by Drazin & Reid [23]. Instead, we present the numerical technique for solving the boundary value problem of ordinary differential equations. The technique involves the spectral-collocation method (see Meirovitch [24], Gottlieb & Orszag [25]), which will also be used in the computation for

the nonlinear theory.

The disturbance velocity components are expressed as

$$V_{10}(x) = \sum_{j=1}^{JJ2} v_j \phi_j(x)$$

$$U_{10}(x) = \sum_{j=1}^{JJ4} u_j \phi_j(x) \tag{2.2.10}$$

where $\phi_j(x)$ is the Chebyshev polynomial of order $j-1$; u_j and v_j are constant coefficients; JJ is the number of the collocation points in (0, 1); $JJ2 = JJ+2$ and $JJ4 = JJ+4$.

We substitute (2.2.10) into (2.2.6)-(2.2.9) and then apply the operator $\int_0^1 \delta(x - x_i).(\ )\, dx$ at the collocation points x_i where $\delta(x - x_i)$ is the Dirac delta function. Thus, at the i-th collocation point, we obtain

$$\sum_{j=1}^{JJ2} v_j [DD^* - (\beta^2 + a_0)]\phi_j(x_i) - \sum_{j=1}^{JJ4} u_j \phi_j(x_i) = 0 \tag{2.2.11}$$

$$\sum_{j=1}^{JJ4} u_j [DD^* DD^* - (2\beta^2 + a_0)DD^* + \beta^2(\beta^2 + a_0)]\phi_j(x_i) + 2T\Omega(x_i)\beta^2 \sum_{j=1}^{JJ2} v_j \phi_j(x_i) = 0 \tag{2.2.12}$$

with boundary conditions

$$\sum_{j=1}^{JJ2} v_j \phi_j(0) = 0 \qquad \sum_{j=1}^{JJ4} u_j \phi_j(0) = 0 \qquad \sum_{j=1}^{JJ4} D^* u_j \phi_j(0) = 0$$

$$\sum_{j=1}^{JJ2} v_j \phi_j(1) = 0 \qquad \sum_{j=1}^{JJ4} u_j \phi_j(1) = 0 \qquad \sum_{j=1}^{JJ4} D^* u_j \phi_j(1) = 0 \tag{2.2.13}$$

For convenience, we define

$$L = DD^* - \beta^2 \qquad P = DD^* DD^* - 2\beta^2 DD^* + \beta^4 \qquad Q = 2\Omega\beta^2 T$$

$$R = -DD^* + \beta^2 \qquad \mathbf{Y}_1 = [v_1, \cdots, v_{JJ2}, u_1, \cdots, u_{JJ4}]^T \tag{2.2.14}$$

Then Eqs. (2.2.11)-(2.2.13) can be written in matrix form. For the case that a_0 is treated as an eigenvalue, we have

$$(\mathrm{M}+ a_0\mathrm{N})\mathrm{Y}_1=0 \tag{2.2.15}$$

where the matrices are $(2*JJ+6)$ by $(2*JJ+6)$ and expressed as

$$\mathrm{M}= \begin{bmatrix}
\phi_1(0) & \cdots & \phi_{JJ2}(0) & 0 & \cdots & 0 \\
\phi_1(1) & \cdots & \phi_{JJ2}(1) & 0 & \cdots & 0 \\
L\phi_1(x_1) & \cdots & L\phi_{JJ2}(x_1) & -\phi_1(x_1) & \cdots & -\phi_{JJ4}(x_1) \\
\vdots & \cdots & \vdots & \vdots & \cdots & \vdots \\
L\phi_1(x_{JJ}) & \cdots & L\phi_{JJ2}(x_{JJ}) & -\phi_1(x_{JJ}) & \cdots & -\phi_{JJ4}(x_{JJ}) \\
0 & \cdots & 0 & \phi_1(0) & \cdots & \phi_{JJ4}(0) \\
0 & \cdots & 0 & \phi_1(1) & \cdots & \phi_{JJ4}(1) \\
0 & \cdots & 0 & D^*\phi_1(0) & \cdots & D^*\phi_{JJ4}(0) \\
0 & \cdots & 0 & D^*\phi_1(1) & \cdots & D^*\phi_{JJ4}(1) \\
Q\phi_1(x_1) & \cdots & Q\phi_{JJ2}(x_1) & P\phi_1(x_1) & \cdots & P\phi_{JJ4}(x_1) \\
\vdots & \cdots & \vdots & \vdots & \cdots & \vdots \\
Q\phi_1(x_{JJ}) & \cdots & Q\phi_{JJ2}(x_{JJ}) & P\phi_1(x_{JJ}) & \cdots & P\phi_{JJ4}(x_{JJ})
\end{bmatrix} \tag{2.2.16}$$

$$\mathrm{N}= \begin{bmatrix}
0 & \cdots & 0 & 0 & \cdots & 0 \\
0 & \cdots & 0 & 0 & \cdots & 0 \\
-\phi_1(x_1) & \cdots & -\phi_{JJ2}(x_1) & 0 & \cdots & 0 \\
\vdots & \cdots & \vdots & \vdots & \cdots & \vdots \\
-\phi_1(x_{JJ}) & \cdots & -\phi_{JJ2}(x_{JJ}) & 0 & \cdots & 0 \\
0 & \cdots & 0 & 0 & \cdots & 0 \\
0 & \cdots & 0 & 0 & \cdots & 0 \\
0 & \cdots & 0 & 0 & \cdots & 0 \\
0 & \cdots & 0 & 0 & \cdots & 0 \\
0 & \cdots & 0 & R\phi_1(x_1) & \cdots & R\phi_{JJ4}(x_1) \\
\vdots & \cdots & \vdots & \vdots & \cdots & \vdots \\
0 & \cdots & 0 & R\phi_1(x_{JJ}) & \cdots & R\phi_{JJ4}(x_{JJ})
\end{bmatrix} \tag{2.2.17}$$

Since the Chebyshev polynomials are known functions, the matrices **M** and **N** can be determined. The boundary value problem of ordinary differential equations is thus reduced to a set of algebraic equations. After solving for a_0 and $\mathbf{Y}_1$, we can evaluate the eigenfunctions u_{10} and v_{10} at any value of x by use of (2.2.10). Among all the eigenvalues obtained, we are only interested in the principal eigenvalue (the largest one) which governs the stability. Note that Eq. (2.2.15) will give 6 abnormal eigenvalues which should not be taken into account. The matrix N is singular since the eigenvalue a_0 does not show up in 6 boundary conditions. Equation (2.2.15) can be changed to

$$(\mathbf{M}^{-1}\mathbf{N}+\frac{1}{a_0}\mathbf{I})\mathbf{Y}_1=0 \tag{2.2.18}$$

which implies

$$\det(\mathbf{M}^{-1}\mathbf{N}+\frac{1}{a_0}\mathbf{I})=0 \tag{2.2.19}$$

Obviously, if $\frac{1}{a_0}=0$, then $\det(\mathbf{M}^{-1}\mathbf{N})=\det(\mathbf{M}^{-1})\det(\mathbf{N})=0$. That is, there appear 6 extremely large but spurious eigenvalues in the eigenvalue spectrum. An alternative method is designed to search the principal eigenvalue and the associated eigenfunction only and thus save a lot of computation time. For brevity, we do not present this method here. For the case that T is treated as an eigenvalue, the problem can be cast in a similar way.

Figure 2.1 is an example of the neutral curve for the wide gap case $\eta=0.5$. Eight collocation points ($JJ=8$) are used. Figure 2.2 is an example of the variation of the linear growth rate a_0 with β at $T=1715$ for the small gap case $\eta=0.95238$ (i.e., $\delta=0.05$). T is slightly greater than $T_{cr}=1695$. In this case, the curve a_0 vs. β can be well approximated by a parabola which will be useful in

Sect. 8.3. where the equation of the parabola will be given.

The use of the Chebyshev polynomials and an appropriate choice of the collocation points guarantee high accuracy of the results. Let us take the computation of the principal eigenvalue at $\beta=3.0$ and $T=4500$ as an example. The variation of a_0 with the number of collocation points JJ is listed as follows

$JJ=8$ $\quad a_0=5.313056$

$JJ=10$ $\quad a_0=5.312527$

$JJ=16$ $\quad a_0=5.312501$

The relative error of a_0 is about 0.01% for $JJ=8$ and 0.0047% for $JJ=10$ if we regard a_0 for $JJ=16$ as an 'exact' value.

2.3 Nonlinear Stability and Fourier Analysis

In the nonlinear stability, we study the disturbances of finite size. All the nonlinear terms are taken into account. Because Taylor vortex flow is periodic in the ς direction, it is natural to represent the disturbances by the Fourier series in ς

$$\begin{bmatrix} U(x,\varsigma,\tau) \\ V(x,\varsigma,\tau) \\ W(x,\varsigma,\tau) \end{bmatrix} = \sum_{n=-\infty}^{\infty} \begin{bmatrix} U_n(x,\tau) \\ V_n(x,\tau) \\ W_n(x,\tau) \end{bmatrix} e^{(-in\beta\varsigma)} \tag{2.3.1}$$

Of course, we may use $in\beta$ in (2.3.1) instead of $-in\beta$, which is optional because U, V, W, are real functions

$$U_n = U_{-n} \qquad V_n = V_{-n} \qquad W_n = W_{-n} \tag{2.3.2}$$

Hence we only need to solve U_n, V_n, W_n for non-negative values of n. We define the amplitudes as follows

$$\begin{cases} A_0 = V_0(x=0.5,\tau) \\ A_n = 2V_n(x=0.5,\tau) \qquad (n \neq 0) \end{cases} \tag{2.3.3}$$

where A_0 is a measure of the distortion of the mean flow (basic flow) and A_n are measures of the spatial harmonics in ς. For example, $A_1 = 2V_1(x=0.5\tau)$.

Substitution of (2.3.1) into (2.1.8)-(2.1.11) leads to

$$[DD^* - n^2\beta^2 - \frac{\partial}{\partial\tau}]V_n - U_n = \frac{1}{2A^2\delta}\sum_{\mu=-\infty}^{\infty}[U_\mu D^* V_{n-\mu} - (n-\mu)\beta(iW_\mu)V_{n-\mu}] \tag{2.3.4}$$

$$[DD^*DD^* - (2n^2\beta^2 + \frac{\partial}{\partial\tau})DD^* + n^2\beta^2(n^2\beta^2 + \frac{\partial}{\partial\tau})]U_n + 2T\Omega n^2\beta^2 V_n$$

$$= n^2\beta^2\left\{\frac{-1}{2A'\delta}\sum_{\mu=-\infty}^{\infty}[U_\mu DU_{n-\mu} - (n-\mu)\beta(iW_\mu)U_{n-\mu}] - \frac{T}{1+\delta x}\sum_{\mu=-\infty}^{\infty}V_\mu V_{n-\mu}\right\}$$

$$+\frac{n^2\beta^2}{2A'\delta}\sum_{\mu=-\infty}^{\infty}\left\{DU_\mu D(iW_{n-\mu}) + U_\mu D^2(iW_{n-\mu}) - (n-\mu)\beta[D(iW_\mu)(iW_{n-\mu})\right.$$

$$\left. + (iW_\mu)D(iW_{n-\mu})]\right\} \tag{2.3.5}$$

$$D^* U_n - in\beta W_n = 0 \tag{2.3.6}$$

with the boundary conditions at $x=0$ and $x=1$

$$U_n = V_n = D^* U_n = 0 \tag{2.3.7}$$

where the independent variable ς has been replaced by the dimensionless wave number β.

Based on the above Fourier analysis, we shall apply two approaches to solve the set of nonlinear equations (2.3.4)-(2.3.7):

(1) numerical method;

(2) high-order perturbation methods.

In the linear theory, a small single disturbance (single-mode) with positive linear growth rate a_0 is assumed to develop independent of other disturbances. In the nonlinear theory, due to the nonlinear interaction, a small single disturbance with wavenumber β will generate corresponding harmonics with wavenumber $n\beta$ ($n=2,3,...$) and distort the mean flow during the evolution of the flow. More features of the nonlinear theory will be discovered and explained.

CHAPTER 3

THE HIGH-ORDER PERTURBATION METHOD FOR SINGLE-MODE

3.1 Formulation for the Evolution of Taylor Vortex Flow

In the single-mode perturbation method, the distortion of the mean flow and higher harmonics are assumed to be exclusively generated by the fundamental through the nonlinear terms. Based on this strong assumption, Herbert [19],[20] proposed the following amplitude expansion

$$\begin{Bmatrix} U_n(x,\tau) \\ V_n(x,\tau) \\ W_n(x,\tau) \end{Bmatrix} = \sum_{m=0}^{\infty} A^{|n|+2m} \begin{Bmatrix} U_{nm}(x) \\ V_{nm}(x) \\ W_{nm}(x) \end{Bmatrix} \qquad (-\infty < n < \infty) \tag{3.1.1}$$

where

$$A = A(\tau) \quad U_{nm} = U_{-nm} \quad V_{nm} = V_{-nm} \quad W_{nm} = W_{-nm}$$

$$U_{00} = V_{00} = W_{00} = 0 \tag{3.1.2}$$

and

$$\begin{cases} V_{10}(x=0.5) = 0.5 \\ V_{nm}(x=0.5) = 0 \qquad (n \neq 1 \text{ and } m \neq 0) \end{cases} \tag{3.1.3}$$

As compared with the definition of amplitudes in (2.3.3), we have

$$A_1 = 2V_1(x=0.5,\tau) = 2A(\tau)V_{10}(x=0.5) = A(\tau) = A \tag{3.1.4}$$

Obviously, $A(\tau)$ is the amplitude of the fundamental. In (3.1.1), the leading term ($m=0$) in the fundamental is of order A; the leading term in the second harmonic is of order A^2; the leading term in the third harmonic is of

order A^3. Those terms with $m>0$ are the higher order corrections to the harmonics or the distortion of the mean flow. Therefore $A(\tau)$ plays the role of a perturbation parameter. Now the single-mode has more meaning than a small single disturbance because it also implies that there is only one perturbation parameter $A(\tau)$. Later, in the two-mode perturbation method (see Chap. 6), two parameters, $A(\tau)$ (the amplitude of the fundamental) and $B(\tau)$ (the amplitude of the second harmonic) are introduced.

For the time derivatives, we apply the well-known Landau equation

$$\frac{dA}{dt} = a_0 A + a_1 A^3 + a_2 A^5 + a_3 A^7 + a_4 A^9 + \cdots = \sum_{k=0}^{\infty} a_k A^{2k+1} \qquad (3.1.5)$$

where a_0 is indeed the linear growth rate as $A \to 0$; $a_1, a_2, \cdots$ are called the second, third, $\cdots$ Landau constants, respectively. Note that these constants are regarded as constants in the sense that they are not functions of time, but they are functions of β and T.

Now we introduce the equivalent forms of (3.1.1) and (3.1.5)

$$\begin{Bmatrix} U_n(x,\tau) \\ V_n(x,\tau) \\ W_n(x,\tau) \end{Bmatrix} = \sum_{m=0}^{\infty} A^n (A\hat{A})^m \begin{Bmatrix} U_{nm}(x) \\ V_{nm}(x) \\ W_{nm}(x) \end{Bmatrix} \quad (n \geq 0)$$

$$\begin{Bmatrix} U_{-n}(x,\tau) \\ V_{-n}(x,\tau) \\ W_{-n}(x,\tau) \end{Bmatrix} = \sum_{m=0}^{\infty} \hat{A}^n (A\hat{A})^m \begin{Bmatrix} U_{-nm}(x) \\ V_{-nm}(x) \\ W_{-nm}(x) \end{Bmatrix} \quad (n > 0) \qquad (3.1.6)$$

$$\frac{dA}{d\tau} = a_0 A + a_1 A(A\hat{A}) + a_2 A(A\hat{A})^2 + \cdots = \sum_{k=0}^{\infty} a_k A(A\hat{A})^k \qquad (3.1.7)$$

or

$$\frac{1}{A}\frac{dA}{d\tau} = \frac{1}{\hat{A}}\frac{d\hat{A}}{d\tau} = a_0 + a_1(A\hat{A}) + a_2(A\hat{A})^2 + \cdots = \sum_{k=0}^{\infty} a_k (A\hat{A})^k$$

where $A=\hat{A}$. Both A and $\hat{A}$ are real. If A is associated with $exp(-i\beta)$, then $\hat{A}$ is associated with $exp(i\beta)$. This is helpful and convenient when we construct and check the perturbation equations by hand. For example, in (3.1.7), it is easy to see that all the terms on both sides of the Landau equation are associated with the same wavenumber β.

It is not difficult to generate (3.1.1). The procedure can be demonstrated as follows. We first compute the functions associated with A and its counterpart $\hat{A}$ (i.e., V_{10} and V_{-10}). Then, due to the quadratic terms, we generate the functions associated with A^2, $A\hat{A}$ and their counterparts at higher order (i.e., V_{01}, V_{20} and V_{-20}). By use of all known functions, we produce at the third order the functions associated with $A^2\hat{A}, A^3$ and their counterparts (i.e., V_{11}, V_{30}, V_{-11} and V_{-30}). In such a way, we can generate the functions at arbitrarily high order. We list some lower order functions as follows

0β	β	2β	3β	4β	5β	6β
	AV_{10}					
$A\hat{A}V_{01}$		A^2V_{20}				
	$A^2\hat{A}V_{11}$		A^3V_{30}			
$A^2\hat{A}^2V_{02}$		$A^3\hat{A}V_{21}$		A^4V_{40}		
	$A^3\hat{A}^2V_{12}$		$A^4\hat{A}V_{31}$		A^5V_{50}	
$A^3\hat{A}^3V_{03}$		$A^4\hat{A}^2V_{22}$		$A^5\hat{A}V_{41}$		A^6V_{60}

The first column represents the distortion of the mean flow because $A^k\hat{A}^k$ implies zero wave number. The second column means

$$V_1=AV_{10}+A^2\hat{A}V_{11}+A^3\hat{A}^2V_{12}+\cdots \tag{3.1.8}$$

When we compare (3.1.8) with (3.1.7), we can see the inherent relation between the fundamental V_1 and the corresponding Landau equation.

Replacing V_1 by $\frac{dA}{d\tau}$ and V_{1m} by a_m in (3.1.8), we obtain (3.1.7). This idea will be used later in the two-mode perturbation method (see Chap. 6) and the side-band stability (see Chap. 8).

We substitute (3.1.6) and (3.1.7) into the system of nonlinear disturbance equations (2.3.4)-(2.3.7). Then we decompose the system into successive linear ordinary differential equations according to: (1) same order; (2) same wave number. As an example of the application of the Landau equation, we show the term $\frac{d}{d\tau}(AV_{10})$, which is the first term in $\frac{dV_1}{d\tau}$,

$$\frac{d}{d\tau}(AV_{10}) = a_0 V_{10} + a_1 A(A\hat{A})V_{10} + a_2 A(A\hat{A})^2 V_{10} + \cdots \tag{3.1.9}$$

The term $a_0 V_{10}$ will show up in the equations of V_{10} where a_0 will be determined. The term $a_1 V_{10}$ will be added to the equation of V_{11} since $a_1 V_{10}$ is associated with $A(A\hat{A})$ where a_1 will be solved. The resulting successive linear perturbation equations are

$$[DD^* - (n\beta)^2 - (n+2m)a_0]V_{nm} - U_{nm} = -\sum_{l=1}^{m}(n+2m-2l)a_l V_{n(m-l)} + R_1 \tag{3.1.10}$$

$$\left\{DD^*DD^* - [2(n\beta)^2+(n+2m)a_0]DD^* + (n\beta)^2[(n\beta)^2+(n+2m)a_0]\right\}U_{nm} + 2T\Omega(n\beta)^2 V_{nm}$$

$$= -\sum_{l=1}^{m}(n+2m-2l)[DD^* - (n\beta)^2]a_l V_{n(m-l)} + R_2 \tag{3.1.11}$$

$$D^* U_{nm} - in\beta W_{nm} = 0 \tag{3.1.12}$$

with the boundary conditions at $x=0$ and $x=1$

$$U_{nm} = V_{nm} = D^* U_{nm} = 0 \tag{3.1.13}$$

where

$$R_1=\sum_{\nu=0}^{n}\sum_{\mu=0}^{m}M[\nu\mu,(n-\nu)(m-\mu)]$$

$$+\sum_{\nu=1}^{m}\sum_{\nu=0}^{m-\nu}\left\{M[-\nu\mu,(n+\nu)(m-\nu-\mu)]+M[(n+\nu)(m-\nu-\mu),-\nu\mu]\right\}$$

$$R_2=\sum_{\nu=0}^{n}\sum_{\mu=0}^{m}N[\nu\mu,(n-\nu)(m-\mu)]$$

$$+\sum_{\nu=1}^{m}\sum_{\nu=0}^{m-\nu}\left\{N[-\nu\mu,(n+\nu)(m-\nu-\mu)]+N[(n+\nu)(m-\nu-\mu),-\nu\mu]\right\} \qquad (3.1.14)$$

and

$$M[\nu\mu,(n-\nu)(m-\mu)]=\frac{1}{2A'\delta}[U_{\nu\mu}D^{*}V_{(n-\nu)(m-\mu)}-(n-\nu)\beta(iW_{\nu\mu})V_{(n-\nu)(m-\mu)}]$$

$$N[\nu\mu,(n-\nu)(m-\mu)]=n^2\beta^2\left\{\frac{1}{2A'\delta}[U_{\nu\mu}DU_{(n-\nu)(m-\mu)}-(n-\nu)\beta(iW_{\nu\mu})U_{(n-\nu)(m-\mu)}]\right.$$

$$\left.-\frac{T}{1+x\delta}V_{\nu\mu}V_{(n-\nu)(m-\mu)}\right\}+\frac{1}{2A'\delta}(n\beta)\left\{DU_{\nu\mu}D(iW_{(n-\nu)(m-\mu)})+U_{\nu\mu}D^2(iW_{(n-\nu)(m-\mu)})\right.$$

$$\left.-(n-\nu)\beta[D(iW_{\nu\mu})(iW_{(n-\nu)(m-\mu)})+(iW_{\nu\mu})D(iW_{(n-\nu)(m-\mu)})]\right\} \qquad (3.1.15)$$

The expressions for the nonlinear terms R_1 and R_2 are tedious. As an example, we show the equations for U_{20}, V_{20}, W_{20} (i.e., $n=2, m=0$)

$$[DD^{*}-(2\beta)^2-2a_0]V_{20}-U_{20}=\frac{1}{2A'\delta}(U_{10}D^{*}V_{10}-\beta iW_{10}V_{10}) \qquad (3.1.16)$$

$$\left\{DD^{*}DD^{*}-[2(2\beta)^2+2a_0]DD^{*}+(2\beta)^2[(2\beta)^2+2a_0]\right\}U_{20}+2T\Omega(2\beta)^2V_{20}$$

$$=(2\beta)^2\left\{\frac{-1}{2A'\delta}[U_{10}DU_{10}-\beta(iW_{10})U_{10}]-\frac{T}{1+x\delta}V_{10}V_{10}\right\}$$

$$+\frac{1}{2A'\delta}(2\beta)\left\{DU_{10}D(iW_{10})+U_{10}D^2(iW_{10})-\beta[D(iW_{10})(iW_{10})+(iW_{10})D(iW_{10})]\right\}$$

(3.1.17)

$$D^* V_{20} - i2\beta W_{20}=0 \tag{3.1.18}$$

with the boundary conditions at $x=0$ and $x=1$

$$U_{20}=V_{20}=D^* U_{20}=0 \tag{3.1.19}$$

where

$$R_1(\mathbf{V}_{10}\mathbf{V}_{10}) =\frac{1}{2A^* \delta}(U_{10}D^* V_{10} - \beta i W_{10}V_{10}) \tag{3.1.20}$$

$$R_2(\mathbf{V}_{10}\mathbf{V}_{10}) =(2\beta)^2\left\{\frac{-1}{2A^* \delta}[U_{10}DU_{10} - \beta(iW_{10})U_{10}] - \frac{T}{1+\delta x}V_{10}V_{10}\right\}$$

$$+\frac{1}{2A^* \delta}(2\beta)\left\{DU_{10}D(iW_{10}) + U_{10}D^2(iW_{10}) - \beta[D(iW_{10})(iW_{10}) + (iW_{10})D(iW_{10})]\right\} \tag{3.1.21}$$

Note that the bold face letter $\mathbf{V}$ is used here. The symbol $\mathbf{V}_{10}$ stands for any one among U_{10}, V_{10}, W_{10}. This symbolic notation will be used later in Sect. 3.3.

We design a program to automatically generate and solve the complicated and lengthy equations (3.1.10)-(3.1.13) for 'arbitrarily high' order.

We can also point out some shortcomings of this method. The amplitude expansion (3.1.1) implies that if the fundamental $A=0$, all the harmonics and the distortion of the mean flow are automatically equal to zero. We shall see that is not always true. Another shortcoming is that we can only prescribe different values of the initial disturbance of the fundamental $A(0)$ in the Landau equation (3.1.5). Hence, the method is incapable of dealing with the interaction between different modes with different initial amplitudes. Other shortcomings will be seen later.

3.2 Formulation for Steady States of Taylor Vortex Flow

The method we use to directly compute steady states relies on the parameter expansion used by Reynolds and Potter [26] to study steady states of the Poiseuille flow and later by Herbert [27] to study steady states of Taylor vortex flow.

To study steady states, all the time derivatives are dropped from the nonlinear system (2.3.4)-(2.3.7). The amplitude expression is the same as (3.1.1) except that $A(\tau)$ is now replaced by the steady state amplitude, A_e, which is no longer a function of time. Of course, the Landau equation is not used. In (2.3.4)-(2.3.7), there are two parameters, wavenumber β and the Taylor number T. The wavenumber appears nonlinearly while the Taylor number T appears linearly. Hence, it is easier to expand T than β. For a fixed β, we expand T as

$$T = T_0 + T_1 A_e^2 + T_2 A_e^4 + T_3 A_e^6 + T_4 A_e^8 + \cdots = \sum_{k=0}^{\infty} T_k A_e^{2k} \qquad (3.2.1)$$

or equivalently,

$$T = T_0 + T_1(A_e \hat{A}_e) + T_2(A_e \hat{A}_e)^2 + T_3(A_e \hat{A}_e)^3 + \cdots = \sum_{k=0}^{\infty} T_k (A_e \hat{A}_e)^k \qquad (3.2.2)$$

where T_0 is the Taylor number at the neutral curve; T_1, T_2, $\cdots$ are the coefficients to be determined.

We substitute (3.2.1) and the amplitude expression into the nonlinear system (2.3.4)-(2.3.7) with the time derivatives dropped. Note that we should apply (3.2.1) to both sides of the equations. The program designed takes care of generating and solving the differential equations and evaluating T_0, T_1, T_2, $\cdots$.

After computing T_0, T_1, $T_2 \cdots$, we can obtain A_e for given T , or obtain T for given A_e by use of (3.2.1). The advantage of this method is obvious if we are only interested in steady states. By use of (3.2.1), it is easy to compute A_e for many different values of T at a fixed β. In contrast, if we use the method for evolution to find A_e, we can only get a single value of A_e for a group of a_0, a_1, a_2, $\cdots$ at fixed β and T. For many different values of T, we need to compute many groups of Landau constants.

Success and shortcomings of this method will become more obvious as compared with the results of the numerical method. For this reason, the presentation of the results is postponed to Sect. 5.5.

3.3 Results of the Evolution

Figures 3.1(a) and 3.1(b) describe the evolution of the amplitude $A(\tau)$ (indeed, $0.5A$) at $\beta=3.3$ and $T=3675$ for the wide gap case $\eta=0.5$, where 9th order is used. In these two figures, we observe that $A(\tau)$ grows almost exponentially at the beginning, which implies that the linear theory is adequate. With growth, the nonlinear terms become more and more important and reduce the growth rate of A until finally a steady state is reached. By comparison of the figures, we recognize that the change of the initial amplitude of a disturbance changes only the time to reach the steady state but not the value of the steady state, A_e. This is a typical example of supercritical stability. For different values of β and T, the single-mode method gives figures similar to Fig. 3.1.

Now we turn our attention to the study of nonzero steady states of A. Figure 3.2 shows the steady states at $T=3500$ for $\eta=0.5$. We get nonzero steady states of A from β^- (the wavenumber of the left branch at the neutral curve) to β^+ (the wavenumber at the right branch of the neutral curve). Figure 3.3 shows the steady states at $T=6000$ for $\eta=0.5$. The results of both 9th and 15th orders are given. In this figure, the curves for the steady state do not cover the whole interval $[\beta^-, \beta^+]$. We have two points $\beta_S=2.078$ and $\beta^+=6.05$ with $A_e=0$. Note that $\beta_S>\beta^-=1.45$. It is easy to understand that $A_e=0$ at β^+ because there the linear growth rate is $a_0=0$. However, a_0 is still positive at β_S. We try different orders of the perturbation expansions (from 3rd to 15th order). The value of β_S does not vary with the increase of the order used though the nonzero amplitude varies with the orders as shown. When we recall the truncated Landau equation (up to the 3rd order)

$$\frac{dA}{dt}=a_0A+a_1A^3 \tag{3.3.1}$$

we can easily obtain the expression for the steady state by setting $\frac{dA}{d\tau}=0$, that is

$$A_e^2=-\frac{a_0}{a_1}$$

For the positive a_0 at β_S, we conclude that the second Landau constant a_1 must tend to $-\infty$ for $A_e=0$. This conclusion is confirmed by Fig. 3.4., where a_1 vs. β is plotted and a_1 does show the singularity at β_S. For those wavenumbers β satisfying $\beta<\beta_S$, a_1 is sometimes positive, producing meaningless result $A_e^2<0$; sometimes it is negative, giving positive A_e^2. But we realize such positive A_e is incorrect. Hence, we find the single-mode method is to be only valid in the interval $[\beta_S, \beta^+]$ rather than the interval $[\beta^-, \beta^+]$. Furthermore, we know that those nonzero values of A_e at wavenumbers close to β_S are not correct because of the singularity at β_S. We shall explain in the next section why and where this singularity occurs.

3.4 Singularity

Having found the singularity phenomenon in the single mode method, we now derive the equation for the occurrence of the singularity from the perturbation equations (3.1.10)-(3.1.13).

For simplicity, we only present the first equation (3.1.10) in (3.1.10)-(3.1.13). From (3.1.10), we get the following equations for U_{10}, V_{10}

$$(DD^{*}-\beta^{2}-a_{0})V_{10}-U_{10}=0 \tag{3.4.1}$$

which is an eigenvalue problem. Solving this equation and its accompanying equations in (3.1.11)-(3.1.13) for U_{10}, V_{10}, W_{10}, we obtain a_0, U_{10}, V_{10}, W_{10}.

For U_{20}, V_{20}, we have

$$[DD^{*}-(2\beta)^{2}-2a_{0}]V_{20}-U_{20}=R_{1}(\mathbf{V}_{10}\mathbf{V}_{10}) \tag{3.4.2}$$

which is an inhomogeneous equation. This equation is not always solvable. To show this, let us consider the equation for $\bar{U}_{10}$, $\bar{V}_{10}$ associated with a wavenumber $\bar{\beta}$ which is equal to 2β

$$[DD^{*}-\bar{\beta}^{2}-\bar{a}_{0}]\bar{V}_{10}-\bar{U}_{10}=0 \tag{3.4.3}$$

that is

$$[DD^{*}-(2\beta)^{2}-\bar{a}_{0}]\bar{V}_{10}-\bar{U}_{10}=0 \tag{3.4.4}$$

By comparing (3.4.2) with (3.4.4), we know from the theory of ordinary differential equation that U_{20} and V_{20} will have a unique solution if

$$\bar{\beta}=2\beta \qquad \bar{a}_{0}\neq 2a_{0} \tag{3.4.5}$$

In the case that

$$\bar{\beta}=2\beta \qquad \bar{a}_{0}=2a_{0} \tag{3.4.6}$$

the equations for U_{20}, V_{20} will have no solutions unless they satisfy solvability condition. For this case, the inner product of the inhomogeneous terms and the eigenfunction of the adjoint system must be equal to zero. Since there is no flexible (undetermined) constant in the inhomogeneous term R_1 (also in R_2), the solvability condition can not be satisfied. Thus in general U_{20}, V_{20} have no solution and become abnormal (extremely large) in the numerical method.

For U_{11} and V_{11}, we have

$$(DD^* - \beta^2 - 3a_0)V_{11} - U_{11} = -a_1 V_{10} + R_1(\mathbf{V}_{10}\mathbf{V}_{10} + \mathbf{V}_{20}\mathbf{V}_{-10} + \mathbf{V}_{-10}\mathbf{V}_{20}) \qquad (3.4.7)$$

where the second Landau constant a_1 is to be determined. When Eq. (3.4.6) is satisfied, a_1 has a singular value because of the abnormal V_{20}. For example, we have shown that the singularity of a_1 occurs at $\beta=2.078$ and $T=6000$ in Fig. 3.4. The calculation shows that $a_0=5.3795$ at $\beta=2.078$ whereas $\bar{a}_0=10.7639$ at $\bar{\beta}=2\beta=4.156$. Hence, $\bar{a}_0=2a_0$, which confirms (3.4.6).

Since the singularity occurs in the low order, increasing the order in the perturbation method, for example, from 3rd to 15th order, does not change the wavenumber for $A_e=0$ where a_1 is singular.

In Fig. 3.5, we plot the singularity line of β_S which is also the line with $A_e=0$ in the β- T plane. Note that this line starts from a particular point P. The corresponding Taylor number, called T_p, intersects the neutral curve at two points, P and Q, such that $\beta_Q=2\beta_P$. These two points, especially the point P, have special significance since $\beta_P=0.5\beta_Q$ and $(a_0)_P=0.5(a_0)_Q=0$. For the wide gap case ($\eta=0.5$), $T_P=3666$, $\beta_P=2.2$ and $\beta_Q=4.4$. For those Taylor numbers satisfying $T_{cr} \leq T \leq T_P$, we can get the steady states of A from β^- to β^+. That is, no singularity occurs.

Moreover, we should point out that we shall obtain abnormal functions U_{n0}, V_{n0}, W_{n0} if

$$n\beta=\overline{\beta} \qquad na_0=\overline{a}_0 \tag{3.4.8}$$

is satisfied ($n \geq 2$). Taking $n=3$ as an example, it is easy to show that a_2 will have a singularity at the wavenumber β which satisfies

$$3\beta=\overline{\beta} \qquad 3a_0=\overline{a}_0 \tag{3.4.9}$$

The wavenumber β satisfying Eq. (3.4.9) is smaller than that satisfying Eq. (3.4.6). For example, at $T=6000$, the wavenumber satisfying (3.4.9) is $\beta=1.703$ which is smaller than $\beta_S=2.078$ as shown in Fig. 3.6. In fact, $a_0=2.320$ for $\beta=1.703$ while $a_0=6.954$ for $3\beta=5.109$. Hence, Eq. (3.4.6) is a special but important case in Eq. (3.4.8) since it causes a singularity in larger wavenumber than other values of n.

CHAPTER 4

FORMULATION OF THE NUMERICAL METHOD

4.1 Formulation

First, we rearrange (2.3.4)-(2.3.7) as

$$\frac{\partial}{\partial\tau}V_n = (DD^* - n^2\beta^2)V_n - U_n - \frac{1}{2A'\delta}\sum_{\mu=-\infty}^{\infty}[U_\mu D^* V_{n-\mu} - (n-\mu)\beta(iW_\mu)V_{n-\mu}] \tag{4.1.1}$$

$$\begin{aligned}\frac{\partial}{\partial\tau}(DD^* - n^2\beta^2)U_n = {} & (DD^*DD^* - 2n^2\beta^2DD^* + n^4\beta^4)U_n + 2T\Omega\, n^2\beta^2 V_n \\ & - n^2\beta^2\left\{\frac{-1}{2A'\delta}\sum_{\mu=-\infty}^{\infty}[U_\mu DU_{n-\mu} - (n-\mu)\beta(iW_\mu)U_{n-\mu}] - \frac{T}{1+x\,\delta}\sum_{\mu=-\infty}^{\infty}V_\mu V_{n-\mu}\right\} \\ & - \frac{n^2\beta^2}{2A'\delta}\sum_{\mu=-\infty}^{\infty}\Big\{DU_\mu D(iW_{n-\mu}) + U_\mu D^2(iW_{n-\mu}) - (n-\mu)\beta[D(iW_\mu)(iW_{n-\mu}) \\ & + (iW_\mu)D(iW_{n-\mu})]\Big\}\end{aligned} \tag{4.1.2}$$

$$D^* U_n - in\beta W_n = 0 \tag{4.1.3}$$

with boundary conditions at $x = 0$ and $x = 1$

$$V_n(x,\tau) = U_n(x,\tau) = D^* U_n(x,\tau) = 0 \tag{4.1.4}$$

Then we separate the variables and apply a spectral-collocation method. We assume that

$$\begin{aligned}V_n(x,\tau) &= \sum_{j=1}^{JJ} V_{nj}(\tau)\phi_j(x) \\ U_n(x,\tau) &= \sum_{j=1}^{JJ2} U_{nj}(\tau)\phi_j(x)\end{aligned} \tag{4.1.5}$$

where $\phi_j(x)$ is the Chebyshev polynomial of order $j-1$; u_j and v_j are constant coefficients; JJ is the number of the collocation points in [0,1] and $JJ2=JJ+2$.

We substitute (4.1.5) into (4.1.1)-(4.1.4) and then apply the operator $\int_0^1 \delta(x - x_i).(\ )\, dx$ at the collocation points x_i. The resulting equations are sets of ordinary differential equations with the independent variable τ at the collocation points x_i. However, the boundary conditions have no time derivatives which make it difficult to write the sets of equations in matrix form. To overcome this obstacle, we convert the boundary conditions to the following ordinary differential equations with respect to time and with initial conditions

$$
\begin{aligned}
U_n(\bar{x},\tau) = 0 \quad &\rightarrow \quad \begin{cases} U_n(\bar{x},\tau) = -k\dfrac{\partial}{\partial\tau} U_n(\bar{x},\tau) \\ U_n(\bar{x},0) = 0 \end{cases} \\
V_n(\bar{x},\tau) = 0 \quad &\rightarrow \quad \begin{cases} V_n(\bar{x},\tau) = -k\dfrac{\partial}{\partial\tau} V_n(\bar{x},\tau) \\ V_n(\bar{x},0) = 0 \end{cases} \\
D^* U_n(\bar{x},\tau) = 0 \quad &\rightarrow \quad \begin{cases} D^* U_n(\bar{x},\tau) = -k\dfrac{\partial}{\partial\tau} D^* U_n(\bar{x},\tau) \\ D^* U_n(\bar{x},0) = 0 \end{cases}
\end{aligned}
\tag{4.1.6}
$$

where $\bar{x}=x_{JJ}=0$ or $\bar{x}=x_1=1$.

Note that 6 constants k are introduced in (4.1.6). If we drop the nonlinear terms in (4.1.1)-(4.1.2) and solve the resulting linear equations, these constants, $-k$, will show up in the eigenvalue spectrum as spurious eigenvalues. Theoretically, their values are arbitrary. But from the viewpoint of numerical stability, k should be positive. Hence, $-k$ is chosen somewhere between the maximum (principal) and minimum eigenvalues. If $-k$ is greater than the principal eigenvalues, it will contaminate the system. Note that for high harmonics (big

values of n), the principal eigenvalue will be negative with a large absolute value. In actual computations, k is of the order 10^3.

After we apply the operator to the boundary conditions, we obtain

$$\sum_{j=1}^{JJ} V_{nj}(\tau)\phi_j(\bar{x}) = 0 \quad \rightarrow \quad \begin{cases} \sum_{j=1}^{JJ} V_{nj}(\tau)\phi_j(\bar{x}) = -k \sum_{j=1}^{JJ} \frac{\partial}{\partial \tau} V_{nj}(\tau)\phi_j(\bar{x}) \\ \sum_{j=1}^{JJ} V_{nj}(0)\phi_j(\bar{x}) = 0 \end{cases} \tag{4.1.7}$$

for brevity, only one boundary condition is shown.

Now we present the resulting equations at $x_i (i = 2, \cdots, JJ-1)$:

$$\sum_{j=1}^{JJ} \frac{\partial}{\partial \tau} V_{nj}(\tau)\phi(x_i) = \sum_{j=1}^{JJ} V_{nj}(\tau)(DD^* - n^2\beta^2)\phi_j(x_i) - \sum_{j=1}^{JJ2} U_{nj}(\tau)\phi_j(x_i)$$

$$- \frac{1}{2A'\delta} \sum_{\mu=-\infty}^{\infty} [U_\mu D_* V_{n-\mu} - (n-\mu)\beta(iW_\mu)V_{n-\mu}] \tag{4.1.8}$$

$$\sum_{j=1}^{JJ2} \frac{\partial}{\partial \tau} U_{nj}(\tau)(DD^* - n^2\beta^2)\phi_j(x_i) = \sum_{j=1}^{JJ2} U_{nj}(\tau)(DD^* DD^* - 2n^2\beta^2 DD^* + n^4\beta^4)\phi_j(x_i)$$

$$+ 2T\Omega n^2\beta^2 \sum_{j=1}^{JJ} V_{nj}(\tau)\phi_j(x_i)$$

$$- \frac{n^2\beta^2}{2A'\delta} \sum_{\mu=-\infty}^{\infty} \Big\{ DU_\mu D(iW_{n-\mu}) + U_\mu D^2(iW_{n-\mu}) - (n-\mu)\beta[D(iW_\mu)(iW_{n-\mu})$$

$$+ (iW_\mu)D(iW_{n-\mu})] \Big\} \tag{4.1.9}$$

$$\sum_{j=1}^{JJ2} [u_{nj}(\tau)D^*\phi_j(x_i) - in\beta w_{nj}(x_i)] = 0 \tag{4.1.10}$$

where all the nonlinear terms are not expanded intentionally. The reason will be clear later.

First we solve the linear part of the problem as a check. That is, we drop all nonlinear terms in (4.1.7)-(4.1.10). The harmonics U_n, V_n and W_n are thus

decoupled. For each value of n, we can formulate (4.1.7)-(4.1.10) as

$$\mathbf{S}_n \frac{\partial}{\partial \tau}\mathbf{Y}_n = \mathbf{Q}_n \mathbf{Y}_n \tag{4.1.11}$$

where

$$\mathbf{Y}_n = [V_{n1}, \cdots, V_{n,JJ}, U_{n1}, \cdots, U_{n,JJ2}]^T \tag{4.1.12}$$

The method used to form $\mathbf{S}_n$ and $\mathbf{Q}_n$ is analogous to that to form $\mathbf{M}$ and $\mathbf{N}$ in the linear theory (see (2.2.16) and (2.2.17)). With the explicit Euler method, (4.1.12) is expressed as

$$\mathbf{S}_n \frac{1}{\Delta\tau}[\mathbf{Y}_n(\tau_i + \Delta\tau) - \mathbf{Y}_n(\tau_i)] = \mathbf{Q}_n \mathbf{Y}_n(\tau_i) \tag{4.1.13}$$

where $\Delta\tau$ is the time step size and $\tau_i = i\Delta\tau$. For $n = 1$ at given β, the eigenfunction with a very small amplitude (norm) is prescribed as an initial disturbance. This disturbance should grow approximately with $exp(a_0)$ if the linear growth rate is positive. However, in the numerical results the disturbance grows much faster. Hence, we need to check the eigenvalue spectrum. Taking $\beta = 3.0$ and $T = 4500$ as an example, the largest (principal) eigenvalue is 5.312501 while the smallest one is -59659.18 when $JJ = 16$ collocation points are used. The stiffness ratio (see Johnson & Riess [28] or Lambert [29]) $\left| \frac{-59659.18}{5.312501} \right|$ is as large as 10^4. In fact, the more collocation points (i.e., the more terms of the Chebyshev polynomials) we use, the stiffer the Eq. (4.1.13). Therefore, use of an implicit method is imperative. Eq. (4.1.11) is then expressed as

$$\mathbf{S}_n \frac{1}{\Delta\tau}[\mathbf{Y}_n(\tau_i + \Delta\tau) - \mathbf{Y}_n(\tau_i)] = \mathbf{Q}_n \mathbf{Y}_n(\tau_i + \Delta\tau)$$

or

$$\frac{1}{\Delta\tau}[\mathbf{Y}_n(\tau_i + \Delta\tau) - \mathbf{Y}_n(\tau_i)] = \mathbf{S}_n^{-1}\mathbf{Q}_n \mathbf{Y}_n(\tau_i + \Delta\tau) \tag{4.1.14}$$

which turns out to be successful. Now let us reconsider the nonlinear system (4.1.7)-(4.1.10). We can formulate this as

$$\begin{bmatrix} \mathbf{S}_0 & 0 & 0 & : & 0 \\ 0 & \mathbf{S}_1 & 0 & : & 0 \\ 0 & 0 & \mathbf{S}_2 & : & 0 \\ : & : & : & : & : \\ 0 & 0 & 0 & : & \mathbf{S}_N \end{bmatrix} \frac{\partial}{\partial \tau} \begin{Bmatrix} \mathbf{Y}_0 \\ \mathbf{Y}_1 \\ \mathbf{Y}_2 \\ : \\ \mathbf{Y}_N \end{Bmatrix} = \begin{bmatrix} \mathbf{Q}_0 & 0 & 0 & : & 0 \\ 0 & \mathbf{Q}_1 & 0 & : & 0 \\ 0 & 0 & \mathbf{Q}_2 & : & 0 \\ : & : & : & : & : \\ 0 & 0 & 0 & : & \mathbf{Q}_N \end{bmatrix} + \begin{Bmatrix} \mathbf{N}_0 \\ \mathbf{N}_1 \\ \mathbf{N}_2 \\ : \\ \mathbf{N}_N \end{Bmatrix} \tag{4.1.15}$$

or

$$\mathbf{S}_n \frac{\partial}{\partial \tau} \mathbf{Y}_n = \mathbf{Q}_n \mathbf{Y}_n + \mathbf{N}_n(\mathbf{Y}_0, \mathbf{Y}_1, \ldots, \mathbf{Y}_N)$$

where $\mathbf{N}_0, \mathbf{N}_1, \mathbf{N}_2, \cdots, \mathbf{N}_N$ are nonlinear terms and each of them is a function of $\mathbf{Y}_0, \mathbf{Y}_1, \cdots, \mathbf{Y}_N$. Direct application of the implicit method to (4.1.15) is quite involved. Hence, we use an implicit method to handle the linear terms and an explicit method for the nonlinear terms. The formula is expressed as

$$\mathbf{S}_n \frac{1}{\Delta \tau} [\mathbf{Y}_n(\tau_i + \Delta \tau) - \mathbf{Y}_n(\tau_i)] = \frac{1}{2} \mathbf{Q}_n [\mathbf{Y}_n(\tau_i + \Delta \tau) + \mathbf{Y}_n(\tau_i)] + \mathbf{N}_n [\mathbf{Y}_0(\tau_i), \mathbf{Y}_1(\tau_i), \ldots, \mathbf{Y}_N(\tau_i)] \tag{4.1.16}$$

If we drop the nonlinear term $\mathbf{N}_n$, Eq. (4.1.16) is reduced to the implicit trapezoidal method with accuracy $(\Delta \tau)^3$. The nonlinear term $\mathbf{N}_n$ is evaluated at time τ_i, thus $\mathbf{Y}_n$ can be solved separately at $\tau_i + \Delta \tau$. Equation (4.1.16) can also be written as

$$\mathbf{Y}_n(\tau_i + \Delta \tau) = (\mathbf{S}_n - \frac{\Delta \tau}{2} \mathbf{Q}_n)^{-1} [(\mathbf{S}_n + \frac{\Delta \tau}{2} \mathbf{Q}_n) \mathbf{Y}_n(\tau_i) + \Delta \tau \mathbf{N}_n(\tau_i)] \tag{4.1.17}$$

This method which is similar to those called semi-implicit or linearly-implicit method (see Lambert [29]) is successful in our work. Other formulations based on the semi-implicit method but with higher accuracy were tried.

But those formulations are not convenient and the improvement in the accuracy is insignificant. Hence, Eq. (4.1.17) is used for most of our numerical work.

4.2 Some Remarks on the Method

The numerical method in general requires more computation time than the perturbation method. For the cases with large positive linear growth rate, a_0 (i.e., at high Taylor numbers and the wavenumber not too far away from the critical wavenumber), the time for a small disturbance to develop into the steady state is often short. But for those cases with small positive linear growth rate, this time is quite long and the perturbation method is more desirable. However, the numerical method reveals some important phenomena which would be hardly discovered by the perturbation method. Moreover, the numerical method can model actual experimental situations much better than the perturbation method. The numerical method is good for the study of the wave interaction. For example, if we use 45 harmonics in the calculation, we can start with 45 nonzero small disturbances and investigate their interaction, which would be impossible for the perturbation method. More advantages and the shortcomings of the numerical method will be discussed later.

The numerical method is indeed a combination of Fourier analysis in the ς direction, spectral-collocation method in the r direction, and a finite difference method in τ (time). The major errors come from the following sources: the truncation of the Fourier series, the truncation of the Chebyshev polynomials and the step size in the finite difference method. That is, the errors depend on the values of N, JJ and $\Delta\tau$. There is no criterion available to estimate the magnitude of errors. Hence we perform numerical experiments to gain some confidence. In Sect. 4.1. we shall show the excellent agreement between the numerical method and the perturbation method in prototype cases. For all the numerical calculations, 8 collocation points ($JJ=8$) are used. Depending on the wavenumbers, the harmonics $N=9, 18, 27, 36, 45$ are used.

The step size of time $\Delta\tau$ is varied from 0.002 to 0.02 based on the linear growth rate. The numerical method is applied to the wide gap case $\eta=0.5$ only. In this case, axisymmetric Taylor vortex flow can exist for values of T much greater than T_{cr}.

CHAPTER 5

SOME RESULTS OF THE NUMERICAL METHOD

5.1 The Evolution and the Overshoot Phenomenon

In this section, we present the results of the numerical method and make some comparison with the single-mode method. For convenience, let us fix the Taylor number at $T=6000$. We shall present results at the following points in the $\beta-T$ plane: $M(5.2, 6000)$, $N(3.5, 6000)$, $R(2.57, 6000)$, $L(2.56, 6000)$, $G(1.3, 6000)$, $H(1.0, 6000)$ shown in Fig. 5.1. Note that the wavenumbers are arranged in descending order. For comparison with the single-mode method, only a single small disturbance $V_1(0)$ is chosen as initial condition for the numerical method for the time being. Recall the normalization of the eigenfunction is $V_{10}(x=0.5)=0.5$. The amplitude of the disturbance is expressed as

$$V_1(0)=0.5A(0)=0.5c \tag{5.1.1}$$

where c is a small constant at our disposal.

For the point M ($\beta=5.2$ and $T=6000$), we show the results of both the perturbation and the numerical method. Figure 5.2(a) is the result of the numerical method where 9 harmonics and the distortion of the mean flow are computed and V_0, V_1, V_2, V_3, V_4 are plotted. Figure 5.2(b) describes the evolution of the amplitude $A(\tau)$ (indeed, $0.5A$ is shown in the figure) where 9th order perturbation expansion is used. Note that in the single-mode method, 9th order is associated with the 9th harmonic. When we plot these two figures and superpose them, we find that the curve of $0.5A$ in Fig. 5.2(b) is almost identical to the curve of V_1 in Fig. 5.2(a). In the steady state, $2V_1=0.1074$ while

$A=0.1089$. This excellent agreement gives us confidence that both methods and the designed programs are correct.

For the point $N(3.5, 6000)$, Fig. 5.3(a) is a plot for the results of the numerical method (9 harmonics) while Fig. 5(b) is a plot for the results of the single-mode method (9th order). When we plot these two figures and superpose them, we see that the curve of $0.5A$ in Fig. 5.3(a) is identical to the curve of V_1 in Fig. 5.3(b) from the time $t=0$ to the time when the maximum amplitudes are reached. However, after reaching the maximum amplitude, $0.5A(\tau)$ keeps this maximum amplitude as its steady state while V_1 decreases to some value and then keeps this new value as its steady state, thus forming an 'overshoot' of the curve V_1. Due to this overshoot, the steady state of A is slightly different from that of V_1 ($2V_1=0.1688$, $A=0.1712$).

The overshoot phenomenon during the evolution was reported by Neitzel [9] on the study of the Taylor vortex flow in finite-length cylinders. In his paper, the amplitude is defined by use of the stream function rather than the fundamental V_1 we use. He suspected that the overshoot was caused by the effect of the finite-length of the cylinders. Our results, however, show that the overshoot exists even for the case of two infinitely long cylinders. The results show that the harmonics take different times to reach their individual steady states. If the fundamental V_1 reaches its maximum but some higher harmonics are still growing and these harmonics have finite values, the interaction between the fundamental and such harmonics may produce the overshoot. In Fig. 5.3(b), we can see that the third harmonic causes the overshoot though not very clearly. To gain a better view, we present an example as shown in Fig. 5.4 at $\beta=2.80$ and $T=9000$ (i.e., the point K in Fig. 5.1.). The maximum of the third harmonic corresponds to the 'valley' of the overshoot of the

fundamental and the second harmonic. We thus claim that the overshoot is an inherent property of Taylor vortex flow independent of the length of the cylinders.

The single-mode method is unable to model the overshoot phenomenon. The reason is quite simple. If we differentiate the Landau equation (3.1.5) with respect to time, we get

$$\frac{d^2A}{d\tau^2} = \frac{dA}{d\tau}[a_0 + 3a_1(A\hat{A}) + 5a_2(A\hat{A})^2 + \cdots] \tag{5.1.2}$$

Obviously, $\frac{d^2A}{d\tau^2}=0$ is satisfied automatically if $\frac{dA}{d\tau}=0$. However, for the overshoot, $\frac{dV_1}{d\tau}=0$ but $\frac{d^2V_1}{d\tau^2}\neq 0$ at the maximum of V_1 (see the point P in Fig. 5.4.).

Because of the overshoot and the singularity we have shown in Sect. 3.3, the results of the single-mode method are inaccurate for smaller wavenumbers at $T=6000$. We are not going to present the results for the evolution of the single-mode method in this section.

In Figs. 5.5(a) and 5.5(b), we show the results of two neighboring points $R(2.57, 6000)$ and $L(2.56, 6000)$, respectively. Fig. 5.5(a) is similar to the previous figures for the numerical method such as Fig. 5.2(a). However, Fig. 5.5(b) displays something new. The fundamental V_1 and all the odd harmonics such as third, fifth, ... finally vanish in the steady state. The second harmonic (with $2\beta=5.12$) takes the place of the fundamental. Hence the flow possesses $2\beta=5.12$ as its wavenumber. More interestingly, the results show that the small disturbance with $\beta=2.56$ develops to the same steady state as a small disturbance with $\hat{\beta}=5.12$. The following is a comparison between the steady state of $\beta=2.56$

and that of $\hat{\beta}=5.12$

$\beta=2.56$	$\hat{\beta}=5.12$
$V_0=-1.612339E-02$	$V_0=-1.612339E-02$
$V_1=0$	
$V_2=5.567141E-02$	$V_1=5.567141E-02$
$V_3=0$	
$V_4=8.991310E-04$	$V_2=8.991310E-04$
$V_5=0$	
$V_6=1.820990E-04$	$V_3=1.820990E-04$

Of course, above results are not occasional. We will explain these results in Sect. 5.4.

According to the linear theory, there will be no Taylor vortex flow if the wavenumber, β, of a small disturbance is less than β^- (the left branch of the neutral curve). This is not true in the nonlinear case. Note that at $T=6000$, $\beta^-=1.45$. Figure 5.6(a) is a plot for $\beta=1.3$. The small disturbance with $\beta=1.3$ finally leads to the steady state with $2\beta=2.6$. The small disturbance with $\beta=1.3$ decays at first, which indicates the validity of the linear theory. However, this small disturbance generates higher harmonics through the nonlinear interaction before it vanishes. The second, third and fourth harmonics soon grow because they have positive growth rate. As we can see from this figure, the interaction between the second, third and fourth harmonics with finite amplitudes is complicated. Finally, the second and all the even harmonics survive while the fundamental and all odd harmonics vanish. Figure 5.6(b) is the plot for a small disturbance with $\beta=1.0$ which leads to $3\beta=3.0$. The following is a comparison between the steady state of $\beta=1.0$ and that of $\hat{\beta}=3.0$

$\beta=1.0$	$\hat{\beta}=3.0$
$V_0=-5.316461E-02$	$V_0=-5.316461E-02$
$V_1=0$	
$V_2=0$	
$V_3=8.319775E-02$	$V_1=8.319775E-02$
$V_4=0$	
$V_5=0$	
$V_6=1.049402E-02$	$V_2=1.049402E-02$

These results will also be further discussed in Sect. 5.4.

5.2 Steady States and the Jump Phenomenon

In Fig. 5.7, we plot the steady state of $2V_1$ obtained from the numerical method (9 harmonics) and A obtained from the single-mode method (9th order) at $T=3675$ for $\eta=0.5$. The Taylor number is almost equal to $T_{cr}=3666$. The agreement between the results of the two methods is very good.

Now we plot the steady state of the fundamental, $2V_1$, and the second harmonic, $2V_2$, at $T=6000$ in Fig. 5.8. The steady state A_e obtained from the single-mode method is also plotted for comparison. We observe that $2V_1$ drops to zero at β_J whose value is between 2.562 and 2.565. Also, at $2\beta_J$, $2V_2$ jumps up from a smaller value to a bigger value which is exactly the value of $2V_1$ at $2\beta_J$. This phenomenon is called the jump phenomenon. For different Taylor numbers, T $(T \geq T_P)$, we can find such jumps and the corresponding wavenumbers, β_J. In Fig. 5.9, the line of occurrence of jump is plotted. Note that this line starts from the particular point P of the neutral curve. We know that the singularity line in the single-mode method also starts from this point. We shall show that the jump phenomenon is a result of the existence of the unstable steady state solution in Sect. 6.2.

By comparison, we can see the difference between the steady state of the numerical method and that of the single-mode method may be caused by the overshoot, the jump or the singularity. For those wavenumbers $\beta>\beta_J$, the difference between two methods are approximately equal to the magnitude of the overshoot. The overshoot phenomenon takes place at high Taylor numbers with wavenumbers close to the critical wavenumber. For those wavenumbers satisfying $\beta_S<\beta<\beta_J$, the difference is due to the jump and the singularity. The results of the numerical method are more accurate and reasonable results than those of the single-mode method. In Fig. 5.9, we sketch the shaded domain

where the the results of the single-mode method are in excellent agreement with those of the numerical method. Hence, we conclude that the single-mode method and the Landau equation produce good results for the values of β and T in the shaded domain.

5.3 Amplitude Diagram and Two-Wave Interaction

So far we have only considered the single small initial disturbance. What would happen if we introduce two initial disturbances to the flow? To answer this question, we show two cases at $\beta=2.58$ and $T=6000$ in Figs. 5.10(a) and 5.10(b). In these two figures, $V_1(0)$ is the same only $V_2(0)$ is slightly different. However, these two neighboring initial conditions lead to different steady states. We can plot many figures like Fig. 5.10(a) and Fig. 5.10(b) for many different pairs of $A(0)$ and $B(0)$ at fixed β and T. But the easier way to study two-wave interaction is to draw an amplitude diagram for the fundamental and the second harmonic. Of course, the evolution and the steady states should be represented in an infinite dimensional space and the amplitude diagram of two harmonics is only a subspace. Figure 5.11 is the amplitude diagram at $\beta=2.58$ and $T=6000$. We observe that there are two attractors A and B which stand for two different stable steady states. More interestingly, there exists a repellor R between the two attractors. This repellor corresponds to an unstable solution. Without drawing the amplitude diagram, it is not easy to discover the repellor because such an unstable solution is never achieved during the evolution. A small part of the path corresponding to the overshoot is also shown. Note that the overshoot only occurs for some pairs of initial amplitudes $A(0)$ and $B(0)$ including the single initial disturbance ($A(0)\neq 0$ but

$B(0)=0$). Indeed there is no overshoot in Figs. 5.10(a) and 5.10(b). Due to the existence of the repellor (the unstable steady solution), the time for a pair of $A(0)$ and $B(0)$ to reach the steady state varies quite largely. If a path of the evolution is close to the repellor, this time will be very long. Hence, the time to reach the steady state depends not only on the wavenumber but also on the combination of the initial amplitudes (i.e., the spectrum of initial disturbances).

We have shown that for some wavenumbers and Taylor numbers, the magnitudes of two initial disturbances will play a very important role. But this is not the complete answer for the problem of two-wave interaction. In fact, for other cases, only the wavenumber of one disturbance will determine the steady state. Thus the magnitudes of the nonzero $A(0)$ and $B(0)$ have no effects on wave selection. We find that as β decreases from 2.58, the distance between the attractor A and the repellor R is shortened. And at β_J, the attractor A is canceled by the repellor R. Hence, the jump phenomenon is caused by the cancellation of the attractor and the repellor. For $\beta<\beta_J$, for example $\beta=2.55$, there is only one attractor B as shown in Fig. 5.12. Obviously, no matter how we introduce $A(0)$ and $B(0)$, we always obtain the stable steady state with $\beta=5.10$. On the other hand, as β increases from 2.58, the distance between the attractor A and the repellor R is enlarged while the distance between the attractor B and the repellor R is shortened. At a certain wavenumber, the repellor R cancels the attractor B and only attractor A exists. Fig. 5.13 is an example with only one attractor A. We always get the stable steady state with $\beta=2.9$ provided $B(0)$ is nonzero. A very important case in this example is the pair of $V_1(0)=0.25E-11$ and $V_2(0)=0.25E-02$. Note that $V_1(0)$ is extremely small and $V_2(0)$ is 10^9 times as big as $V_1(0)$. Hence, V_2 reaches its steady state first. But

the final stable steady state has $\beta=2.9$. The corresponding figure of evolution for this case will be shown in Fig. 6.9. From this example, we conclude that the steady state with $\beta=5.8$ is unstable to any small disturbance with $\beta=2.9$.

It is quite expensive and difficult to apply the numerical method to the study of the interaction of two waves, especially searching the location of the repellor in the amplitude diagram (i.e., the value of the unstable solution). To overcome such difficulties, we establish the two-mode perturbation method given in Chap. 6.

5.4 Existence of Multiple Steady States

We are going to show the following important fact for steady state solutions which may be stable or unstable:

If velocity components $U(x)$, $V(x)$, $W(x)$ are the steady state solution for a fixed wavenumber β, they are also one of the steady solutions for wavenumbers β/n where $n=2, 3, 4, \cdots$.

The above fact indicates the possibility of multiple steady state solutions for small wavenumber (large wavelength), which will be shown in Fig. 5.14.

To study the steady state, we drop all the time derivative terms in (2.3.4)-(2.3.7). The Fourier series (2.3.1) then becomes

$$\begin{bmatrix} U(x,\varsigma) \\ V(x,\varsigma) \\ W(x,\varsigma) \end{bmatrix} = \sum_{n=-\infty}^{\infty} \begin{bmatrix} U_n(x) \\ V_n(x) \\ W_n(x) \end{bmatrix} e^{(-in\beta\varsigma)} \tag{5.4.1}$$

Now the harmonics U_n, V_n, W_n are functions of x only. It will be enough to consider only one equation (i.e., Eq. (2.3.4)) in this derivation. Eq. (2.3.4) is reduced to

$$[DD^* - n^2\beta^2]V_n - U_n = \frac{1}{2A'\delta} \sum_{\mu=-\infty}^{\infty} [U_\mu D^* V_{n-\mu} - (n-\mu)\beta(iW_\mu)V_{n-\mu}] \tag{5.4.2}$$

Suppose that at a fixed β, there exists a steady state solution

$$\begin{Bmatrix} U(x) \\ V(x) \\ W(x) \end{Bmatrix} = \cdots + \begin{Bmatrix} U_{-3} \\ V_{-3} \\ W_{-3} \end{Bmatrix} e^{(-i3\beta\varsigma)} + \begin{Bmatrix} U_{-2} \\ V_{-2} \\ W_{-2} \end{Bmatrix} e^{(-i2\beta\varsigma)} + \begin{Bmatrix} U_{-1} \\ V_{-1} \\ W_{-1} \end{Bmatrix} e^{(-i\beta\varsigma)} + \begin{Bmatrix} U_0 \\ V_0 \\ W_0 \end{Bmatrix}$$

$$+ \begin{Bmatrix} U_1 \\ V_1 \\ W_1 \end{Bmatrix} e^{(i\beta\varsigma)} + \begin{Bmatrix} U_2 \\ V_2 \\ W_2 \end{Bmatrix} e^{(i2\beta\varsigma)} + \begin{Bmatrix} U_3 \\ V_3 \\ W_3 \end{Bmatrix} e^{(i3\beta\varsigma)} + \cdots \tag{5.4.3}$$

For $n=0$, Eq. (5.4.2) becomes

$$DD^{*}V_0 - U_0 = \frac{1}{2A'\delta}\sum_{\mu=-\infty}^{\infty}[U_\mu D^{*}V_{-\mu} - (-\mu)\beta(iW_\mu)V_{-\mu}] \tag{5.4.4}$$

and the subscripts μ and $-\mu$ are listed as follows

μ: ... -5 -4 -3 -2 -1 0 1 2 3 4 5 ...

$-\mu$: ... 5 4 3 2 1 0 -1 -2 -3 -4 -5 ...

For $n=1$, Eq. (5.4.2) becomes

$$[DD^{*} - \beta^2]V_1 - U_1 = \frac{1}{2A'\delta}\sum_{\mu=-\infty}^{\infty}[U_\mu D^{*}V_{1-\mu} - (1-\mu)\beta(iW_\mu)V_{1-\mu}] \tag{5.4.5}$$

and the subscripts μ and $1-\mu$ are listed as follows

μ: ... -5 -4 -3 -2 -1 0 1 2 3 4 5 ...

$1-\mu$: ... 6 5 4 3 2 1 0 -1 -2 -3 -4 ...

For $n=2$, Eq. (5.4.2) becomes

$$[DD^{*} - (2\beta)^2]V_2 - U_2 = \frac{1}{2A'\delta}\sum_{\mu=-\infty}^{\infty}[U_\mu D^{*}V_{2-\mu} - (2-\mu)\beta(iW_\mu)V_{2-\mu}] \tag{5.4.6}$$

and the subscripts μ and $2-\mu$ are listed as follows

μ: ... -5 -4 -3 -2 -1 0 1 2 3 4 5 ...

$2-\mu$: ... 7 6 5 4 3 2 1 0 -1 -2 -3 ...

Now let us consider the steady state solution $\overline{U}_{\overline{n}}$, $\overline{V}_{\overline{n}}$, $\overline{W}_{\overline{n}}$ at $\overline{\beta}=\beta/2$.

Equation (5.4.2) becomes

$$[DD^{*} - \overline{n}^2\overline{\beta}^2]\overline{V}_{\overline{n}} - \overline{U}_{\overline{n}} = \frac{1}{2A'\delta}\sum_{\overline{\mu}=-\infty}^{\infty}[\overline{U}_{\overline{\mu}}D^{*}\overline{V}_{\overline{n}-\overline{\mu}} - (\overline{n}-\overline{\mu})\overline{\beta}(i\overline{W}_{\overline{\mu}})\overline{V}_{\overline{n}-\overline{\mu}}] \tag{5.4.7}$$

For $\bar{n}=0$, Eq. (5.4.7) becomes

$$DD^{*}\bar{V}_0 - \bar{U}_0 = \frac{1}{2A'\delta}\sum_{\bar{\mu}=-\infty}^{\infty}[\bar{U}_{\bar{\mu}}D^{*}\bar{V}_{-\bar{\mu}} - (-\bar{\mu})\bar{\beta}(i\bar{W}_{\bar{\mu}})\bar{V}_{-\bar{\mu}}] \tag{5.4.8}$$

For $\bar{n}=1$, Eq. (5.4.7) becomes

$$[DD^{*} - \bar{\beta}^2]\bar{V}_1 - \bar{U}_1 = \frac{1}{2A'\delta}\sum_{\bar{\mu}=-\infty}^{\infty}[\bar{U}_{\bar{\mu}}D^{*}\bar{V}_{1-\bar{\mu}} - (1-\bar{\mu})\bar{\beta}(i\bar{W}_{\bar{\mu}})\bar{V}_{1-\bar{\mu}}] \tag{5.4.9}$$

For $\bar{n}=2$, Eq. (5.4.7) becomes

$$[DD^{*} - 2\bar{\beta}^2]\bar{V}_2 - \bar{U}_2 = \frac{1}{2A'\delta}\sum_{\bar{\mu}=-\infty}^{\infty}[\bar{U}_{\bar{\mu}}D^{*}\bar{V}_{2-\bar{\mu}} - (2-\bar{\mu})\bar{\beta}(i\bar{W}_{\bar{\mu}})\bar{V}_{2-\bar{\mu}}] \tag{5.4.10}$$

Let us consider (5.4.7). Besides the zero (trivial) solution, one possible solution is that $\bar{U}_{\bar{n}}$, $\bar{V}_{\bar{n}}$, $\bar{W}_{\bar{n}}$ are all nonzero. Furthermore, the third possible solution is that $\bar{U}_{\bar{n}}$, $\bar{V}_{\bar{n}}$, $\bar{W}_{\bar{n}}$ with odd $\bar{n}$ are all zero but $\bar{U}_{\bar{n}}$, $\bar{V}_{\bar{n}}$, $\bar{W}_{\bar{n}}$ with even $\bar{n}$ are all nonzero. Now let us focus on the third possible solution. For $\bar{n}=0$, if $\bar{\mu}$ is odd, all the terms with odd $\bar{\mu}$ vanish on the right hand side of (5.4.8). Hence, the list of the subscripts is reduced to

$\bar{\mu}$: ... -4 -2 0 2 4 ...

$-\bar{\mu}$: ... 4 2 0 -2 -4 ...

For $\bar{n}=1$, all the terms on the right hand side of (5.4.9) are equal to zero since either of $\bar{\mu}$ and $1-\bar{\mu}$ must be odd. And all the terms on the left hand side are also equal to zero since $\bar{U}_1$, $\bar{V}_1$, $\bar{W}_1$ are equal to zero. That is, Eq. (5.4.9) can be dropped. Similarly, we can see that all the equations with odd subscript $\bar{n}$ in (5.4.2) vanish.

For $\bar{n}=2$, the list of the subscripts is reduced to

$\bar{\mu}$: ... -6 -4 -2 0 2 4 6 ...

$2-\bar{\mu}$: ... 8 6 4 2 0 -2 -4 ...

Now in (5.4.10) both $\bar{\mu}$ and $2-\bar{\mu}$ are even. If we do the following replacements in (5.4.10):

$2\bar{\beta}$	$\rightarrow$	β
$(2-\bar{\mu})\bar{\beta}$	$\rightarrow$	$(1-\mu)\beta$
$\sum_{\bar{\mu}=-\infty}^{\infty}$	$\rightarrow$	$\sum_{\mu=-\infty}^{\infty}$
$\bar{U}_2, \bar{V}_2, \bar{W}_2$	$\rightarrow$	$\hat{U}_2, \hat{V}_2, \hat{W}_2$
($\bar{\mu}$ is even)		(μ is all integer)

then we can rewrite (5.4.10) as

$$[DD^{*}-\beta^2]\hat{V}_1-\hat{U}_1=\frac{1}{2A'\delta}\sum_{\mu=-\infty}^{\infty}[\hat{U}_\mu D^{*}\hat{V}_{1-\mu}-(1-\mu)\beta(i\bar{W}_\mu)\bar{V}_{1-\mu}] \qquad (5.4.11)$$

Obviously, Eq. (5.4.11) is essentially the same as (5.4.5) except that $\hat{U}_1, \hat{V}_1, \hat{W}_1$ are used in (5.4.11) rather than U_1, V_1, W_1.

For other even subscripts, we do the following replacements in (5.4.7):

$\bar{n}\,\bar{\beta}$	$\rightarrow$	$n\,\beta$
$(\bar{n}-\bar{\mu})\bar{\beta}$	$\rightarrow$	$(n-\mu)\beta$
$\sum_{\bar{\mu}=-\infty}^{\infty}$	$\rightarrow$	$\sum_{\mu=-\infty}^{\infty}$
$\bar{U}_{\bar{n}}, \bar{V}_{\bar{n}}, \bar{W}_{\bar{n}}$	$\rightarrow$	$\hat{U}_n, \hat{V}_n, \hat{W}_n$
($\bar{\mu}$ is even)		(μ is all integer)

then all the equations with even $\bar{n}$ in (5.4.7) are rewritten as

$$[DD^* - n^2\beta^2]\hat{V}_n - \hat{U}_n = \frac{1}{2A'\delta}\sum_{\mu=-\infty}^{\infty}[\hat{U}_\mu D^*\hat{V}_{n-\mu} - (n-\mu)\beta(i\hat{W}_\mu)\hat{V}_{n-\mu}] \quad (5.4.12)$$

By comparing (5.4.12) with (5.4.2), we obtain

$$\overline{U}_{\bar{n}} = \hat{U}_n = U_n \qquad \overline{V}_{\bar{n}} = \hat{V}_n = V_n \qquad \overline{W}_{\bar{n}} = \hat{W}_n = W_n \quad (5.4.13)$$

Based on (5.4.3) and (5.4.13), we conclude that the steady state solution U_n, V_n, W_n for β is also a steady state solution for $\overline{U}_{\bar{n}}$, $\overline{V}_{\bar{n}}$, $\overline{W}_{\bar{n}}$ for $\overline{\beta}=\beta/2$ where all $\overline{U}_{\bar{n}}$, $\overline{V}_{\bar{n}}$, $\overline{W}_{\bar{n}}$ with odd $\bar{n}$ are equal to zero. We have shown an example for this case in Sect. 5.1, that is, the example for $\beta=1.3$ and $T=6000$.

The previous procedure of proof can be easily extended to $\overline{\beta}=\beta/n$ $(n \geq 3)$. For example, if the steady state solution (U_n, V_n, W_n) does exist, there is at least a possible steady solution $(\overline{U}_{\bar{n}}, \overline{V}_{\bar{n}}, \overline{W}_{\bar{n}})$ for $\overline{\beta}=\beta/3$ which is nonzero as $\bar{n}=\cdots,-9,-6,-3,0,3,6,9,\cdots$ and zero for other values of $\bar{n}$. We have shown an example for this case in Sect. 5.1, that is, the example for $\beta=1.0$ and $T=6000$.

We now explain why there are multiple steady state solutions for small wavenumbers (large wavelengths). In Fig. 5.14, the curve labeled by β is the steady state amplitude V_1 (the amplitude of the fundamental) obtained by the numerical method at $T=6000$ for $\eta=0.5$. According to the fact we have just proved, we can generate a curve labeled 2β by use of the curve labeled β. A point P_1 on the curve labeled by β is moved horizontally to the point P_2 on the curve labeled 2β with the wavenumber one half of the wavenumber of the point P_1 and the same amplitude as that of the point P_1. This new curve (labeled by 2β) tells us that a small single disturbance, for example, with $\beta=2.50$ will develop to a steady state with wavenumber $2\beta=5.0$. Similarly, we can generate an infinite number of curves labeled by $n\beta$ $(n \geq 2)$. Only several

such curves are shown in Fig. 5.14. From this figure, we know that for a disturbance with small wavenumber, there is a multiplicity of steady state solutions. For example, the disturbance with $\beta=1.0$ will have four possible solutions: $3\beta=3.0$, $4\beta=4.0$, $5\beta=5.0$, $6\beta=6.0$ because if we draw a vertical line at $\beta=1.0$, it will intersect the curves labeled 3β, 4β, 5β, 6β.

Obviously, the smaller the wavenumber, the greater the number of possible steady state solutions. Note that according to the linear theory, the disturbances with $\beta=2.0, 3.0, 4.0, 5.0, 6.0$ have positive linear growth rates, but the numerical method excludes the steady state for $\beta=2.0$.

In the experiments, only one steady state solution will be realized. In Sect. 6.2 and Sect. 7.2, We shall show that some stable steady state solution for a large wavenumber β may become unstable steady state solution for a small wavenumber. For example, a stable steady state solution for β may become an unsteady state solution for $\frac{n\beta}{n+1}$ where $n=1, 2, 3, \cdots$.

From the derivation, we realize that the important fact results from the quadratic terms of the Navier-Stokes equations. Hence, we conclude that the fact is not only valid for the Taylor vortex flow problem but also for some special cases of the Navier-Stokes equations with spatially periodic steady state solutions (e.g., Benard convection rolls).

5.5 Comparison on Steady States with the Parameter Expansion Method

In Sect. 4.2, we formulated the perturbation method based on a parameter expansion. We now compare the results of this method with those of the numerical method.

In Fig. 5.15, we plot three curves of the steady state amplitude of the fundamental, A_e, at $\beta=4.0$ corresponding to the 9th, 15th, 21st orders, respectively. Also we plot three data points of the numerical method in which 9 harmonics are computed. The numerical method shows that A_e becomes horizontal as T is greater than about 6000. For example, $A_e=.14957438$ at $T=6000$ and $A_e=.15008064$ at $T=9000$. When we apply the numerical method, both T and β are fixed. However, for the perturbation method based on the parameter expansion, only β is fixed while T is expanded. Hence it is difficult to determine what order in the perturbation method based on the parameter expansion is comparable with 9 harmonics in the numerical method. That is, there is no direct relation available for us to compare the accuracy of these two methods. What we observe is that the higher the order in the parameter expansion, the better the agreement with the numerical method.

From the numerical method, we know that the amplitude of the fundamental $A_e=0$ in the region with small β and large T. What would happen if we apply the parameter expansion in such region? Figure 5.16 answers this question. At $\beta=2.5$, the parameter expansion produces finite amplitudes at $T=6000$ and $T=9000$ whereas the numerical method gives zero amplitude at these two values of T and shows a sudden drop (jump) of the amplitude between $T=4500$ and $T=6000$. We sketch the amplitude A_e in Fig. 5.17. We

know that the jump phenomenon at a fixed T is due to the existence of the unstable solution. Now we can see that there should be jump phenomena for some fixed wavenumbers, one of which is the case we are discussing. It is not a surprise that the parameter expansion can not model such jump phenomenon which needs at least two values of T for a fixed A_e at a given β. However, the parameter expansion, $T = T_0 + T_1 A_e^2 + T_2 A_e^4 + \cdots$, is a polynomial which can give only one value of T for a fixed A_e.

We now conclude that the parameter expansion is unable to model the jump phenomenon no matter how many terms in the expansion are calculated. Note this above conclusion is not only valid for the expansion in terms of parameter T, but also valid for the parameter expansion $\beta = \beta_0 + \beta_1 A_e^2 + \cdots$ as T is fixed. Consequently, there is no need to try an expansion of β, which is more complicated since β appears nonlinearly in (2.3.4)-(2.3.7).

The results show that all the coefficients T_k are positive as long as $\beta \geq 2.2$. However, if we decrease β a little away from 2.2, for example, $\beta = 2.199$, an interesting phenomenon occurs. All the coefficients become negative suddenly except T_0 (the Taylor number at the neutral curve). Table 5.1 is the comparison of the coefficients at $\beta = 2.2$ and $\beta = 2.199$. We realize that the sudden change of the sign for all $T_k (k > 0)$ is caused by singularities of T_k. Table 5.2 illustrates the singularity of T_1, T_2, T_3, and T_4. As all T_k $(k > 0)$ become negative, the only physically possible solution of A_e is $A_e = 0$. The reason is simple because any nonzero A_e will lead to meaningless results, $T < T_0$, from $T = T_0 + T_1 A_e^2 + T_2 A_e^4 + \cdots$.

When β is decreased further away from $\beta = 2.2$, for example, $\beta = 2.0$, many coefficients $T_k (k \geq 3)$ change the sign from negative back to positive. Hence, we get $A_e = 0$ at the 3rd and 5th orders but get nonzero A_e at higher orders.

Obviously, such nonzero A_e is incorrect. Hence, we conclude that $A_e=0$ for $\beta<2.2$ as shown in the unshaded region in Fig. 5.18. Note that one of the boundaries of the shaded region is a vertical line at $\beta=2.2$ which intersects the neutral curve at the particular point P. We have seen this special point P before in the results of the single-mode perturbation method.

CHAPTER 6

THE HIGH-ORDER PERTURBATION METHOD FOR TWO MODES

To gain deeper insight into the jump phenomenon discovered by the numerical method, we propose a high order perturbation method for two modes (two-mode method). In this method, the singularity appearing in the single-mode method will be removed. Also the stable and unstable solutions of the fundamental and the second harmonic will be found.

6.1 Formulation for the Evolution of Taylor Vortex Flow

We introduce two perturbation parameters: $A(\tau)$ and $B(\tau)$. Both $A(\tau)$ and $B(\tau)$ are assumed to be of the same order. The general expressions for amplitudes are difficult to obtain. Rather, we present the first several terms of the fundamental as

$$\begin{Bmatrix} U_1(x,\tau) \\ V_1(x,\tau) \\ W_1(x,\tau) \end{Bmatrix} = A \begin{Bmatrix} U_{11}^{1}(x) \\ V_{11}^{1}(x) \\ W_{11}^{1}(x) \end{Bmatrix} + \hat{A}B \begin{Bmatrix} U_{12}^{6}(x) \\ V_{12}^{6}(x) \\ W_{12}^{6}(x) \end{Bmatrix} + A^2\hat{A} \begin{Bmatrix} U_{13}^{10}(x) \\ V_{13}^{10}(x) \\ W_{13}^{10}(x) \end{Bmatrix} + AB\hat{B} \begin{Bmatrix} U_{13}^{15}(x) \\ V_{13}^{15}(x) \\ W_{13}^{15}(x) \end{Bmatrix} + \cdots \tag{6.1.1}$$

and the first several terms of the second harmonic as

$$\begin{Bmatrix} U_2(x,\tau) \\ V_2(x,\tau) \\ W_2(x,\tau) \end{Bmatrix} = B \begin{Bmatrix} U_{21}^{2}(x) \\ V_{21}^{2}(x) \\ W_{21}^{2}(x) \end{Bmatrix} + A^2 \begin{Bmatrix} U_{22}^{3}(x) \\ V_{22}^{3}(x) \\ W_{22}^{3}(x) \end{Bmatrix} + A\hat{A}B \begin{Bmatrix} U_{23}^{12}(x) \\ V_{23}^{12}(x) \\ W_{23}^{12}(x) \end{Bmatrix} + B^2\hat{B} \begin{Bmatrix} U_{23}^{18}(x) \\ V_{23}^{18}(x) \\ W_{23}^{18}(x) \end{Bmatrix} + \cdots \tag{6.1.2}$$

where

$$V_{11}^{1}(x=0.5)=0.5 \qquad V_{21}^{2}(x=0.5)=0.5 \tag{6.1.3}$$

and the hat has the same meaning as in the single-mode method.

Other functions V_{np}^{q} for the distorted mean flow, fundamental, second harmonic and higher harmonics are equal to zero at $x=0.5$, where the first subscript n indicates the multiple of the wavenumber (for example, 2 indicates 2β); the second subscript p indicates the order; and the superscript q stands for the ordinal number of the functions showing up in the program. Since U_n, V_n, W_n are real, we have

$$U_{np}^{q}=U_{-np}^{q} \qquad V_{np}^{q}=V_{-np}^{q} \qquad W_{np}^{q}=W_{-np}^{q} \tag{6.1.4}$$

As compared with the definition of amplitudes in (2.3.3), we have

$$\begin{aligned} A_1&=2V_1(x=0.5\tau)=2A(\tau)V_{11}^{1}(x=0.5)=A(\tau)=A \\ A_2&=2V_2(x=0.5\tau)=2B(\tau)V_{21}^{2}(x=0.5)=B(\tau)=B \end{aligned} \tag{6.1.5}$$

which show that $A(\tau)$ is indeed the amplitude of the fundamental whereas $B(\tau)$ the amplitude of the second harmonic. In this method, the distortion of the mean flow and the higher harmonics are assumed to be exclusively generated by the fundamental and the second harmonic through the nonlinear terms.

We list the first several functions (up to the third order) as follows

0β	β	2β	3β	4β	5β	6β
	AV_{11}^{1}	BV_{21}^{2}				
$A\hat{A}V_{02}^{4}$ $B\hat{B}V_{02}^{8}$	$\hat{A}BV_{12}^{6}$	$A^2V_{22}^{3}$	ABV_{32}^{5}	$B^2V_{42}^{7}$		
$A^2\hat{B}V_{03}^{13}$	$A^2\hat{A}V_{13}^{10}$ $AB\hat{B}V_{13}^{15}$	$A\hat{A}BV_{23}^{12}$ $B^2\hat{B}V_{23}^{18}$	$A^3V_{33}^{9}$ $\hat{A}B^2V_{33}^{16}$	$A^2BV_{43}^{11}$	$AB^2V_{53}^{14}$	$B^3V_{63}^{17}$

From the second column and the third column, it is easy to understand how we derive the amplitude expressions. Note that terms $A^2\hat{A}V_{13}^{10}$ and $AB\hat{B}V_{13}^{15}$ are associated with the same wavenumber β and the same order (third order) but they have different combinations of A and B, which is a new feature of this method.

Replacing V_1, V_{11}^1, V_{12}^6 by $\frac{dA}{d\tau}$, a_0, a_1, $\cdots$ in (6.1.1), we get

$$\frac{dA}{d\tau} = a_0 A + a_1 \hat{A}B + a_2 A^2\hat{A} + a_3 AB\hat{B}$$

$$+ a_4 A^3\hat{B} + a_5 \hat{A}B^2\hat{B} + a_6 A^3\hat{A}^2 + a_7 \hat{A}^3B^2 + a_8 AB^2\hat{B}^2 + \cdots \qquad (6.1.6)$$

Replacing V_2, V_{21}^2, V_{22}^3 by $\frac{dB}{d\tau}$, b_0, b_1, $\cdots$ in (6.1.2), we get

$$\frac{dB}{d\tau} = b_0 B + b_1 A^2 + b_2 A\hat{A}B + b_3 B^2\hat{B}$$

$$+ b_4 A^3\hat{A} + b_5 \hat{A}^2B^2 + b_6 A^2\hat{A}^2B + b_7 A\hat{A}B^2\hat{B} + b_8 B^3\hat{B}^2 + \cdots \qquad (6.1.7)$$

Both equations (6.1.6) and (6.1.7) are called the Landau type equations and the coefficients $a_0, a_1, \cdots, b_0, b_1, \cdots$ are called the Landau constants in the sense that they are not functions of time. As one example of applications of the Landau equations, we show the term $\frac{d}{d\tau}(BV_{21}^2)$, which is the first term in $\frac{dV_2}{d\tau}$,

$$\frac{d}{d\tau}(BV_{21}^2) = b_0 BV_{21}^2 + b_1 A^2 V_{21}^2 + b_2 A\hat{A}BV_{21}^2 + b_3 B^2\hat{B}V_{21}^2 + \cdots \qquad (6.1.8)$$

In Eq. (6.1.8), the term $b_0 V_{21}^2$ will show up in the equation of V_{21}^2 which is an eigenvalue problem for b_0. The term $b_1 V_{21}^2$ will be added to the equation of V_{22}^3 since $b_1 V_{21}^2$ is associated with A^2. Recall that the singularity occurs in the

functions associated with A^2 in the single-mode method. Now this singularity is removed because the Landau constant b_1 is determined by satisfying the solvability condition for equation of V_{22}^3. The term $b_2 V_{21}^2$ will be added to the equation of V_{23}^{12} since $b_2 V_{21}^2$ is associated with $A\hat{A}B$.

As another example of the application of the Landau equations, we show the term $\frac{d}{d\tau}(\hat{A}BV_{12}^6)$, which is the second term in $\frac{dV_1}{d\tau}$,

$$\frac{d}{d\tau}(\hat{A}BV_{12}^6) = (a_0 + b_0)\hat{A}BV_{12}^6 + a_1 AB\hat{B}V_{12}^6 + b_1\hat{A}A^2V_{12}^6 + \cdots \qquad (6.1.9)$$

where the term $(a_0 + b_0)V_{12}^6$ will show up in the equation of V_{12}^6, the term $a_1 V_{12}^6$ will be added to the equation of V_{13}^{15}, and the term $b_1 V_{12}^6$ will be added to the equation of V_{13}^{10}. In the derivation of (6.1.9), both Landau equations have been used.

Substituting (6.1.1)-(6.1.7) into the nonlinear system (2.3.4)-(2.3.7), we decompose the system into successive linear ordinary differential equations according to : (1) same wavenumber; (2) same order; (3) same combinations of A and B. As before, the program designed can generate, solve the differential equations and evaluate the Landau constants.

6.2 Applications of the Method

After determining the Landau constants, we can use the Landau equations (6.1.6)-(6.1.7) to study:

(1) the interaction the fundamental $A(\tau)$ and the second harmonic $B(\tau)$;

(2) the jump phenomenon and steady state solutions, A_e and B_e;

The properties of the Landau equations approximate some of the properties of the Navier-Stokes equations. Note that solving the Landau equations is a very simple task. Now the study of the Navier-Stokes equations is converted to the study of the Landau equations.

First, we present the application to the evolution of disturbance amplitudes. Figure 6.1.(a) is obtained by the two-mode perturbation method (9th order) at $\beta=2.58$ and $T=6000$ while the Fig. 6.2(b) is obtained by the numerical method (9 harmonics) at the same β and T. In both figures, only a small disturbance of $A(\tau)$ is initialized while the initial value of $B(\tau)$ is equal to zero. When we plot these two figures and superpose them, we can see that $0.5A(\tau)$ and $0.5B(\tau)$ obtained by the two-mode method are almost identical to the corresponding curves V_1 and V_2 by the numerical method from the time $t=0$ to the time that $0.5A(\tau)$ and $0.5B(\tau)$ almost reach their maximum values. However, unlike V_1 and V_2, $A(\tau)$ and $B(\tau)$ do not exhibit any overshoot. Consequently, the steady states of $0.5A$ and $0.5B$ are different from those of V_1 and V_2.

The two-mode method can be used to study two wave interaction. In Figure 6.2.(a), two nonzero small disturbances $A(0)$ and $B(0)$ are initialized at $\beta=2.58$ and $T=6000$ for the wide gap case. As compared with Fig. 6.2.(b) obtained from the numerical method, we can see that the two-mode method

gives good approximate results of the evolution. At any fixed β and T, we can easily plot a family of such figures of two wave interaction by choosing different pairs of $A(0)$ and $B(0)$ since solving Landau equations (6.1.6)-(6.1.7) is a simple and quick process. On the other hand, the numerical method requires tens and sometimes hundreds times of computation time used for the two-mode method to obtain same family of curves.

Amplitude diagrams are useful in the study of wave interaction. Figure 6.3 is an amplitude diagram at $\beta=2.58$ and $T=6000$. As compared with Fig. 5.11 obtained from the numerical method, we observe that both figures agree qualitatively and show the existence of a repellor, R. However, both figures only give the rough location of the repellor. The main difference between these two figures is that the locations of the attractor, A, and the repellor, R, are not the same and there is no overshoot showing up in the two-mode method.

The question why the two-mode method can not exhibit the overshoot is not solved yet. We wrote two different programs for the method. But we obtained exactly the same results, which seems to exclude the possibility of errors in programming. Perhaps, to model the overshoot, a three mode method is needed since we have seen the indication in Fig. 5.4 where the overshoot corresponds to the growth of the third harmonic. Another question is that the steady states A_e obtained from the two-mode method sometimes have better accuracy but sometimes have worse accuracy than the single-mode method. The reason for this is unknown as yet.

To solve the steady states directly, we set $\frac{dA}{d\tau}=\frac{dB}{d\tau}=0$ in (6.1.6)-(6.1.7) then obtain the following equations

$$0 = a_0 A + a_1 \hat{A} B + a_2 A^2 \hat{A} + a_3 A B \hat{B}$$
$$+ a_4 A^3 \hat{B} + a_5 \hat{A} B^2 \hat{B} + a_6 A^3 \hat{A}^2 + a_7 \hat{A}^3 B^2 + a_8 A B^2 \hat{B}^2 + \cdots \quad (6.2.1)$$

$$0 = b_0 B + b_1 A^2 + b_2 A \hat{A} B + b_3 B^2 \hat{B}$$
$$+ b_4 A^3 \hat{A} + b_5 \hat{A}^2 B^2 + b_6 A^2 \hat{A}^2 B + b_7 A \hat{A} B^2 \hat{B} + b_8 B^3 \hat{B}^2 + \cdots \quad (6.2.2)$$

which can be solved by some numerical techniques similar to the bisection method.

Figures 6.4 and 6.5 are the plots of steady states at $T=4500$ and $T=6000$, respectively. In these two figures, both A_e and B_e obtained from the 9th order two-mode method are plotted. Besides, A_e from the 9th order single-mode method and the steady state of $2V_1$ from the numerical method are also plotted. At some wavenumbers, Eqs. (6.2.1)-(6.2.2) give three solutions with physical significance. For example, at $\beta=2.58$ and $T=6000$, we get

solution	A_e	B_e
1	0.	$1.11171E-01$
2	$1.04846E-01$	$6.41049E-02$
3	$1.62391E-01$	$3.56543E-02$

In Fig. 6.5, we label these three solutions by $A1$, $A2$ and $A3$ for the fundamental and $B1$, $B2$ and $B3$ for the second harmonic. Obviously, Solutions 1 and 3 are stable and Solution 2 is unstable. By recalling Fig. 6.3 which is the amplitude diagram for $\beta=2.58$ and $T=6000$, we observe that the stable Solutions 1 and 3 correspond to the locations of the attractors, A and B, in the amplitude diagram while the unstable Solution 2 corresponds to the location of the repellor, R. In Figs. 6.4 and 6.5, the Solutions 2 and 3 are plotted with the triangle symbol. As for the Solution 1, we notice that when $A_e=0$, Eqs.

(6.2.1)-(6.2.2) are reduced to one equation

$$0 = b_0 B + b_3 B^2 \hat{B} + b_8 B^3 \hat{B}^2 + \cdots \tag{6.2.3}$$

which is same as the Landau equation of the single-mode method. To avoid confusing the figures, we do not plot the Solution 1 with the triangle symbol. By varying wavenumbers, we obtain curves representing the three solutions. When the unstable Solution 2 merges the stable Solution 3, the jump phenomenon occurs, which implies that only Solution 1 can exist. Hence, Taylor vortex flow has wavenumber 2β. Note that the slope of the amplitude curve is vertical at the jump in both Figs. 6.4 and 6.5. At $T=4500$, the jump takes place at the same wavenumber as that obtained from the numerical method - a very good agreement. At $T=6000$, the agreement is not as good as that at $T=4500$. As T increases further, for example at $T=9000$, the discrepancy between the two methods becomes bigger. The β_J from the numerical method is 2.61 while the β_J from the two-mode method is 2.48.

The intervals where the unstable solutions exist are listed as follows

T	$[\beta_J, \beta_U]$	$[2\beta_J, 2\beta_U]$
4500	2.446– 2.475	4.892– 4.95
6000	2.51– 2.78	5.20– 5.56
9000	2.48– 3.22	4.96– 6.44

Figure 6.6 is an illustration of the intervals obtained at the 9th order. The results of the calculation show that the location of the jump (wavenumber β_J) is almost not affected by the order used. For example, the 3rd order gives the same β_J as the 9th order.

We know that in the single-mode method, the results of A_e are good only for those large β if T is large. In contrast, the two-mode method is only suitable to the right neighborhood of β_J. Note that in Figs. 6.4 and 6.5, we only display A_e in the right neighborhood of β_J. For those wavenumbers β satisfying $\beta>0.5\beta^+$, the mode B will have wavenumber 2β greater than β^+ (the wavenumber of the right branch of the neutral curve). Hence, mode B has the negative linear growth rate b_0 which would cause a failure of the perturbation method. Davey & Nguyen [30] found that the perturbation method based on the Landau equation is invalid in the stable domain where the linear growth rate is negative. Indeed, when wave number is increased to some value beyond $\beta>0.5\beta^+$, singularities of some Landau constants appear and the amplitude of B becomes abnormal (infinitely large). Consequently, we conclude that the two-mode method is not suitable for $T<T_p$.

The presence of the unstable solution is very important in the stability analysis. Besides the jump phenomenon, we are able to explain some phenomena of wave interaction.

Figure 6.7 is a sketch of the steady state amplitude. As $\beta<\beta_J$ but β is close to β_J, the single disturbance (i.e., $A(0)\neq 0$ but $B(0)=0$) will lead to the steady state with 2β no matter how small $A(0)$ is. Now if we start with $A(0)\neq 0$ and $B(0)\neq 0$ ($B(0)$ may be small or big), we can definitely say that the steady state must have wavenumber 2β. In such a case, the single disturbance is a special but very important case since the wave selection depends only on the wavenumber, β, and the magnitudes of $A(0)$ and $B(0)$ do not play any role provided $A(0)$ is nonzero. Furthermore, we can conclude that the steady state with 2β is stable to the small disturbance β if $\beta<\beta_J$ but β is close to β_J.

For the two intervals $[\beta_J, \beta_U]$ and $[2\beta_J, 2\beta_U]$ where the three solutions exist, the initial amplitudes, $A(0)$ and $B(0)$, play a role in wave selection (see Fig. 6.7). Depending on the magnitudes of $A(0)$ and $B(0)$, we may get a steady state with β or 2β.

Now let us investigate the interval $[\beta_U, 0.5\beta^+]$ and the associated interval $[2\beta_U, \beta^+]$. Note that the fundamental and the second harmonic of the unstable Solution 2 merge to the corresponding ones of the stable Solution 1 at β_U and $2\beta_U$, respectively. Hence, there is only one solution with $A_e \neq 0$ and $B_e \neq 0$ in these intervals. This conclusion is very interesting. Suppose that there is a steady state with β inside the interval $[2\beta_U, \beta^+]$ which may result from a small disturbance with β. This steady state will be stable if there are no disturbances with smaller wavenumbers in the flow. However, this steady state is unstable to the disturbance inside the interval $[\beta_U, 0.5\beta^+]$ since in such case the steady state becomes the 'second' harmonic. Figure 6.8 is a convincing example at $\beta=5.8$ and $T=6000$. At first, a disturbance with $\beta=5.8$ is introduced which soon develops to its steady state. At $t=4.0$, a new disturbance with $\bar{\beta}=\beta/2=2.9$ is introduced. This disturbance is very small but it affects the steady state with $\beta=5.8$. Finally, the flow has new wavenumber $\bar{\beta}=2.9$. The original steady state with $\beta=5.8$ now has smaller value of amplitude and becomes the second harmonic in the steady state of the flow. The numerical method also produces similar result as shown in Fig. 6.9. Since $V_1(0)$ is extremely small, V_2 soon grows to its steady state with finite amplitude while V_1 is still very small. But V_1 continues to grow and eventually becomes the fundamental of the steady state while V_2 becomes smaller and serves as the second harmonic of the steady state. Thus we conclude that the steady states in $[2\beta_U, \beta^+]$ are unstable to the small disturbances in $[\beta_U, 0.5\beta^+]$. The steady

state in $[2\beta_U, \beta^+]$ is shifted to the steady state inside $[\beta_U, 0.5\beta^+]$. Such shift phenomenon is similar to the jump phenomenon because the steady state of the fundamental changes from zero to finite while the steady state of the second harmonic decreases to a smaller finite value. In Fig. 6.7, we denote such shift ('jump') by arrows at β_U and $2\beta_U$. Also we denote the jump phenomenon by arrows at β_J and $2\beta_J$.

We can use Fig. 6.6. to explain the hysteresis phenomenon. Suppose that a steady state is set up at the point 0. As the Taylor number T decreases quasi-steadily to the point 1 $(2\beta_U)$, the steady state is shifted to the point 2 (β_U) according to the previous discussion. That is, the number of the cells in a finite length of cylinder is reduced by one half. If T decreases further, the flow keeps this new wavenumber. But instead if we increase T to the point 4, the wavenumber of the flow will be changed from β back to 2β (point 5) because of the jump phenomenon. The Taylor number for the change from 2β to β is smaller than that for the change from β to 2β. This is the so-called hysteresis phenomenon, which was studied by Benjamin and Mullin [6],[7],[8] for some short cylinders. The case we explain here is analogous to the 'one-to-two cells'. They concluded that the hysteresis is caused by the end effect (imperfection) which produces unstable solutions. However, our work shows that the unstable solutions and the resulting hysteresis phenomenon are the inherent properties of the flow in the infinitely long cylinders. Perhaps, the experiments in short cylinders make the hysteresis phenomenon more observable.

6.3 Discussion on the Multi-Mode Method.

The attempt to extend the two-mode method to a multi-mode method will suffer some troubles. We now point out some of shortcomings of the multi-mode method based on our experiences on the single-mode and two-mode methods. First, we should not apply the multi-mode method unconditionally. We have mentioned that the two-mode method is not appropriate for $T<T_p$. We can also argue that the three mode method may not be suitable for those Taylor numbers which have β_J satisfying $\beta_J>\beta^+/3$. For example, at $T=4500$, $\beta_J=2.45$ and $\beta^+=5.16$, which means $3\beta_J>\beta^+$. Of course, for relatively high Taylor numbers with $\beta_J<\beta^+/3$, three mode method may give us some good results such as β_J. However, the amount of work needed would increase significantly. When we apply the 9th order single-mode method, we need to determine only 5 Landau constants and solve 25 equations. But when we use the 9th order two-mode method, we have to determine 48 Landau constants and solve 238 equations. Hence, we can only use low orders in the multi-mode method due to the economic reasons. More seriously, because the perturbation method can only be applied to the range of $[\beta^-, \beta^+]$, the multi-mode method is unable to handle with those disturbances with very small wave number and their interaction because these wavenumbers are less than β^-. In contrast, there is no such restriction in principle in the numerical method.

Though we shall not establish a multi-mode method, we present a modified two-mode method to study the interaction of two waves with $n\beta$ and $(n+1)\beta$, respectively. The method is based on the following two facts appearing in the two-mode method: (1) the intervals of multiple solutions are almost independent of the order used; (2) for $\beta<\beta_J$, $A=\frac{dA}{d\tau}=0$ and the two Landau

equations are reduced to one equation which turns out to be the Landau equation of the single-mode. Suppose that there are 3 modes A, B and C with β, 2β and 3β respectively. If $\beta<\beta^-$, $T\leq T_P$ and 2β and 3β are inside $[\beta^-, \beta^+]$, then at the steady state, $A=\frac{dA}{d\tau}=0$ and $\frac{dB}{d\tau}=\frac{dC}{d\tau}=0$. The Landau equation for A is dropped while the Landau equations for B and C are reduced to (up to the 3rd order)

$$0=b_0B+b_1(B\hat{B})B+b_2(C\hat{C})B \tag{6.3.1}$$

$$0=c_0C+c_1(C\hat{C})C+c_2(B\hat{B})C \tag{6.3.2}$$

The interaction between 2β and 3β mainly through the distortion of the mean flow, i.e., terms $B\hat{B}$ and $C\hat{C}$. By solving (6.3.1)-(6.3.2), we can study the interaction of two waves with 2β and 3β respectively. That is, we can obtain the intervals with stable and unstable solutions for B and C.

The necessary condition for this method is $A=0$. During the evolution A is not always equal to zero. Hence, this method is only useful for the study of steady state solutions. If $C=0$ in (6.3.1)-(6.3.2), the jump occurs. Then (6.3.2) is discarded and (6.3.1) is reduced to

$$0=b_0B+b_1B^2\hat{B} \tag{6.3.3}$$

which is exactly the Landau equation for the single-mode method. Therefore, another condition is that this method should only be applied to those intervals $[\beta^-, \beta^+]$ where the single-mode method can give good results. Of course, this method can also be extended to the study of interaction between two waves with $n\beta$ and $(n+1)\beta$ respectively provided $(n-1)\beta$ is less than β^-. The results of this method will be presented in Sect. 7.2.

CHAPTER 7

STABILITY DIAGRAM AND WAVE INTERACTION

The results of this chapter are obtained from the numerical method except part of Sect. 7.2. The program designed for the numerical method allows us to prescribe initial conditions in terms of many modes and study their nonlinear interaction. However, the number of combinations of many modes (i.e., the number of disturbance spectra) can be tremendous and thus makes it difficult to extract systematic information from the results. Hence, we shall first study the results for a single disturbance, which can be considered as a continuation of Sect. 5.1.

7.1 Stability Diagram for Single-Mode

Let us consider $T=6000$. We have shown that near β_J, a small change of the wavenumber can lead to totally different steady states (with β or 2β). Such a wavenumber is called a turning point in this work. Also we showed that a single disturbance with $\beta=1.3$ develops to the steady state with $2\beta=2.6$ (see Fig. 5.6(a)) while the single disturbance with $\beta=1.0$ develops to the steady state with $3\beta=3.0$ (see Fig. 5.6(b)). Hence, two questions arise. The first one is whether there is a new turning point β_{2J} between $\beta=1.0$ and $\beta=3.0$. Another question is whether the smaller β will lead to a steady state with $n\beta$ ($n=3,4,\cdots$). The numerical results give positive answers for both problems. We plot V_1 and V_2 in the $\beta-A_e$ plane (wavenumber - steady state amplitude plane) in Fig. 7.1(a) and V_1 and V_3 in Fig. 7.1(b). As β decreases from β^+, V_1, V_2 and V_3 draw their individual paths in $\beta-A_e$ plane. At β_J (labeled by

1-2(L)) V_1 drops to zero while at $2\beta_J$ (labeled by 1-2(R)) V_2 jumps up to the path formed by V_1. Also in Fig. 7.1(b), V_3 drops to zero at $3\beta_J$. As β decreases from β_J, V_1 and V_3 are equal to zero, forming horizontal lines while V_2 moves along the path formed by V_1 (see the corresponding points P_1 and P_2 in Fig. 7.1(a)). As β reaches $\beta_{2J}=1.282$, labeled by 2-3, V_2 drops to zero at $2\beta_{2J}=2.564$, labeled by 2-3(L). Meanwhile, V_3 jumps up from zero to the path formed by V_1 at $3\beta_{2J}$, labeled by 2-3(R), as shown in Fig. 7.1(b). As β decreases further from β_{2J}, V_3 moves along the path formed by V_1. When β reaches another turning point $\beta_{3J}=0.90$, V_3 also drops to zero at $3\beta_{3J}$, labeled by 3-4(L), while V_4 jumps up to the path of V_1 at $4\beta_{3J}$. Note that the interval I $[3\beta_{3J}, 3\beta_{2J}]$ where the steady state has 3β, is smaller than the interval I $[2\beta_{2J}, 2\beta_J]$ where steady state has 2β. Following this procedure, we can find other turning points β_{nJ} at smaller wavenumbers and smaller associated intervals I $[n\beta_{nJ}, n\beta_{(n-1)J}]$. But for small wavenumbers, the numerical method becomes rather inefficient. If we use 9 harmonics for the interval $[\beta_J, \beta^+]$, we need to use 18 harmonics for the interval $[\beta_{2J}, \beta_J]$ to obtain the same accuracy because a disturbance leads to the steady state with 2β. For the interval $[\beta_{5J}, \beta_{4J}]$, we thus need 45 harmonics, which takes very long computation time. Hence it is not easy to locate the turning points.

For different Taylor numbers, we apply the previous procedure to search for the turning points and associated intervals. The results are summarized in Fig. 7.2. Let us focus on $T=6000$ first. The turning points β_J, β_{2J}, β_{3J}, β_{4J} are located at the lines 1-2(L), 2-3, 3-4, 4-5 respectively. And their corresponding jumps, $2\beta_J$, $2\beta_{2J}$, $3\beta_{2J}$, $3\beta_{3J}$, $\cdots$ are located at the lines 1-2(R), 2-3(L), 2-3(R), 3-4(L), $\cdots$, respectively. Any small disturbance with wavenumber located between the line 1-2(L) and the line 2-3 will lead to the steady state with 2β

inside $[2\beta_{2J}, 2\beta_J]$. Any disturbance with β located between the line $(n-1)-n$ and the line $n-(n+1)$ will lead to the steady state with $n\beta$ inside $[n\beta_{nJ}, n\beta_{(n-1)J}]$. Take the point X ($\beta=1.0$, $T=6000$) as an example. Since this point is located between the line 2-3 and the line 3-4, it will lead to the steady state with $3\beta=3.0$ inside $[3\beta_{3J}=2.70, 3\beta_{2J}=3.846]$.

The $\beta-T$ plane of this figure is divided into three regions: 1. stable region where Couette flow is stable; 2. unstable region where Couette flow is unstable but stable Taylor vortex flow can not show up; 3. unstable region where Couette flow is unstable and stable Taylor vortex flow may show up. The line separating the stable region 1 and the unstable regions 2 and 3 is called the neutral curve which is a modification of the well-known neutral curve from the linear theory. According to the linear theory, the neutral curve is the one with zero linear growth rate. But for the points Y ($\beta=1.5$, $T=3210$) and X, though they have negative linear growth rates, Couette flow is unstable due to the nonlinear interaction. Hence, they should be inside the unstable region. The modified neutral curve is obtained by scaling. The points on the neutral curve have wavenumber β^- (the left branch) or β^+ (the right branch). Now we draw a family of curves with β^-/n and β^+/n ($n=2,3,\cdots$). The envelope of this family of curves forms the modified neutral curve. The intersection points on the modified neutral curve such as points $P, B, C, D, \cdots$ play an important role because the lines 1-2(L), 2-3, 3-4, 4-5 $\cdots$ start from these points. Meanwhile, the parts of these scaled neutral curves which are inside the unstable region lose their significances though they have zero linear growth rate.

Of course, a single initial disturbance is a very special case which implies that the path of the evolution always starts from some point of the A_1-axis in an infinite dimensional space of amplitudes. But it represents a special class of

spectra. In Fig. 7.3, a single disturbance with $\beta=1.3$ at $T=6000$ is prescribed at $t=0$. Then at $t=0.4$ it develops as Spectrum 1 while at $t=0.55$ to Spectrum 2. If at $t=0$, Spectrum 1 or 2 is initialized instead of the single disturbance, we shall get the same steady state in less time. We have shown in Sect. 6.2 that for small wavenumber β inside $[\beta_{2J}, \beta_J]$ it would be enough to study a single disturbance for two-wave interaction because only the wavenumber plays a role in the wave selection for this case. Therefore, this result is very important: the smaller the wavenumber (i.e., the larger the wavelength) of a single disturbance, the narrower is the band of steady states it will lead to. In the experiments of finite-length cylinders, the ends have effects on the flow. That is, the ends may produce strong disturbances with small wavenumber (large wavelength) determined by the length of the cylinders. This situation may be approximated by the case of a single disturbance. Hence, the experimental data points obtained from long cylinders may fall in a smaller band in the β- T plane than those from short cylinders.

7.2 Multi-Wave Interaction

In this section, we first present some results at $T=T_P=3666$ obtained from the modified two-mode perturbation method (see Sect. 6.3). Then we present some numerical results at $T=6000$. All results are for $\eta=0.5$.

At $T=T_P=3666$, we have no need to consider the interaction between the fundamental with β and the second harmonic with 2β because either of the waves has wavenumber located outside (β^-, β^+). Figure 7.4 shows the result of interaction between the wave with 2β and the wave with 3β. In the interval $[2\beta_{2J}=2.47, 2\beta_{2U}=2.71]$ there are 3 solutions $B1$, $B2$ and $B3$ for the wave with 2β while in the interval $[3\beta_{2J}=3.705, 3\beta_{2U}=4.005]$ there are 3 solutions $C1$, $C2$ and $C3$ for the wave with 3β. The figure has two obvious differences from Fig. 6.5 for the interaction between the wave with β and the wave with 2β: (1) at $2\beta_{2J}$, the slope of the stable Solution $B3$ and the slope of the unstable Solution $B2$ are not the same, hence forming a cusp; (2) also at $3\beta_{2J}$, the unstable Solution $C2$ and the stable Solution $C3$ form a cusp at zero amplitude. The jump phenomenon occurs at $\beta_{2J}=1.235$. That is, the second harmonic drops to zero at $2\beta_{2J}=2.47$ while the third harmonic jumps from zero up to the amplitude curve created by the fundamental at $3\beta_{2J}=3.705$. Hence, for a disturbance with $\beta<\beta_{2J}$, the fundamental and the second harmonic are zero and the stable steady state with 3β exists. Now let us consider another case. Suppose there is a steady state with $\bar{\beta}$ inside $(\beta^-, 2\beta_{2J})$ We know that the steady state can exist from β^- to β^+ as long as $T\leq T_P$ though it may not be always stable. We also know that in $[\beta^-, 2\beta_{2J}]$ there is only one stable solution for the wave with 2β, that is, the Solution $B1$ with zero amplitude. Hence, this steady state is unstable to a very small disturbance with large wavenumber $\hat{\beta}=3\bar{\beta}/2$ because the difference $\hat{\beta}-\bar{\beta}=\bar{\beta}/2$ will serve as the fundamental while the disturbance

with $\hat{\beta}$ will become the third harmonic. Finally, the flow will have wavenumber $\hat{\beta}$. Therefore, the steady state with $\bar{\beta}$ is shifted to that with $\hat{\beta}=3\bar{\beta}/2$. On the other hand, the stable Solution $B1$ and the unstable Solution $B2$ merge at $2\beta_{2U}$ and meanwhile the stable Solution $C1$ and the unstable Solution $C2$ merge at $3\beta_{2U}$ such that a steady state solution with $\bar{\beta}$ inside $[3\beta_{2S}, \beta^+]$ becomes unstable to a very small disturbance with $\hat{\beta}=2\bar{\beta}/3$. Therefore, the steady state with $\bar{\beta}$ is shifted to that with $\hat{\beta}=2\bar{\beta}/3$. Hence, the interval I_S $[2\beta_{2J}, 3\beta_{2U}]$ is the interval where stable steady state with 2β or 3β can exist.

Fig. 7.5 shows the result for the interaction between the wave with 3β and the wave with 4β, which is similar to the results in Fig. 7.4. The jump takes place at a smaller wavenumber $\beta_{3J}=0.84$. The interval I_S is smaller than that in Fig. 7.4. Similarly, the results for the interaction between the wave with $n\beta$ and the wave with $(n+1)\beta$ can be obtained. But the result for the interaction between the wave with 3β and the wave with 4β in Fig. 7.5 indicates a problem because 5β is inside $[\beta^-=2.20, \beta^+=4.40]$. Hence this result is valid for the case the fifth harmonic is actually suppressed to zero. Otherwise, we need to consider the interaction between three waves with 3β, 4β and 5β respectively. Similar problems occurs for other n $(n \geq 4)$. The calculation shows that I_S has a minimum value. The smallest interval I_S is that for the interaction between the wave with 4β and the wave with 5β ($[4\beta_{4J}=2.54, 5\beta_{4U}=3.975]$ where $\beta_{4J}=0.635$).

We have shown some examples of interactions between two waves (β and 2β) for $T=6000$ in Sect. 5.3. Now we present additional examples of interaction between two waves where the two waves are not restricted to have wavenumber β and 2β. Fig. 7.6 is an example for two waves $\beta_3=3.6$ and $\beta_4=4.8$. Because of the nonlinear interaction, the difference of these two waves

$\beta=\beta_4-\beta_3=1.2$ will play the role of the fundamental. Hence, $\beta_3=3.6$ serves as the third harmonic while $\beta_4=4.8$ as the fourth harmonic. In this figure, two small disturbances are prescribed. The amplitude of the disturbance with $\beta=4.8$ is one thousand times as large as that with $\beta=3.6$. The disturbance with $\beta=4.8$ soon develops to the steady state with finite amplitude while the disturbance with $\beta=3.6$ is still extremely small. But the steady state with $\beta=4.8$ can not suppress the growth of the disturbance with $\beta=3.6$. As time progresses, the disturbance with $\beta=3.6$ grows slowly though it has larger linear growth rate than that with $\beta=4.8$. That is, the existence of the steady state with $\beta=4.8$ reduces the growth of the small disturbance with $\beta=3.6$. Finally, the disturbance with $\beta=3.6$ reaches its steady state whereas the original steady state with $\beta=4.8$ is totally suppressed. Hence, we conclude that the finite amplitude Taylor vortex flow with $\beta=4.8$ is unstable to a small disturbance with $\beta=3.6$. As compared with $\beta=4.8$, the wavenumber $\beta=3.6$ is closer to the critical wavenumber $\beta_{cr}=3.16$

The second example is shown in Fig. 7.7. The disturbances of the fundamental $A(0)$ and the second harmonic $B(0)$ are prescribed. However, the situation is different from the the case we discussed in Sect. 5.3 because now both $\beta=1.2$ and $2\beta=2.4$ are beyond the interval $[\beta_J, \beta^+]$. Hence, neither A or B can develop to the steady state. The second harmonic B first reaches its peak value but soon it is suppressed by the fourth harmonic D. The fourth harmonic keeps its steady state for a certain time but eventually is destroyed by the third harmonic C. Hence, the wavenumber of the flow changes twice during the evolution and the final steady state has wavenumber $3\beta=3.6$. Note that $A(0)$ plays a key role here though it is very small ($A(0)=0.01B(0)$). If $A(0)=0$, then we will obtain the fourth harmonic D as a steady state.

Now we consider an example of interaction of four waves in Fig. 7.8. These four waves are $\beta=1.2$, $2\beta=2.4$, $3\beta=3.6$ and $4\beta=4.8$. Their initial amplitudes are also sketched in Fig. 7.8. Though the second harmonic and the fourth harmonic have larger initial values than the fundamental and the third harmonic, the third harmonic finally becomes the fundamental of the steady state. More cases for this example have been performed and the results are summarized in Table 7.1. Sixteen different spectra are studied and all lead to the same steady state with $3\beta=3.6$. Obviously, these results are caused by two reasons: (1). a steady state can not exist if the wavenumber is less than $\beta_J=2.562$; (2). the steady state with $4\beta=4.8$ is unstable to the disturbance with $3\beta=3.6$.

At $T=6000$, four examples of the interaction between four waves are studied. In these four examples, the wavenumbers of the fundamental and the second harmonic are less than $\beta_J=2.562$. Hence, there will be only two possible steady states. For each example, different disturbance spectra are prescribed. we list these examples as follows

EXAMPLE	β	2β	3β	4β
1	1.2	2.4	<u>3.6</u>	4.8
2	1.1	2.2	<u>3.3</u>	4.4
3	1.08	2.16	<u>3.24</u>	4.32
4	1.05	2.10	<u>3.15</u>	<u>4.20</u>

The underscored indicates the stable steady states. The first three examples show that the wave with 4β is unstable to the wave with 3β. That is, 4β is not inside the interval I_S. The Example 4 shows that either 3β or 4β can exist as steady state, depending on their initial amplitudes. Hence, 4β is inside the

interval I_S. Consequently, there should be a turning point between $4\beta=4.32$ and $4\beta=4.20$. However its exact location is not easy and too expensive to obtain by the numerical method.

We also try an example for the interaction between three waves and an example for the interaction between five waves, which are listed as follows

EXAMPLE	β	2β	3β	4β	5β
5	1.3	2.6	3.9		
6	0.79	1.58	2.37	3.16	3.95

In the Example 5, either the steady state with 2β or 3β can exist as a stable steady state while in the Example 6, either the steady state with 4β or 5β can exist as a stable steady state, depending on the initial amplitude spectra.

In summary, the results from the two-mode method and the numerical method show that there is a subregion containing the critical wavenumber β_{cr} in the β– T plane. Outside this subregion, stable steady state solutions do not exist and the wavenumbers of the disturbances determine the wave selection. If the disturbances are inside the subregion, the selection of the steady state depends on the initial spectra or the wavenumbers of the disturbances. This subregion may be defined as

$$\text{subregion} = \cap \quad \text{all } I_S$$

where $\cap$ is the symbol of the intersection and I_S is obtained from interaction between the wave with $n\beta$ and the wave with $(n+1)\beta$ for different Taylor numbers. Of course, this definition is only concerned with the interaction between two waves. For interaction between more than two waves, the subregion may be smaller or unchanged. This problem needs further investigation.

7.3 The Oscillation Phenomenon

An unexpected oscillation phenomenon takes place at high Taylor numbers and some small wavenumbers for a single small disturbance chosen as an initial condition. Fig. 7.9 is the plot of amplitude growth for a small disturbance with $\beta=1.25$ at $T=9000$. The fundamental and other harmonics reach their individual peaks periodically at different times. Hence, Taylor vortex flow does not develop into a steady state and its wavenumber can not determined. According to the relation $t=d^2\tau/\nu$ in (2.1.12), the period of the oscillation is short (e.g., $t=18.2$ seconds if $d=3cm$ and $\nu=0.424cm^2/\text{sec}$ for this figure). The amplitude diagrams corresponding to this case are quite interesting. We plot the amplitude diagram for the fundamental and second harmonic in Fig. 7. 10(a) as well as the amplitude diagram for the fundamental and third harmonic in Fig. 7.10(b). From these two figures, we can imagine that there is a limit cycle which looks like a 'heart' in the infinite dimensional space. Figs. 10(a) and (b) show two projections of this limit cycle. Figure 7.11 is a plot for a small disturbance with $\beta=1.16$ at $T=12000$. The oscillation is more complicated and is reminiscent of period-doubling. In some cases, the flow shows oscillatory behavior for some time but finally approaches a steady state. Figure 7. 12 shows such an example for a disturbance with $\beta=0.675$ at $T=9000$.

Figure 7.13 is a plot of the intervals of wavenumbers for $T=9000$ and $T=12000$ where the oscillation lasts for quite a long time and seems not to approach a steady state. The oscillation occurs at some special wavenumbers in the left neighborhood of β_{2J} or β_{4J}. It may be exciting to explore the details of the oscillation phenomenon. But such exploration is very time consuming and too expensive because we have to trace the evolution for very long time. Moreover, we should consider the question: whether such oscillation can be

realized in experiments. Hence, we introduce two small disturbances with $\beta=1.25$ and $2\beta=2.50$ at $T=9000$ as shown in Fig. 7.14. The corresponding amplitude diagrams are given in Fig. 15(a) and (b). We know from Fig. 7.9 that the single disturbance with $\beta=1.25$ can cause oscillation. Due to the presence of the second disturbance, however, the oscillation can not last for long time and a steady state with $3\beta=3.6$ is achieved. Accordingly, we may observe the oscillation for a short time at the beginning of some experiment and meanwhile the wavenumber of Taylor vortex flow can not be measured.

CHAPTER 8

SIDE-BAND STABILITY

8.1 Introduction

In order to explain the wave selection phenomenon that Taylor vortex flow actually shows up with wavenumber β close to the critical wavenumber β_{cr}. Eckhaus [17] introduced the concept of side-band stability: a Taylor vortex flow with wavenumber with β in the unstable region determined by the linear theory may be unstable to some small axisymmetric disturbances with different wavenumbers from β. During the nonlinear interaction with the Taylor vortex flow, the small disturbances may grow with time. As a result, these small disturbances would destroy the original Taylor vortex flow and finally develop to a stable Taylor vortex flow with a new wavenumber. In such case, we are obviously not talking about the stability of circular Couette flow (basic flow). Rather, we are dealing with the stability of Taylor vortex flow (secondary flow) with respect to some special small disturbances (noises) which are axisymmetric as the Taylor vortex flow. In other words, we deal with a quite special problem of secondary stability. Furthermore, this is essentially a linear stability problem of the secondary flow. Based on this concept, Eckhaus found the following formula for the neighborhood of the critical point (β_{cr}, T_{cr})

$$\bar{\beta}(T) = \beta_{cr} + \frac{1}{\sqrt{3}} [\beta^*(T) - \beta_{cr}] \tag{8.1.1}$$

or equivalently,

$$\begin{cases} \bar{\beta}^- = \beta_{cr} - \frac{1}{\sqrt{3}}(\beta_{cr} - \beta^-) \\ \bar{\beta}^+ = \beta_{cr} + \frac{1}{\sqrt{3}}(\beta^+ - \beta_{cr}) \end{cases}$$

where β^* is the wavenumber of the neutral curve for a prescribed T, that is, β^* stands for either β^+ or β^-; $\bar{\beta}$ is the wavenumber of the side-band stability curve for the same T ; $\bar{\beta}^-$ and $\bar{\beta}^+$ represent the left and the right branches of the side-band stability curve respectively. Note that T does not appear explicitly in (8.1.1). The side-band stability curve $\bar{\beta}(T)$ has been shown in Fig. 1.2. Stable Taylor vortex flow can only exist in the region encompassed by the side-band stability curve. In the regions between the neutral curve and the side-band stability curve, there is no steady state Taylor vortex flow.

The analysis of Eckhaus is restricted to a discrete spectrum. Kogelman and DiPrima [18] extended Eckhaus' analysis to a band of small axisymmetric disturbances (continuous spectrum). Eventually, they obtained the same relation (8.1.1) for the side-band stability curve.

All the aforementioned analyses are based on the single-mode perturbation method (up to the third order) for evolution in which the Landau equation is applied. Although the concept of the side-band stability is quite simple, the analyses are regarded as intricate and difficult to understand even by DiPrima himself [1]. We consider it adequate to rederive (8.1.1) in a relatively elementary way. We shall present the derivation in Sect. 8.3.

Nakaya [19] proposed a method to carry out the computation up to the fifth order. He obtained a narrower region of the stable Taylor vortex flow shown in Fig. 8.1. However, his result seems doubtful. First, the singularity appearing in the perturbation method was not found in his paper. Second, our results show that the high-order perturbation method does not change the side-band stability curve for low Taylor numbers. Our results will be presented in Sect. 8.4.

8.2 Formulation

The idea of formulation is as follows: For a Taylor vortex flow with wavenumber β, a pair of small axisymmetric disturbances with wavenumbers $\beta-\Delta\beta$ and $\beta+\Delta\beta$ respectively is introduced. The Taylor vortex flow is called mode A and its amplitude is also denoted by A. The disturbances with wavenumbers $\beta+\Delta\beta$ and $\beta-\Delta\beta$ are called mode B and mode C and their amplitudes are denoted by B and C respectively. The quantity $\Delta\beta$ is called the wave shift, which is a small but nonzero number. The amplitudes of B and C are assumed to be very small as compared with A such that any terms associated with the product composed of these two modes such as $C^2, B^2, BC, B^2C, \cdots$ can be neglected. If either or both of the disturbances grow with time due to the interaction with the Taylor vortex flow, the Taylor vortex flow is regarded as unstable.

We use two approaches to study the side-band stability. In Approach 1, the amplitude of Taylor vortex flow is a function of time. Thus we apply the Landau equation there. In Approach 2, we consider the stability of the steady state. Thus the parameter expansion is used. Note that previous work by other researchers only used the Approach 1.

(a) Approach 1

For the Taylor vortex flow (i.e, Mode A), we use the same amplitude expression and the Landau equation as those in the single-mode perturbation method. For convenience, we restate them as follows

$$\begin{Bmatrix} U_n(x,\tau) \\ V_n(x,\tau) \\ W_n(x,\tau) \end{Bmatrix} = \sum_{m=0}^{\infty} A^n (A\hat{A})^m \begin{Bmatrix} U_{nm}(x) \\ V_{nm}(x) \\ W_{nm}(x) \end{Bmatrix} \qquad (n \geq 0)$$

$$\begin{Bmatrix} U_{-n}(x,\tau) \\ V_{-n}(x,\tau) \\ W_{-n}(x,\tau) \end{Bmatrix} = \sum_{m=0}^{\infty} \hat{A}^n (A\hat{A})^m \begin{Bmatrix} U_{-nm}(x) \\ V_{-nm}(x) \\ W_{-nm}(x) \end{Bmatrix} \quad (n>0) \tag{8.2.1}$$

$$\frac{dA}{d\tau} = a_0 A + a_1 A(A\hat{A}) + a_2 A(A\hat{A})^2 + \cdots = \sum_{k=0}^{\infty} a_k A(A\hat{A})^k \tag{8.2.2}$$

For the small disturbances of Modes B C, we derive the following amplitude expressions

$$\begin{Bmatrix} U_n^+(x,\tau) \\ V_n^+(x,\tau) \\ W_n^+(x,\tau) \end{Bmatrix} = BA^{n-1} \sum_{m=0}^{\infty} (A\hat{A})^m \begin{Bmatrix} U_{nm}^B(x) \\ V_{nm}^B(x) \\ W_{nm}^B(x) \end{Bmatrix} + \hat{C}A^{n+1} \sum_{m=1}^{\infty} (A\hat{A})^{m-1} \begin{Bmatrix} U_{nm}^{\hat{C}}(x) \\ V_{nm}^{\hat{C}}(x) \\ W_{nm}^{\hat{C}}(x) \end{Bmatrix} \tag{8.2.3}$$

$$\begin{Bmatrix} U_n^-(x,\tau) \\ V_n^-(x,\tau) \\ W_n^-(x,\tau) \end{Bmatrix} = CA^{n-1} \sum_{m=0}^{\infty} (A\hat{A})^m \begin{Bmatrix} U_{nm}^C(x) \\ V_{nm}^C(x) \\ W_{nm}^C(x) \end{Bmatrix} + \hat{B}A^{n+1} \sum_{m=1}^{\infty} (A\hat{A})^{m-1} \begin{Bmatrix} U_{nm}^{\hat{B}}(x) \\ V_{nm}^{\hat{B}}(x) \\ W_{nm}^{\hat{B}}(x) \end{Bmatrix} \tag{8.2.4}$$

where U_n^+ indicates that U is associated with $n\beta+\Delta\beta$ while U_n^- indicates that U is associated with $n\beta-\Delta\beta$; $V_{10}^B(x=0.5) = V_{10}^C(x=0.5) = 0.5$ and the other functions in (8.2.3)-(8.2.4) are equal to zero at $x=0.5$ (normalization).

We list some lower order functions and their corresponding amplitude combinations as follows

$\Delta\beta$	$\beta-\Delta\beta$	$\beta+\Delta\beta$	$2\beta-\Delta\beta$	$2\beta+\Delta\beta$	$3\beta-\Delta\beta$	$3\beta+\Delta\beta$
	C	B				
$B\hat{A}$ $\hat{C}A$			CA	BA		
	$CA\hat{A}$ $\hat{B}A^2$	$BA\hat{A}$ $\hat{C}A^2$			CA^2	BA^2

Let us consider the following two functions

$$V_1^+ = BV_{10}^B + B(A\hat{A})V_{11}^B + B(A\hat{A})^2V_{12}^B + \cdots + \hat{C}A^2V_{11}^{\hat{C}} + \hat{C}A^2(A\hat{A})V_{12}^{\hat{C}} + \cdots \tag{8.2.5}$$

$$V_1^- = CV_{10}^C + C(A\hat{A})V_{11}^C + C(A\hat{A})^2V_{12}^C + \cdots + \hat{B}A^2V_{11}^{\hat{B}} + \hat{B}A^2(A\hat{A})V_{12}^{\hat{B}} + \cdots \tag{8.2.6}$$

Replacing $V_1^+, V_{10}^B, V_{11}^B, \cdots, V_{11}^{\hat{C}}, V_{12}^{\hat{C}}, \cdots$ by $\frac{dB}{d\tau}, b_0, b_1, \cdots, \bar{b}_1, \bar{b}_2, \cdots$ in (8.2.5), we obtain

$$\begin{aligned}\frac{dB}{d\tau} &= b_0B + b_1B(A\hat{A}) + b_2B(A\hat{A})^2 + \cdots + \bar{b}_1\hat{C}A^2 + \bar{b}_2\hat{C}A^2(A\hat{A}) + \cdots \\ &= B[b_0 + b_1(A\hat{A}) + b_2(A\hat{A})^2 + \cdots] + \hat{C}[\bar{b}_1A^2 + \bar{b}_2A^2(A\hat{A}) + \cdots] \\ &= \sum_{k=0}^{\infty} b_k B(A\hat{A})^k + \sum_{l=1}^{\infty} \bar{b}_l \hat{C}A^2(A\hat{A})^{l-1}\end{aligned} \tag{8.2.7}$$

Replacing $V_1^-, V_{10}^C, V_{11}^C, \cdots, V_{11}^{\hat{B}}, V_{12}^{\hat{B}}, \cdots$ by $\frac{dC}{d\tau}, c_0, c_1, \cdots, \bar{c}_1, \bar{c}_2, \cdots$ in (8.2.6), we obtain

$$\begin{aligned}\frac{dC}{d\tau} &= c_0C + c_1C(A\hat{A}) + c_2C(A\hat{A})^2 + \cdots + \bar{c}_1\hat{B}A^2 + \bar{c}_2\hat{B}A^2(A\hat{A}) + \cdots \\ &= C[c_0 + c_1(A\hat{A}) + c_2(A\hat{A})^2 + \cdots] + \hat{B}[\bar{c}_1A^2 + \bar{c}_2A^2(A\hat{A}) + \cdots] \\ &= \sum_{k=0}^{\infty} c_k C(A\hat{A})^k + \sum_{l=1}^{\infty} \bar{c}_l \hat{B}A^2(A\hat{A})^{l-1}\end{aligned} \tag{8.2.8}$$

Equations (8.2.7)-(8.2.8) are called the Landau equations and the coefficients $b_0, b_1, \cdots, \bar{b}_0, \bar{b}_1, \cdots, c_0, c_1, \cdots, \bar{c}_0, \bar{c}_1, \cdots$ are called the Landau constants.

Substituting (8.2.1)-(8.2.4) and (8.2.7)-(8.2.8) into the nonlinear system (2.3.4)-(2.3.7), we decompose the system into successive linear ordinary

differential equations according to: (1) same wavenumber; (2) same order; (3) same combination of A, B and C. The program designed can generate and solve the differential equations and evaluate the Landau constants. Some resulting differential equations will be shown in the next section.

(b) Approach 2

For Taylor vortex flow (i.e, Mode A), we use the same amplitude expression and parameter expression as those in the single-mode perturbation method where A_e is used instead of $A(\tau)$. For convenience, we restate the parameter expression as follows

$$T = T_0 + T_1(A_e \hat{A}_e) + T_2(A_e \hat{A}_e)^2 + T_3(A_e \hat{A}_e)^3 + \cdots = \sum_{k=0}^{\infty} T_k (A_e \hat{A}_e)^k \qquad (8.2.9)$$

For the Modes B and C, we employ the amplitude expressions (8.2.3)-(8.2.4) and the Landau equations (8.2.7)-(8.2.8) except that $A(\tau)$ now is replaced by A_e.

The rest of this approach is analogous to the Approach 1. These two different approaches are implemented in a single program.

8.3 Simplified Derivation of Side-Band Stability Curve

First, we present some relations between the Landau constants which are useful in the further derivation. We claim that as $\Delta\beta \to 0$

$$a_0 = b_0 = c_0 \tag{8.3.1}$$

and

$$\begin{aligned} b_1 &= 2a_1 \qquad & \bar{b}_1 &= \bar{a}_1 \\ c_1 &= 2a_1 \qquad & \bar{c}_1 &= \bar{a}_1 \end{aligned} \tag{8.3.2}$$

We select following examples from the perturbation equations to verify the above relations

(a) Consider one of the two equations for the functions U_{10}^A, V_{10}^A, W_{10}^A (associated with the wavenumber β)

$$(DD^* - \beta^2 - a_0)V_{10}^A - U_{10}^A = 0$$

and the corresponding one for the functions U_{10}^B, V_{10}^B, W_{10}^B (associated with the wavenumber $\beta+\Delta\beta$)

$$[DD^* - (\beta+\Delta\beta)^2 - b_0]V_{10}^B - U_{10}^B = 0$$

Obviously, as $\Delta\beta \to 0$, due to the normalization of the functions, we obtain

$$b_0 = a_0 \qquad U_{10}^B = U_{10}^A \qquad V_{10}^B = V_{10}^A \tag{8.3.3}$$

Equation (8.3.3) is also true if we compare another equation for the functions U_{10}^A, V_{10}^A, W_{10}^A and the corresponding one for the functions U_{10}^B, V_{10}^B, W_{10}^B (for simplicity, we do not list these two equations here).

Similarly, we can show that

$$c_0 = a_0 \qquad U_{10}^C = U_{10}^A \qquad V_{10}^C = V_{10}^A \tag{8.3.4}$$

Hence, Eq. (8.3.1) is verified.

(b) Consider one of the two equations for the functions U^A_{20}, V^A_{20}, W^A_{20}, (associated with 2β)

$$[DD^* - (2\beta)^2 - 2a_0]V^A_{20} - U^A_{20} = \frac{1}{2A'\delta}[2(U^A_{10}D^* V^A_{10} - i\beta W^A_{10}V^A_{10} + \frac{\delta}{1+\delta x}U^A_{10}V^A_{10})]$$

and the corresponding one for the functions U^B_{20}, V^B_{20}, W^B_{20} (associated with $2\beta+\Delta\beta$)

$$[DD^* - (2\beta+\Delta\beta)^2 - (b_0+a_0)]V^B_{20} - U^B_{20} = \frac{1}{2A'\delta}[U^A_{10}D^* V^B_{10} + U^B_{10}D^* V^A_{10}$$

$$- i\beta(W^A_{10}V^B_{10} + W^B_{10}V^A_{40}) + \frac{\delta}{1+\delta x}(U^A_{10}V^B_{10} + U^B_{10}V^A_{10})]$$

It is easy to see that as $\Delta\beta \to 0$

$$V^B_{20} = 2V^A_{20} \qquad U^B_{20} = 2U^A_{20} \qquad W^B_{20} = 2W^A_{20} \tag{8.3.5}$$

(c) Likewise, it is not difficult to show that as $\Delta\beta \to 0$

$$V^B_{01} = V^A_{01} \qquad U^B_{01} = U^A_{01} \qquad W^B_{01} = W^A_{01} \tag{8.3.6}$$

(d) As the final example, consider one of the two equations for the functions U^A_{11}, V^A_{11}, W^A_{11}

$$(DD^* - \beta^2 - 3a_0)V^A_{11} - U^A_{11} = \frac{1}{2A'\delta}[2a_1 V^A_{10} + U^A_{01}D^* V^A_{10} + U^A_{10}D^* V^A_{01} + U^A_{-10}D^* V^A_{20}$$

$$+ U^A_{20}D^* V^A_{-10} - i\beta W^A_{01}V^A_{10} + \frac{\delta}{1+\delta x}(U^A_{01}V^A_{10} + U^A_{10}V^A_{01} + U^A_{-10}V^A_{20} + U^A_{20}V^A_{-10})]$$

and the corresponding one for the functions U^B_{11}, V^B_{11}, W^B_{11} (associated with $\beta+\Delta\beta$)

$$[DD^* - (\beta+\Delta\beta)^2 - (b_0 + 2a_0)]V^B_{11} - U^B_{11} = \frac{1}{2A'\delta}[(2a_1 + b_1)V^B_{10} + U^A_{01}D^* V^B_{10} + U^B_{10}D^* V^A_{01} +$$

$$U^A_{10}D^* V^B_{01} + U^B_{01}D^* V^A_{10} + U^A_{-10}D^* V^B_{20} + U^B_{20}D^* V^A_{-10} - i\beta(W^B_{01}V^A_{10} + W^A_{01}V^B_{10})$$

$$+\frac{\delta}{1+\delta x}(U_{01}^{A}V_{10}^{B}+U_{01}^{B}V_{10}^{A}+U_{10}^{A}V_{01}^{B}+U_{10}^{B}V_{01}^{A}+U_{-10}^{A}V_{20}^{B}+U_{20}^{B}V_{-10}^{A})]$$

By comparison and full use of all the information shown in the previous examples, it is apparent that

$$b_1=2a_1 \qquad\qquad V_{11}^{B}=2V_{11}^{A} \tag{8.3.7}$$

Thus we verify one of the relations in (8.3.2). The other relations in (8.3.2) can be verified similarly.

The Landau equations (up to the third order) are

$$\frac{dA}{d\tau}=a_0A+a_1A^3 \tag{8.3.8}$$

$$\frac{dB}{d\tau}=B(b_0+b_1A^2)+C(\bar{b}_1A^2) \tag{8.3.9}$$

$$\frac{dC}{d\tau}=C(c_0+c_1A^2)+B(\bar{c}_1A^2) \tag{8.3.10}$$

When $\frac{dA}{dt}=0$, we obtain the steady state amplitude A_e

$$A_e^2=-\frac{a_0}{a_1}>0 \tag{8.3.11}$$

where $a_0>0$ and $a_1<0$.

Consider the vicinity of the critical point $(\beta_{cr},\ T_{cr})$ as shown in Fig. 8.2. The Taylor number T_1 is chosen sufficiently close to T_{cr} and greater than T_{cr}. The first Landau constant a_0 of Mode A is not a function of time but a function of β and T. We expand a_0 in Taylor series at fixed T_1

$$a_0(\beta,T_1)=\hat{a}_0+\frac{\partial a_0}{\partial\beta}\Big|_{cr}(\beta-\beta_{cr})+\frac{1}{2}\frac{\partial^2 a_0}{\partial\beta^2}\Big|_{cr}(\beta-\beta_{cr})^2+\cdots \tag{8.3.12}$$

where $\hat{a}_0=a_0(\beta_{cr},\ T_1)$. Note that as T_1 is close to T_{cr}, the neutral curve is almost symmetric with respect to β_{cr}. Therefore, it is reasonable to use a

parabola as an approximation of (8.3.12). That is, a_0 is assumed to be symmetric with respect to the point (β_{cr}, T_1). We have shown in Fig. 2.2 that the above assumption is very good (the critical point for this figure is at $\beta_{cr}=3.13$ and $T_{cr}=1695$). Fig. 8.2 gives the geometric interpretation of the approximation of a_0. Due to the symmetry of the parabola, $|\beta^+ - \beta_{cr}| = |\beta_{cr} - \beta^-|$. Let

$$\frac{\beta-\beta_{cr}}{\beta^+-\beta_{cr}} = \hat{\beta}, \qquad \frac{\Delta\beta}{\beta^+-\beta_{cr}} = \Delta\hat{\beta}. \tag{8.3.13}$$

where both $\hat{\beta}$ and $\Delta\hat{\beta}$ are dimensionless, and their absolute values are not greater than 1, for example, $\bar{\beta}=0$ when $\beta=\beta_{cr}$, and $\bar{\beta}=1$ when $\beta=\beta^+$.

The approximation of (8.3.12) is expressed in the form of parabola

$$a_0 = \hat{a}_0\left(1 - \frac{\beta - \beta_{cr}}{\beta^+ - \beta_{cr}}\right)\left(1 + \frac{\beta-\beta_{cr}}{\beta_{cr}-\beta^-}\right) = \hat{a}_0(1 - \hat{\beta}^2) \tag{8.3.14}$$

For Modes B and C, the first Landau constants are approximately as

$$b_0 = \hat{a}_0\left[1 - \left(\frac{(\beta+\Delta\beta)-\beta_{cr}}{\beta^+-\beta_{cr}}\right)^2\right] = \hat{a}_0[1 - (\hat{\beta} + \Delta\hat{\beta})^2]$$

$$c_0 = \hat{a}_0\left[1 - \left(\frac{(\beta-\Delta\beta)-\beta_{cr}}{\beta^+-\beta_{cr}}\right)^2\right] = \hat{a}_0[1 - (\hat{\beta} - \Delta\hat{\beta})^2] \tag{8.3.15}$$

which implies that b_0 and c_0 obey the same parabola of a_0, since b_0 and c_0 have the same form as a_0 for $\Delta\beta\to 0$.

In the following derivation, all the second Landau constants are treated as invariants with respect to β and T in the vicinity of the critical point, namely,

$$a_1 = a_{1_{cr}} \qquad b_1 = b_{1_{cr}} \qquad \bar{b}_1 = \bar{b}_{1_{cr}} \qquad c_1 = c_{1_{cr}} \qquad \bar{c}_1 = \bar{c}_{1_{cr}} \tag{8.3.16}$$

If Mode A is in the steady state, Eqs. (8.3.9)-(8.3.10) become

$$\frac{dB}{dt} = B(b_0 + b_1 A_e^2) + C(\bar{b}_1 A_e^2) = B(b_0 - b_1 \frac{a_0}{a_1}) + C(-\bar{b}_1 \frac{a_0}{a_1}) = B(b_0 - 2a_0) + C(-a_0) \tag{8.3.17}$$

$$\frac{dC}{dt} = C(c_0 + c_1 A_e^2) + B(\bar{c}_1 A_e^2) = C(c_0 - c_1 \frac{a_0}{a_1}) + B(-\bar{c}_1 \frac{a_0}{a_1}) = C(c_0 - 2a_0) + B(-a_0) \tag{8.3.18}$$

Eqs. (8.3.17) and (8.3.18) are linear homogeneous differential equations. Let $B = \rho \exp(\lambda t)$, $C = \mu \exp(\lambda t)$, then

$$\begin{bmatrix} (b_0 - 2a_0) - \lambda & -a_0 \\ -a_0 & (c_0 - 2a_0) - \lambda \end{bmatrix} \begin{bmatrix} \rho \\ \mu \end{bmatrix} = \begin{bmatrix} 0 \\ 0 \end{bmatrix} \tag{8.3.19}$$

which leads to

$$\lambda^2 - \lambda(b_0 + c_0 - 4a_0) + [b_0 c_0 - 2a_0(b_0 + c_0) + 3a_0^2] = 0$$

or in terms of the dimensionless quantities (see Eq. (8.3.13))

$$\lambda^2 + 2\hat{a}_0[(1 - \hat{\beta}^2) + \Delta\hat{\beta}^2]\lambda + \hat{a}_0^2 \Delta\hat{\beta}^2(2 - 6\hat{\beta}^2 + \Delta\hat{\beta}^2) = 0 \tag{8.3.20}$$

where the negative root of λ has been dropped. The positive root of λ is

$$\lambda = -\hat{a}_0[(1 - \hat{\beta}^2) + \Delta\hat{\beta}^2] + \hat{a}_0 \sqrt{(1 - \hat{\beta}^2)^2 + 4\hat{\beta}^2 \Delta\hat{\beta}^2} \tag{8.3.21}$$

Note that the amplitude of Mode A is finite while the amplitudes of Modes B and C are assumed as infinitesimal. The eigenvalue λ is indeed the linear growth rate for the Modes B and C. If $\lambda < 0$, both B and C decay and the Mode A is in stable steady state. The small axisymmetric disturbances are suppressed by the existing Taylor vortex flow (Mode A). However, if $\lambda > 0$, both Modes B and C will grow and one of them will replace Mode A. Consequently, Mode A no longer is a stable steady state. In other words, the study of side-band stability of Mode A is the study of linear stability of Modes B and C in

presence of a Taylor vortex flow with finite amplitude.

Note that $\hat{a}_0$ ($\hat{a}_0 = a_0(\beta_{cr}, T_1)$) is greater than zero in the region of interest. For positive λ, we obtain

$$\sqrt{(1-\hat{\beta}^2)^2 + 4\hat{\beta}^2\Delta\hat{\beta}^2} > (1-\hat{\beta}^2) + \Delta\hat{\beta}^2$$

$$\hat{\beta}^2 > \frac{1}{3} + \frac{1}{6}\Delta\hat{\beta}^2$$

or in dimensional form

$$\left(\frac{\beta-\beta_{cr}}{\beta^+-\beta_{cr}}\right)^2 > \frac{1}{3} + \frac{1}{6}\left(\frac{\Delta\beta}{\beta^+-\beta_{cr}}\right)^2 \tag{8.3.22}$$

For negative λ, we obtain

$$\sqrt{(1-\hat{\beta}^2)^2 + 4\hat{\beta}^2\Delta\hat{\beta}^2} < (1-\hat{\beta}^2) + \Delta\hat{\beta}^2$$

$$\hat{\beta}^2 < \frac{1}{3} + \frac{1}{6}\Delta\hat{\beta}^2$$

or in dimensional form

$$\left(\frac{\beta-\beta_{cr}}{\beta^+-\beta_{cr}}\right)^2 < \frac{1}{3} + \frac{1}{6}\left(\frac{\Delta\beta}{\beta^+-\beta_{cr}}\right)^2 \tag{8.3.23}$$

The side-band stability curve is obtained when $\lambda = 0$ and $\Delta\beta \to 0$

$$\begin{cases} \overline{\beta}^- = \beta_{cr} - \frac{1}{\sqrt{3}}(\beta_{cr} - \beta^-) \\ \overline{\beta}^+ = \beta_{cr} + \frac{1}{\sqrt{3}}(\beta^+ - \beta_{cr}) \end{cases} \tag{8.3.24}$$

Equation (8.3.24) is identical to (8.1.1). Hence, we complete the proof of (8.1.1) in a simpler way.

8.4 Results

Because the original analyses of Eckhaus and Kogelman and DiPrima are restricted to the small gap case ($\eta=\frac{r_1}{r_2}\to 1$, i.e., $\delta=\frac{1-\eta}{\eta}\to 0$), we apply the high-order perturbation method to the small gap case ($\delta=0.05$, i.e., $\eta=0.95238$) as well as the wide gap case ($\delta=1.0$, i.e., $\eta=0.5$). For convenience, the side-band stability curve determined by (8.1.1) (i.e., $\bar{\beta}=\beta_{cr}+\frac{1}{\sqrt{3}}(\beta^*-\beta_{cr})$) is called the predicted side-band stability curve (3rd order).

(a) Approach 1

First, we consider the wide gap case in Table 8.1. We display the results of the neutral curve and the 3rd order predicted curve. The wavenumber $\bar{\beta}_p^-$ and $\bar{\beta}_p^+$ are the left and right branches of the predicted curve respectively whereas β^- and β^+ are the left and right branches of the neutral curve respectively. In Table 8.2 and Fig. 8.3, we show the points $((\bar{\beta}^-, T)$ and $(\bar{\beta}^+, T))$ of the side-band stability curves obtained from different orders. Theoretically, these points should have exactly zero linear growth rate. But indeed they correspond to extremely small positive growth rate since it is difficult to accurately locate the points with zero growth rate in the calculation.

By comparison between Tables 8.1 and 8.2, we observe that at low Taylor numbers ($T\leq T_P=3666$), the points from different orders almost coincide with those of the predicted curve. Such agreement implies: (1) at low Taylor numbers the previous analyses of Eckhaus and others are very good and the assumptions they imposed in the analyses are reasonable; (2) the increase of the order of the perturbation does not narrow the region in which stable Taylor vortex flow can exist.

As T is increased, we observe from Table 8.2 and Fig. 8.3 that the points from different orders begin to deviate from the predicted curve. In Fig. 8.3 we also plot the singularity line of the second Landau constant a_1 which is also the zero amplitude line in the single-mode perturbation method. Moreover, we plot the line of the jump β_J (i.e., the $1-2(L)$ line) obtained from the numerical method. We can see the points $(\bar{\beta}^-, T)$ of the third order approaches to and then falls on the singularity line as T is increased. Accordingly, we conclude that due to the singularity of a_1, all the points $(\bar{\beta}^-, T)$ from different orders at relatively high Taylor numbers $(T > T_P)$ are not reliable.

Now we turn to describe the results for the small gap case. In Table 8.3. We display the results for the neutral curve and the 3rd order predicted curve. In Table 8.4 and Fig. 8.4, we show the points $((\bar{\beta}^-, T)$ and $(\bar{\beta}^+, T))$ of the side-band stability curves obtained from different orders. Table 8.4 and Fig 8.4 show that the results for the small gap case are similar to those for the wide gap case at low Taylor numbers. For the left branch of the side-band stability curve $\bar{\beta}^-$ at high Taylor numbers, the differences between the results of different orders and the results for the predicted curve are larger than the differences in the wide gap case.

(b) Approach 2

We apply this approach to both wide and small gap cases. Figure 8.5 is the results for the wide gap case while Fig. 8.6 is the results for the small gap case. In both figures, once again we see that at low Taylor numbers $(T < T_P)$ the perturbation method of different orders produce results very close to to the third order predicted curve. However, in both figures, the left branches of the $\bar{\beta}^-$ curves produced by the perturbation method of different orders terminate

as β is decreased to certain values. Obviously, this phenomenon is related to singularity in the single-mode analysis based on the parameter expansion described in Sect. 5.5. Furthermore, for the right branch of the side-band stability curve $\overline{\beta}^{+}$ at high Taylor numbers, the differences between the results of different orders and the predicted curve are larger than those in Approach 1.

Note that the wave shift $\Delta\beta=0.02$ is used in both small and wide gap cases for both approaches. Choosing different values of $\Delta\beta$ causes little change in the the results (i.e., the points in the $(\beta- T)$ plane) provided $\Delta\beta$ is sufficiently small. In Table 8.5, we give an example of the effect of the wave shift on the computed Taylor numbers of side-band stability curve by use of Approach 2.

In summary, both approaches confirm the previous analyses (up to the third order) of Eckhaus, Kogelman and DiPrima at low Taylor numbers. More importantly, both approaches show that the high-order perturbation method hardly change the predicted side-band stability curve at low Taylor numbers. Another important conclusion is that we should not extend the predicted curve to high Taylor numbers, especially the left branch ($\overline{\beta}^{-}$), because of the singularity and the poor accuracy at high Taylor numbers in the single-mode perturbation method.

8.5 Discussion

The study of the side-band stability curve is based on a special model of interaction between three waves. That is, one wave with finite amplitude has wavenumber β and a pair of small disturbances have wavenumbers $\beta-\Delta\beta$ and $\beta+\Delta\beta$, respectively. The finite amplitude is obtained from the single-mode method which produces accurate results for low Taylor numbers $T \leq T_P$. We may ask the following questions: (1). What will happen to the interaction between one mode with finite amplitude and one small disturbance with $\beta-\Delta\beta$ or $\beta+\Delta\beta$? (2). Do we need to introduce more pairs of small disturbances in the study of side-band stability?

The first question is easy to answer because this is indeed a special case of two-wave interaction which is a reduced case of the previous three-wave interaction. The Landau equation is reduced to

$$\frac{dB}{d\tau} = B(b_0 + b_1 A^2) \tag{8.5.1}$$

The derivation of the new side-band stability curve is analogous to the previous one but simpler. We are not going to present the derivation here. Rather, we just give the result

$$\begin{cases} \overline{\beta}^- = \beta_{cr} - \frac{1}{\sqrt{2}}(\beta_{cr} - \beta^-) \\ \overline{\beta}^+ = \beta_{cr} + \frac{1}{\sqrt{2}}(\beta^+ - \beta_{cr}) \end{cases} \tag{8.5.2}$$

The region determined by (8.5.2) is bigger than that given by (8.1.1). This result makes it necessary to investigate the second question. Let us consider a special model of interaction between five waves. In addition to the previous model with three waves, a new pair of small disturbances $\beta+\Delta\overline{\beta}$ (Mode

D) and $\beta - \Delta\bar{\beta}$ (Mode E) is introduced. The new wave shift $\Delta\bar{\beta}$ is a small quantity which is nonzero and different from $\Delta\beta$. For example, $\Delta\bar{\beta}$ may be equal to $2\Delta\beta$. The corresponding Landau equations are

$$\frac{dA}{d\tau} = a_0 A + a_1 A^3 \tag{8.5.3}$$

$$\frac{dB}{d\tau} = B(b_0 + b_1 A^2) + C(\bar{b}_1 A^2) \tag{8.5.4}$$

$$\frac{dC}{d\tau} = C(c_0 + c_1 A^2) + B(\bar{c}_1 A^2) \tag{8.5.5}$$

$$\frac{dD}{d\tau} = D(d_0 + d_1 A^2) + E(\bar{d}_1 A^2) \tag{8.5.6}$$

$$\frac{dE}{d\tau} = E(e_0 + e_1 A^2) + D(\bar{e}_1 A^2) \tag{8.5.7}$$

Note that Eqs. (8.5.6) and (8.5.7) are not coupled with Eqs. (8.5.4) and (8.5.5). Hence, the derivation is analogous to that in Sect. 8.3 and we still get the same side-band stability curve as (8.1.1) when $\Delta\beta \to 0$ and $\Delta\bar{\beta} \to 0$. That is, the model of three waves is sufficient for the study of the side-band stability for low Taylor numbers.

The analysis of the side-band stability is based on the consideration that a steady state of Taylor vortex flow may be unstable to some axisymmetric disturbances with very small amplitudes. Based on the same consideration, we define in Sect. 7.2 a subregion where stable Taylor vortex flow can exist. The boundary of this subregion plays a similar role to the side-band stability curve. However, the definition is only concerned with the two-wave interaction and the wavenumber of the small disturbance is not arbitrary (i.e., it is either $n\beta$ or $(n+1)\beta$ where n is an integer). In contrast, the wave shift $\Delta\beta$ used in the side-band stability analysis is arbitrary but small. That is, there are two

different ways to determine the subregion. Hence, we would like to know whether the results obtained from these two ways are consistent or not. We note that at $T=3666$ the smallest interval I_S during two-wave interaction is the interval $[4\beta_{4J}=2.54,\ 5\beta_{4U}=3.975]$ during the interaction between the wave with 4β and the wave with 5β. Note that at $T=3666$, $\beta^-=2.20$ and $\beta^+=4.40$. Thus, Eq. (8.1.1) gives $[\overline{\beta}^-=2.61,\ \overline{\beta}^+=3.80]$ while Eq. (8.5.2) leads to $[\overline{\beta}^-=2.48,\ \overline{\beta}^+=4.03]$. These results are consistent.

So far it seems that the analysis of the side-band stability is reasonable, though the results at high Taylor numbers are doubtful. At high Taylor numbers, perhaps the left branch $\overline{\beta}^-$ of the side-band stability curve should be replaced by a line which is between the curve β_J (i.e., 1-2 (L) line) and the vertical line of β_{cr} (see Fig. 8.2). The right branch $\overline{\beta}^+$ also needs modification. For example, at $T=6000$ and $\eta=0.5$, the third order perturbation gives the smallest $\overline{\beta}^+=4.67$ as shown in Table 8.2. But from the Examples 3 and 4 in Sect. 7.2, we know that $\overline{\beta}^+$ is less than 4.32. Hence, the right branch should be bent such that it is closer to the vertical line of β_{cr}. Unfortunately, applying the numerical method to obtain the side-band stability curve is not a appropreate way because the computation is too expensive and time consuming. Due to the limitation of the two-mode method (see Sect. 6.3), the attempt to study the side-band stability at relatively high Taylor numbers based on the finite amplitude obtained from the two-mode method is not worthwhile. A better method would be highly desirable for the study of side-band stability curve at high Taylor numbers.

CHAPTER 9

SUMMARY

We have studied axisymmetric Taylor vortex flow in some range of Taylor numbers and wavenumbers and its stability with respect to axisymmetric disturbances with different wavenumbers. By use of a numerical method and perturbation methods, we find stable and unstable steady state solutions and some associated phenomena such as the occurrence of jump and hysteresis. The results indicate that unstable steady state solutions play a key role in wave selection. Because unstable steady state solutions exist in a small region of wavenumbers consisting of the critical wavenumber β_{cr}, a steady state Taylor vortex flow with large (or small) wavenumber is unstable and thus replaced by a new steady state with wavenumber close to β_{cr}. In this small region, the wavenumbers and initial amplitudes of disturbances determine the wavenumber of the flow; but outside this region, only the wavenumbers of the disturbances have effect on the wave selection such that the steady state has a wavenumber close to β_{cr}. Due to the nonlinear interaction and the existence of unstable steady state solutions, at high Taylor numbers, a small disturbance with small wavenumber β can develop to a stable Taylor vortex flow with wavenumber $n\beta$ inside the small region. The wavenumber of this disturbance may be so small that it is in the stable region determined by the linear theory. Hence, some concepts such as the stable and unstable regions and the neutral curve from the linear theory require new interpretations.

We show the existence of multiple steady state solutions for small wavenumber (large wavelength). We conclude that the smaller the

wavenumber, the greater the number of possible steady state solutions. This conclusion is not only valid for the Taylor vortex flow problem but also for some special cases of Navier-Stokes equations with spatially periodic steady state solutions (e.g., Benard convection rolls).

The numerical method is very important in this work. Most of discoveries were obtained first by the numerical method. The two-mode perturbation method provides good approximations and requires less computation than the numerical method. The amplitude equations help us gain deeper insight into the problem. The two-mode perturbation method is successful because it shows the existence of the stable and unstable solutions, thus explaining the jump phenomenon and the hysteresis phenomenon, and produces good results of the amplitudes at wavenumbers close to the jump.

Because the singularity occurs at high Taylor numbers, the single-mode perturbation method based on the Landau equation gives good results only at low Taylor numbers ($\frac{T}{T_{cr}} \leq \frac{3666}{3100} = 1.18$ for $\eta = 0.5$) or high Taylor numbers with wavenumbers very close to the right branch of the neutral curve (see Fig. 5.9). Moreover, this method can not be used for the study of wave interaction. Another method based on a parameter expansion has similar troubles.

The unstable solutions and side-band stability are closely related. Hence, the analysis of the side-band stability is reasonable. The derivation of the side-band stability curve (up to the third order) given in here is much simpler than previous analysis by Kogelman and DiPrima. High-order perturbation methods are applied to the calculation of the side-band stability curve. Our results show that the side-band stability curve is nearly independent of the order used at low Taylor numbers. Accordingly, Nakaya's results for the fifth

order are doubtful. The side-band stability curve produced is accurate at low Taylor numbers but incorrect at relatively high Taylor numbers. A better method would be highly desirable for the study of side-band stability curve at high Taylor numbers.

Our results show that the hysteresis phenomenon and the overshoot phenomenon during the evolution of the flow are the inherent properties of Taylor vortex flow between infinitely long cylinders. Therefore, we should not overemphasize the end effects in the interpretation of the results of the experiments and the calculations for the finite-length cylinders. The oscillation phenomenon found in the calculation is interesting. However, such phenomenon may occur in some experiments only for a short time.

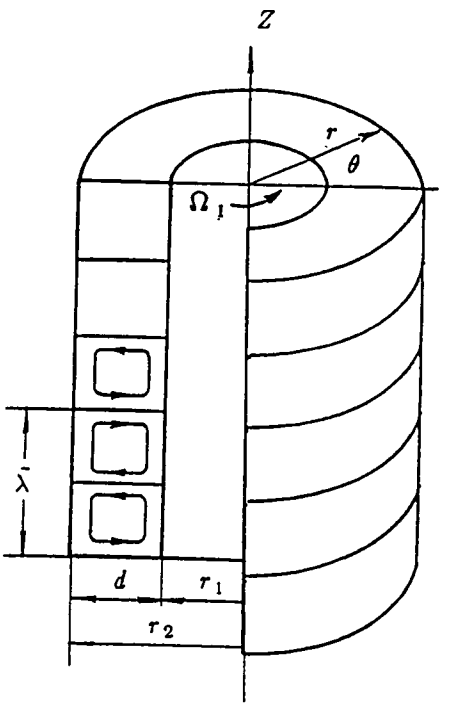

Fig.1.1. Sketch of Taylor vortex flow

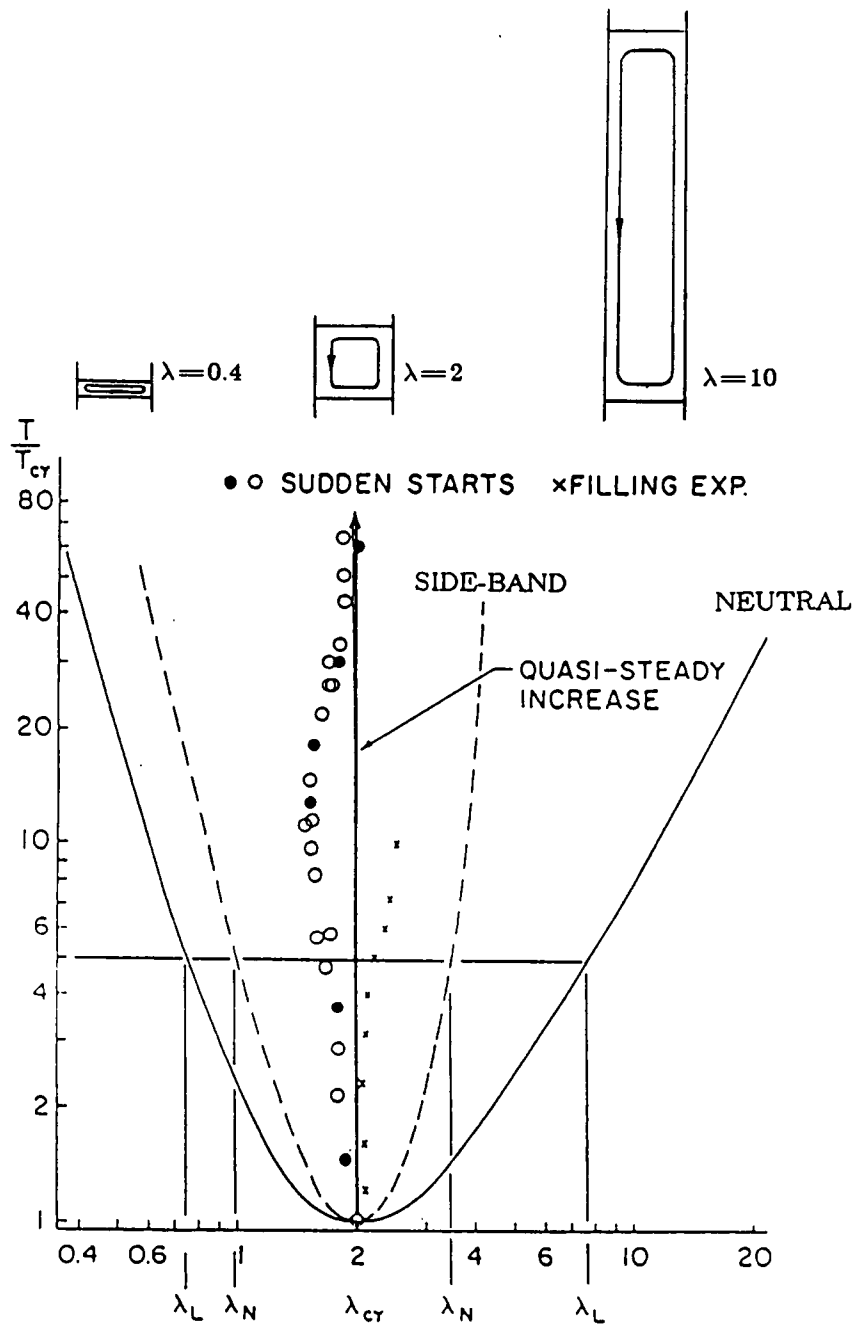

Fig.1.2. Experimental results by Burkhalter & Koschmieder [4]

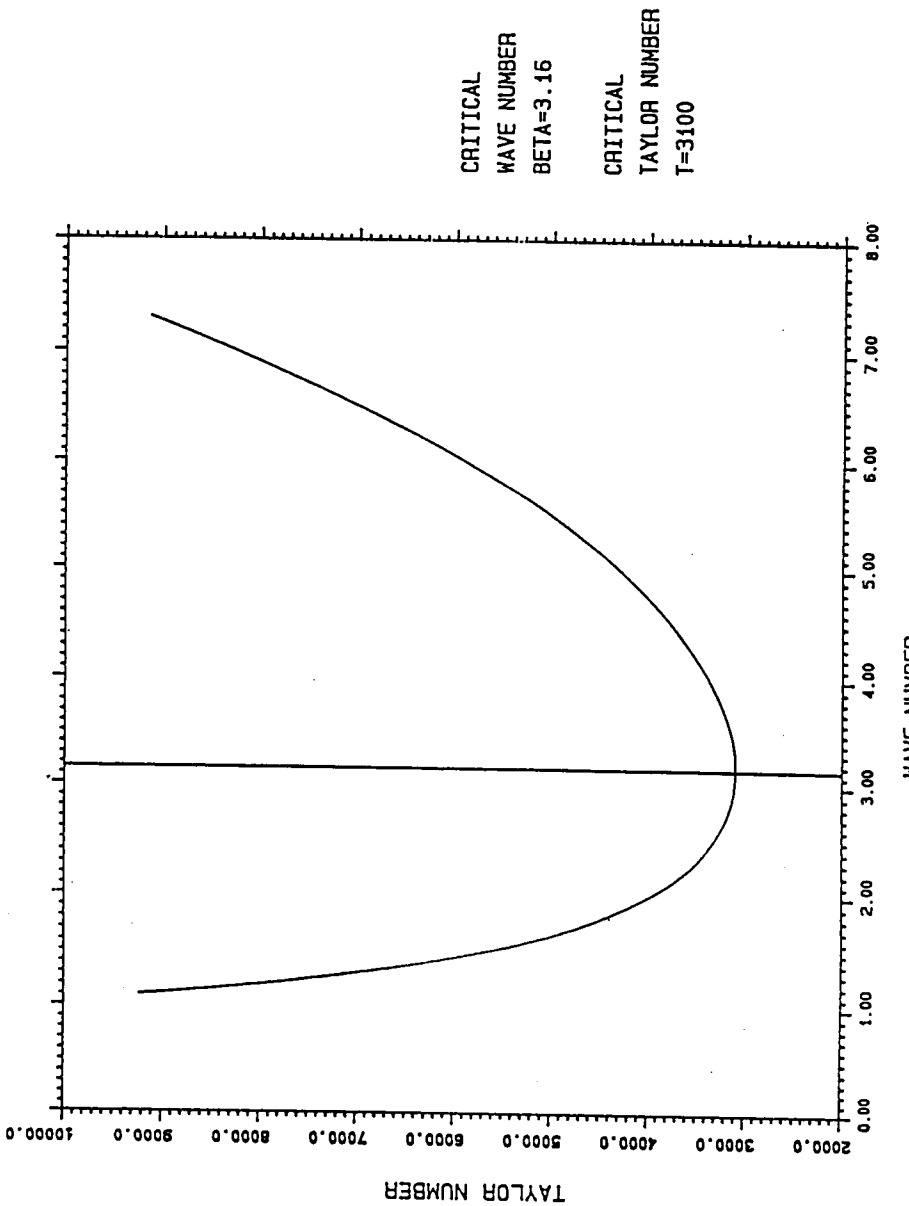

Fig.2.1. Neutral curve for wide gap case (η=0.5)

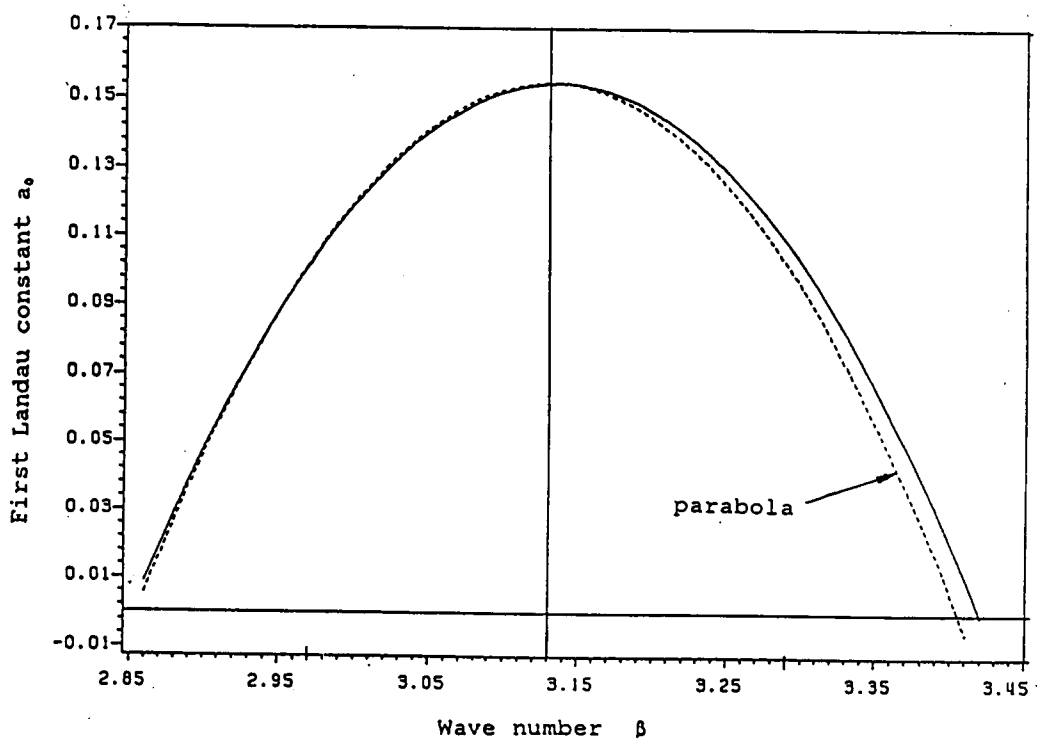

Fig.2.2. Linear growth rate a_0 (first Landau constant) at $T=1715$ for small gap case ($\eta=0.9524$ i.e., $\delta=0.05$). Note that $T_{cr}=1695$ and $\beta_{cr}=3.13$

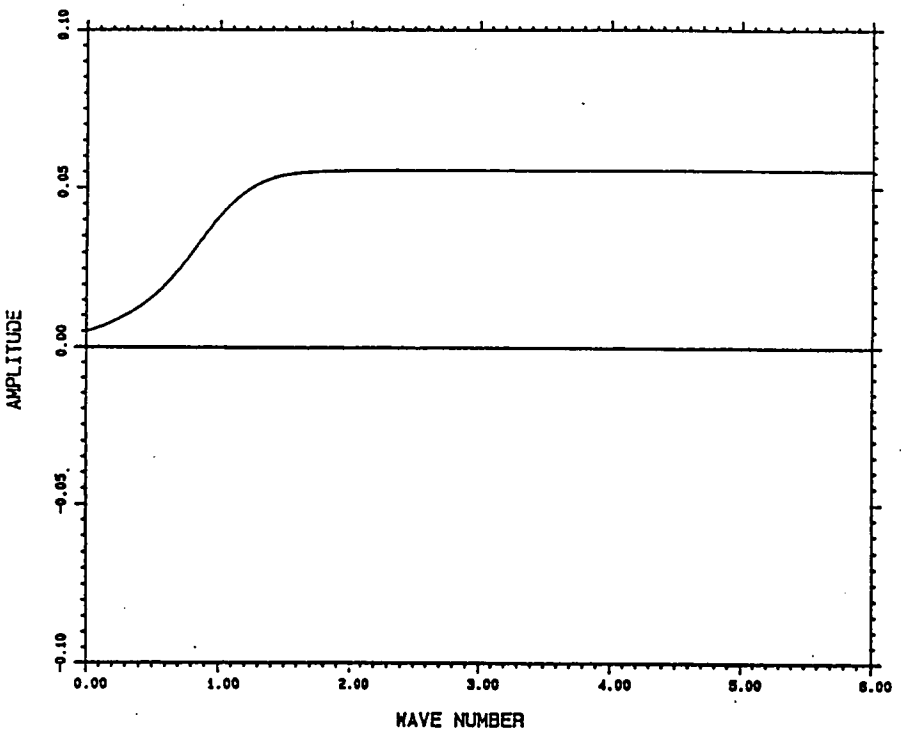

(a)

WAVE NUMBER: 3.3

NOTE:
THE FIGURE SHOWS
0.5*AMPLITUDE

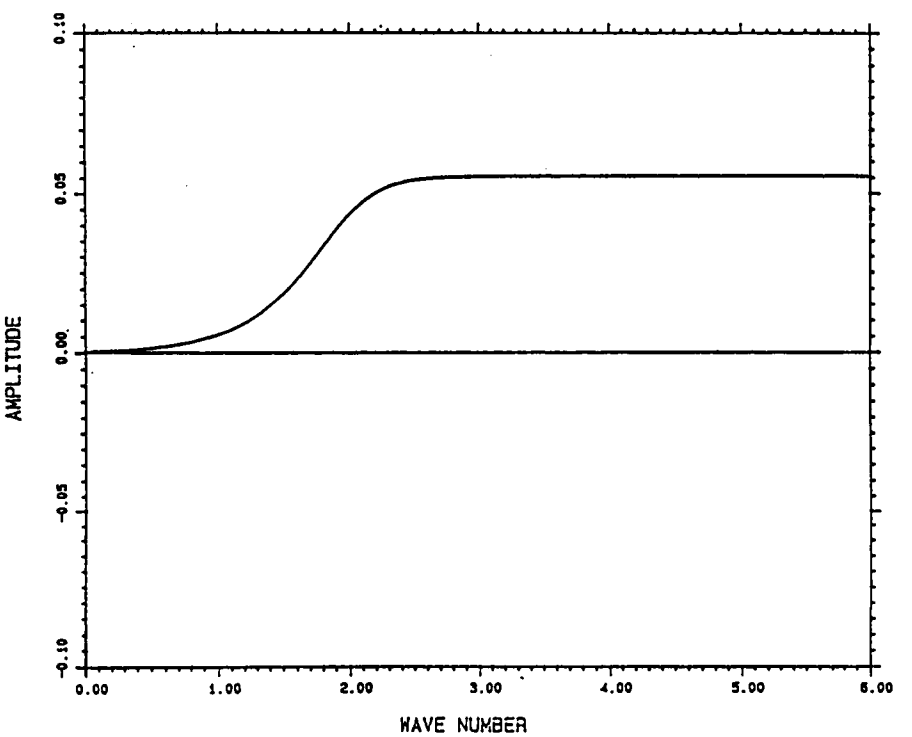

(b)

WAVE NUMBER: 3.3

NOTE:
THE FIGURE SHOWS
0.5*AMPLITUDE

Fig.3.1. Evolution of amplitude $0.5*A(\tau)$ at $\beta=3.3$ and $T=3675$ for $\eta=0.5$ obtained from 9th order single mode method
(a). $A(0)=0.01$ (b). $A(0)=0.001$

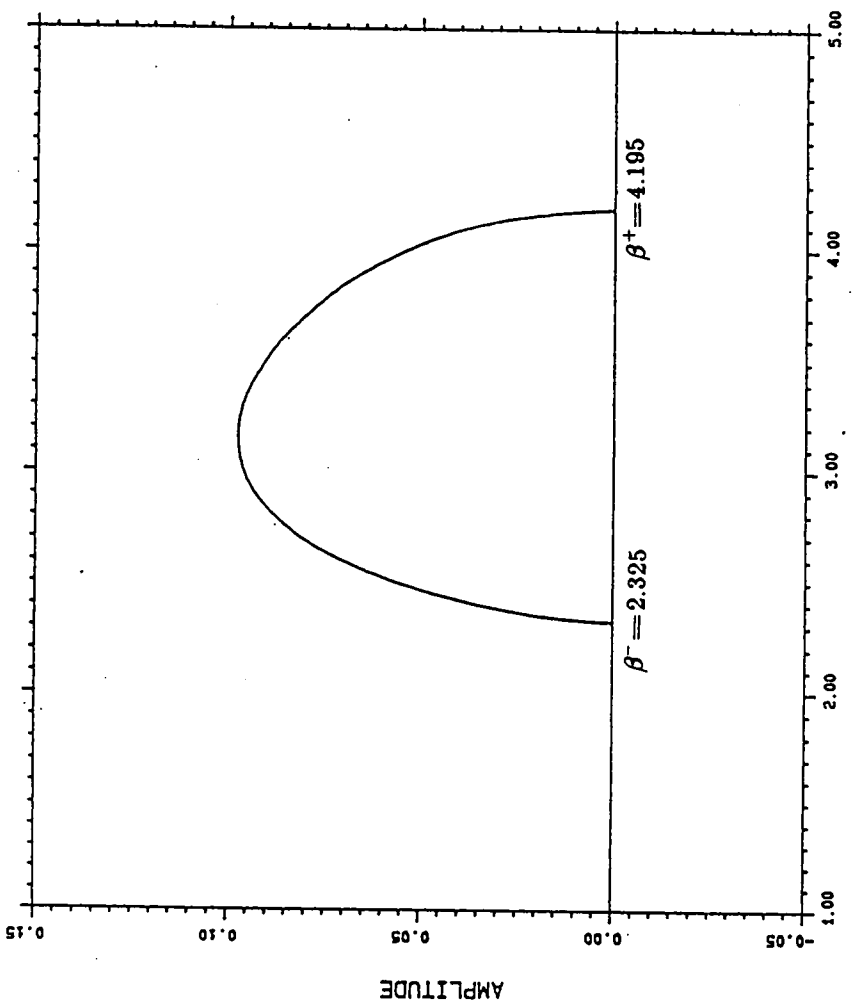

Fig.3.2. Steady states at $T=3500$ for $\eta=0.5$ obtained from 9th order single mode method

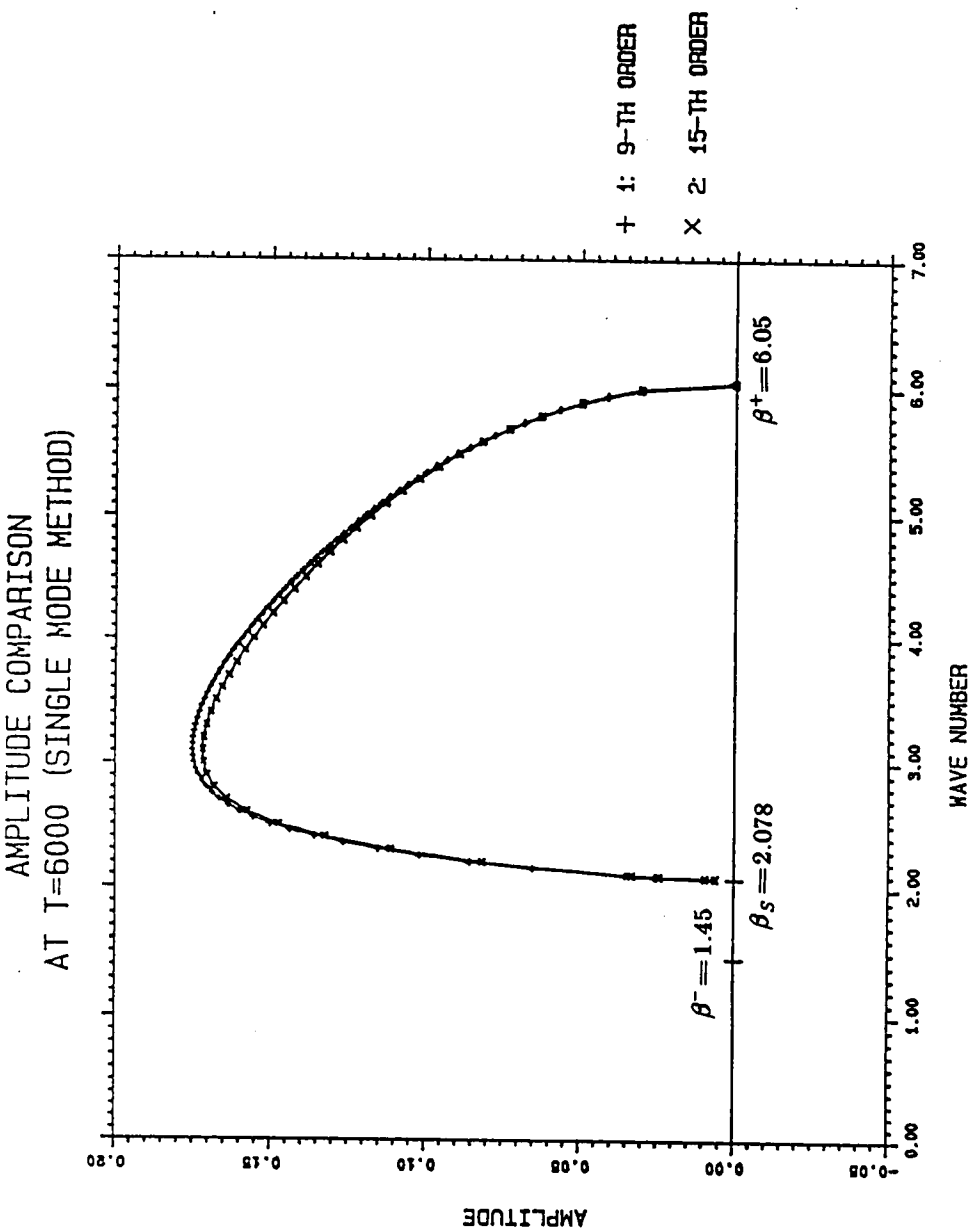

Fig.3.3 Steady states at $T=6000$ for $\eta=0.5$ obtained from 9th and 15th order single mode method.

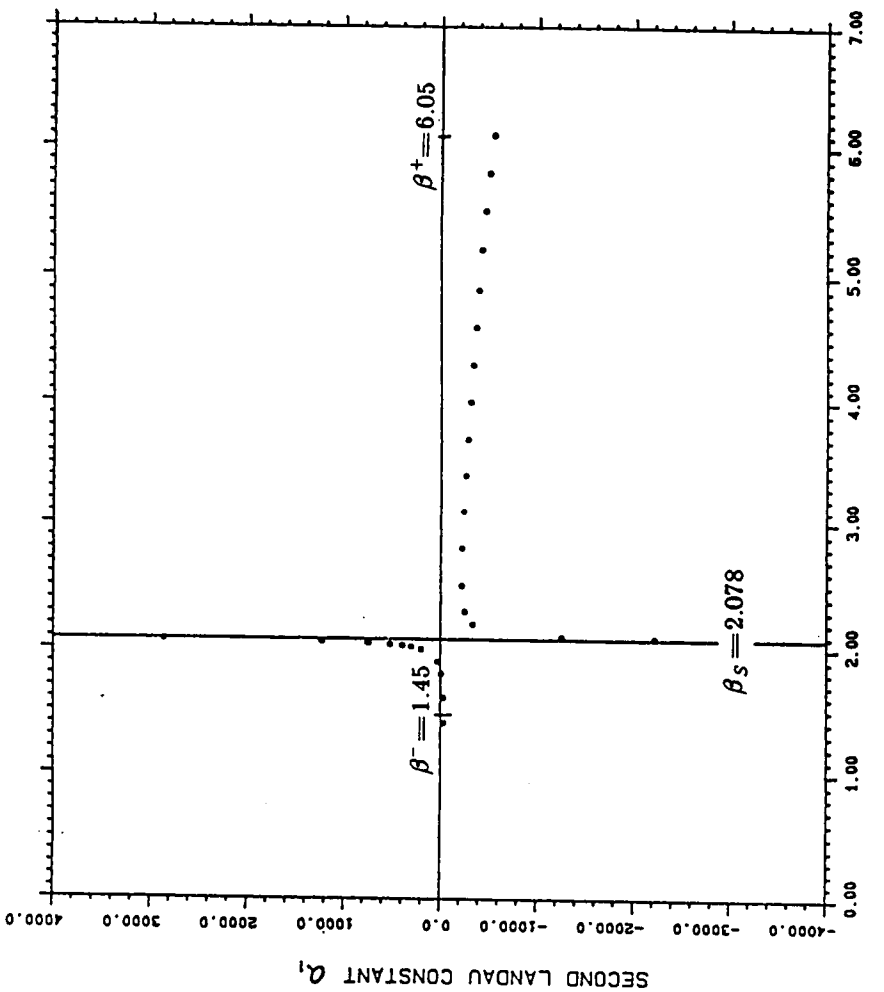

Fig.3.4. Singularity of second Landau constant a_1 at $T=6000$ for $\eta=0.5$

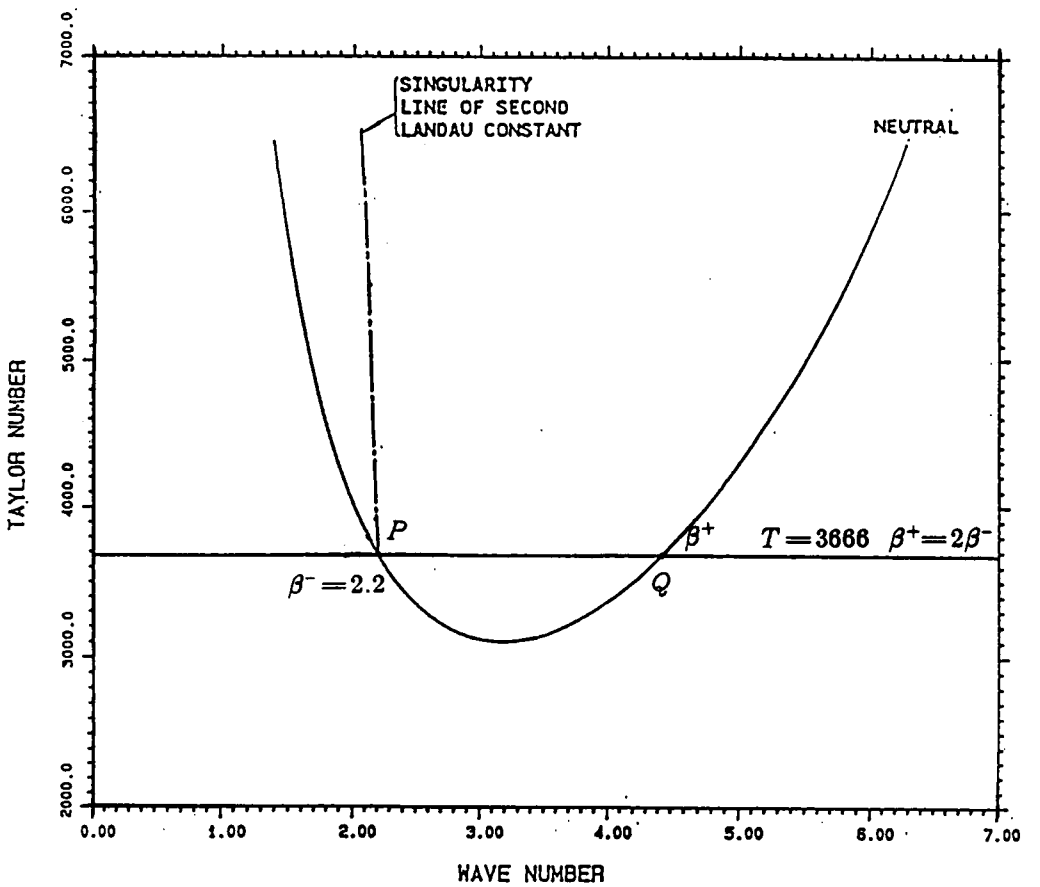

Fig.3.5. Singularity line for $\eta=0.5$

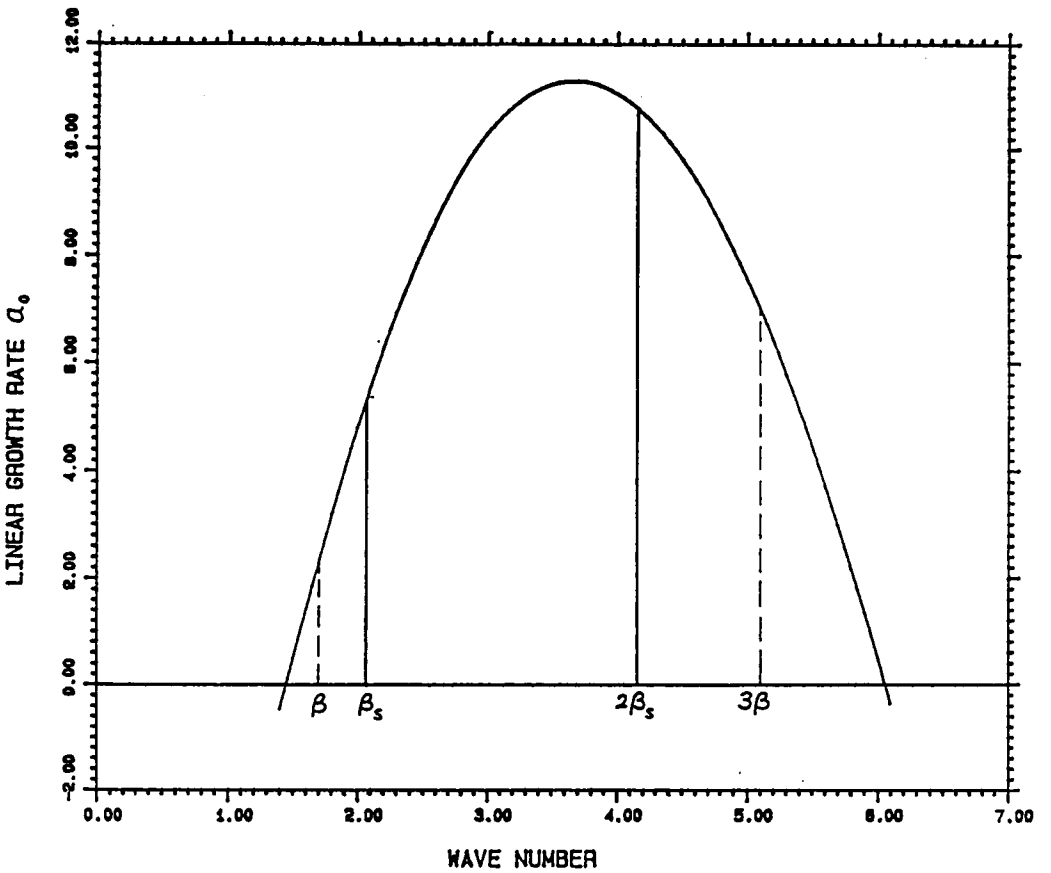

Fig.3.6. Linear growth rate a_0 at $T=6000$ for $\eta=0.5$ Note that a_0 at $2\beta_S$ is twice that at β_S and a_0 at 3β is three times that at β.

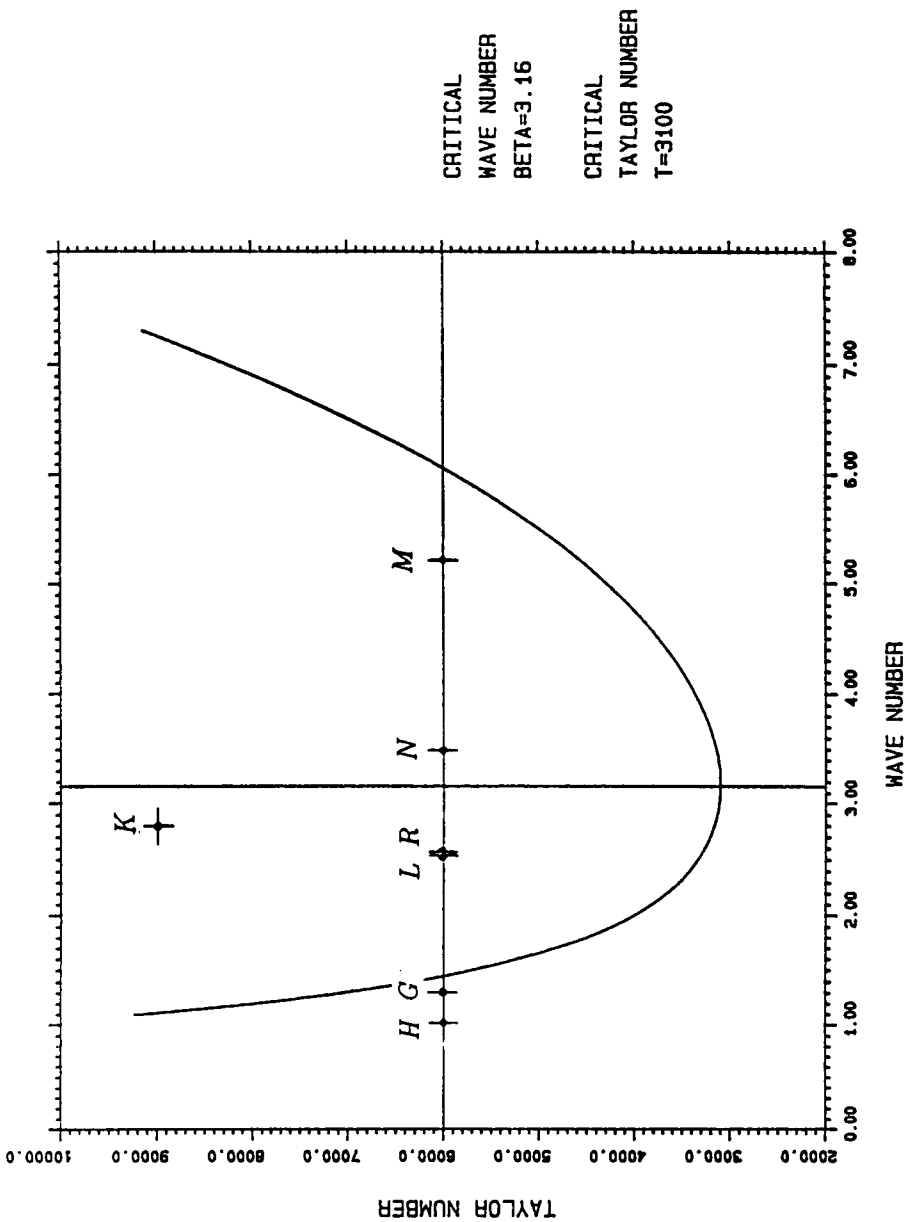

Fig.5.1. The points whose evolution will be presented in Sect. 5.1. for η=0.5

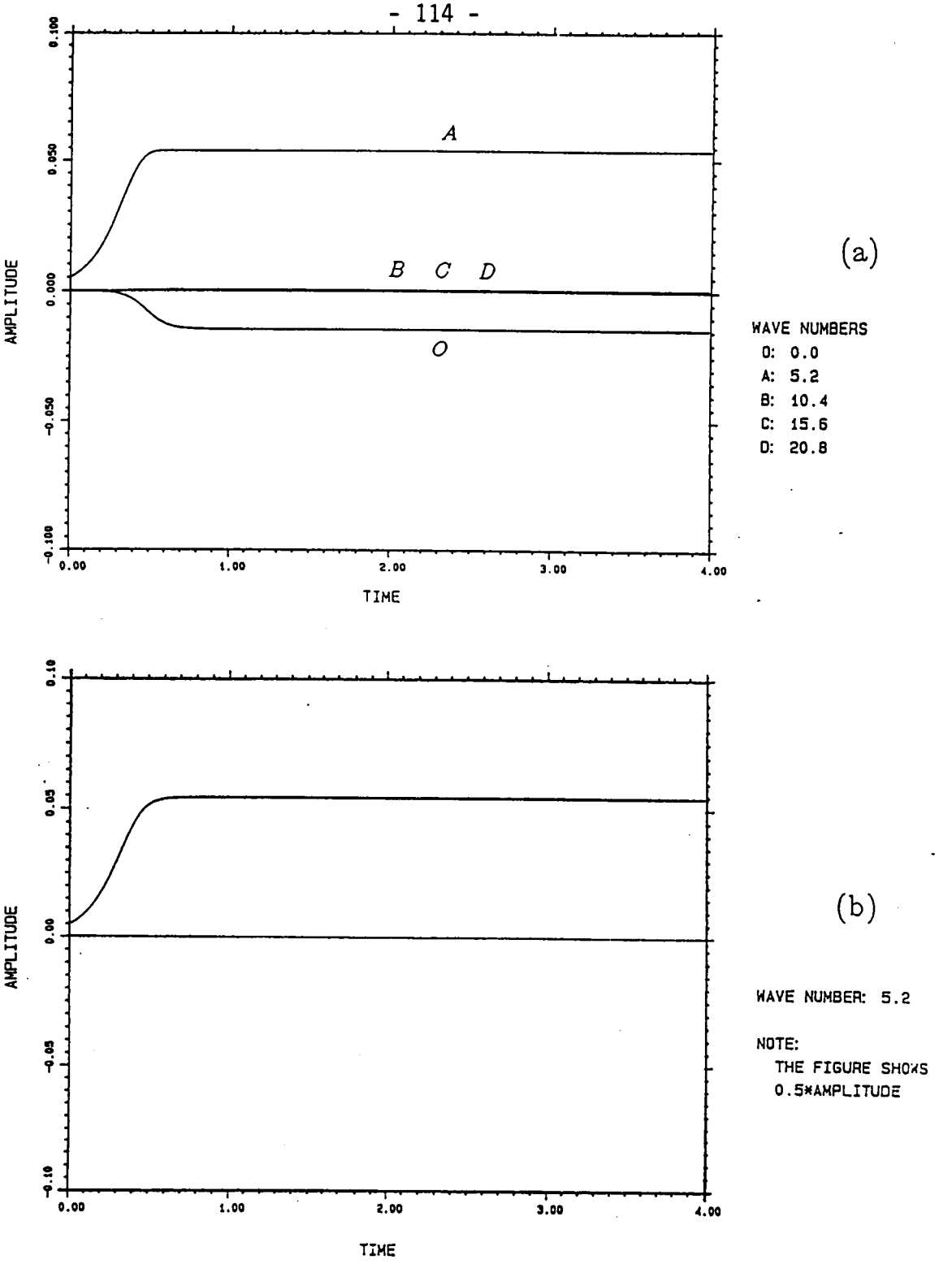

Fig.5.2. Evolution of amplitudes at β=5.2 and T=6000 for η=0.5
(a). numerical method (9 harmonics)
(b). single mode method (9th order)

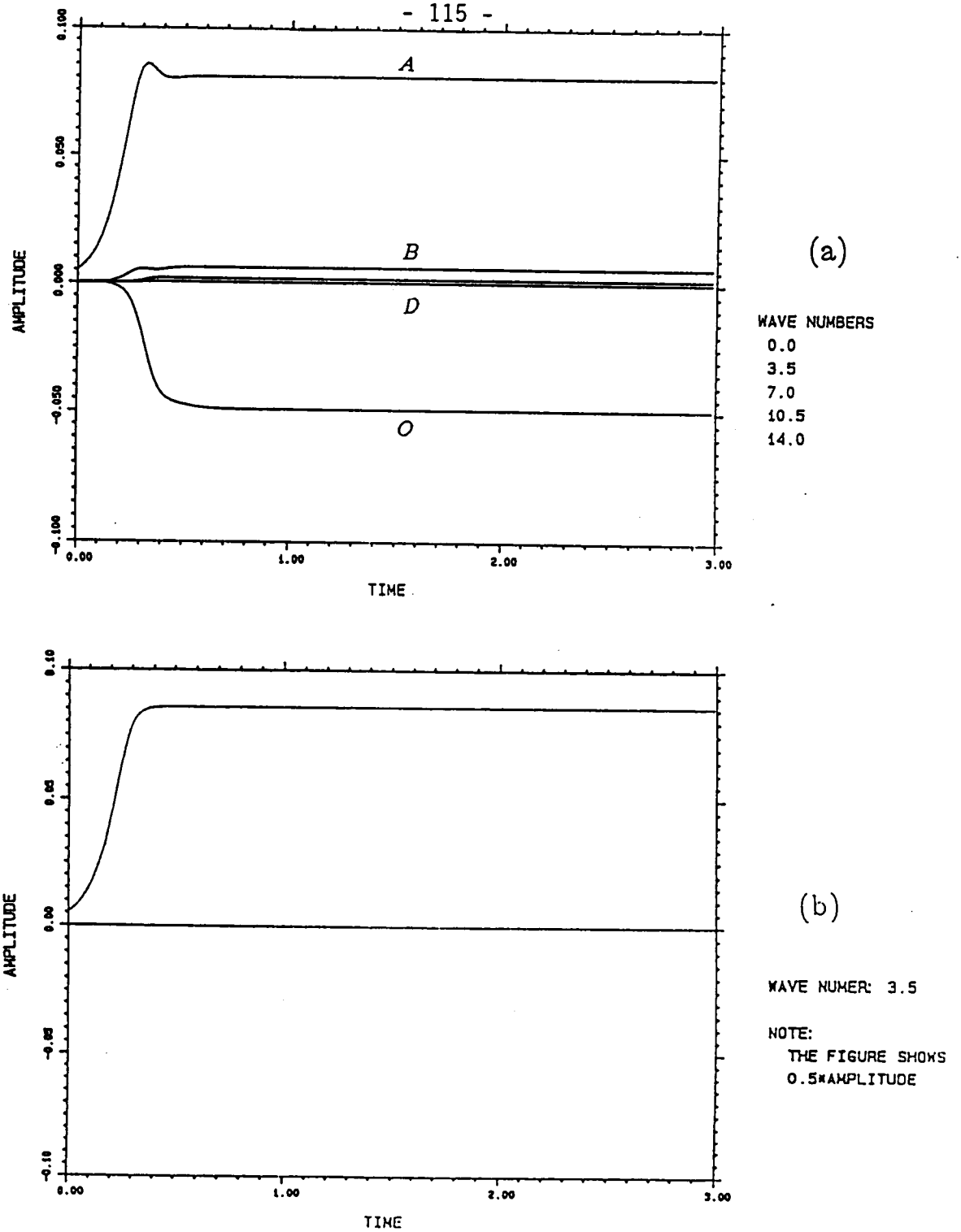

Fig.5.3. Evolution of amplitudes at β=3.5 and T=6000 for η=0.5
(a). numerical method (9 harmonics)
(b). single mode method (9th order)

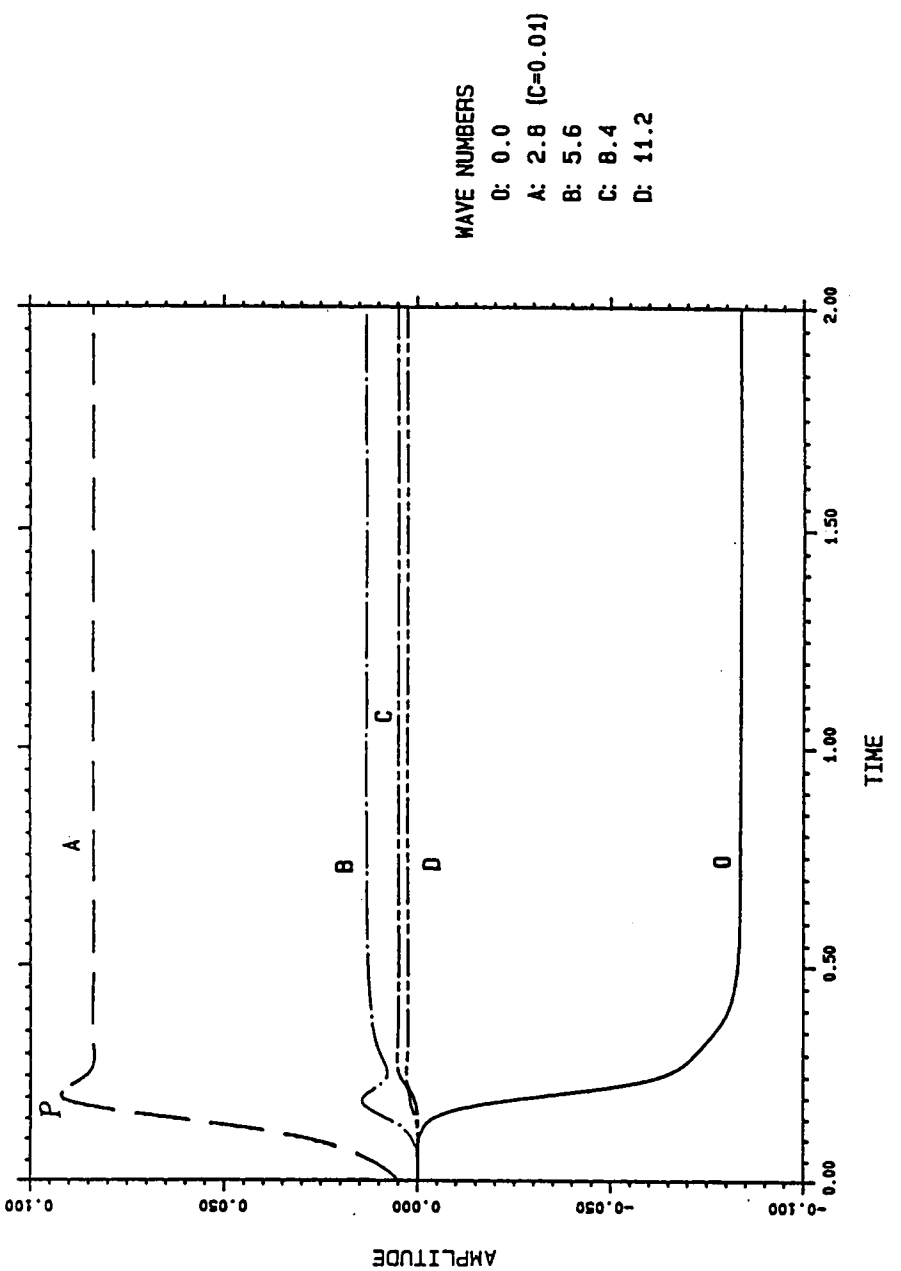

Fig.5.4. Evolution of amplitudes at β=2.8 and T=9000 for η=0.5 obtained by numerical method (9 harmonics);

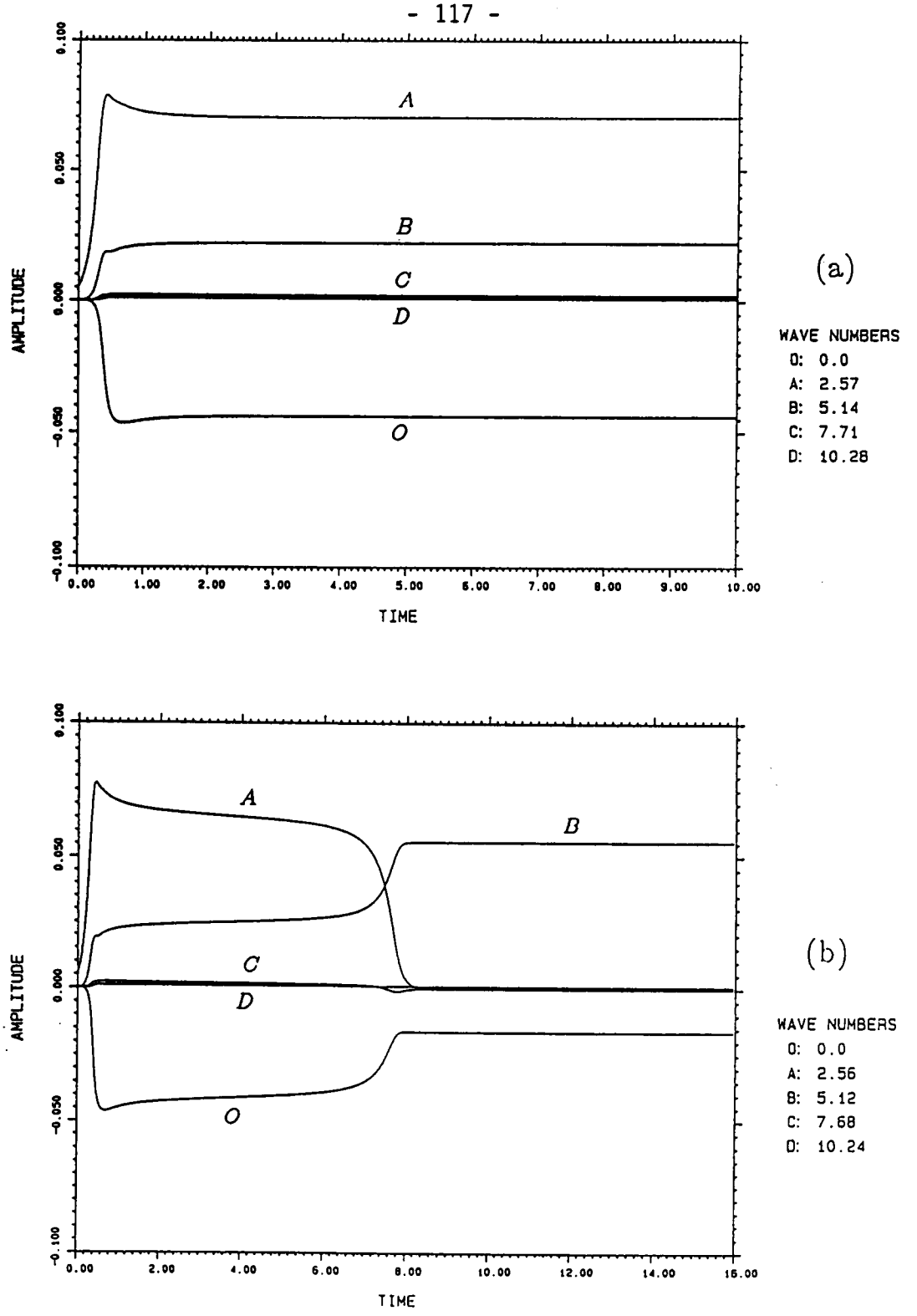

Fig.5.5. Evolution of amplitudes at $T=6000$ for $\eta=0.5$ obtained by numerical method (9 harmonics);

(a). $\beta=2.57$ (b). $\beta=2.56$

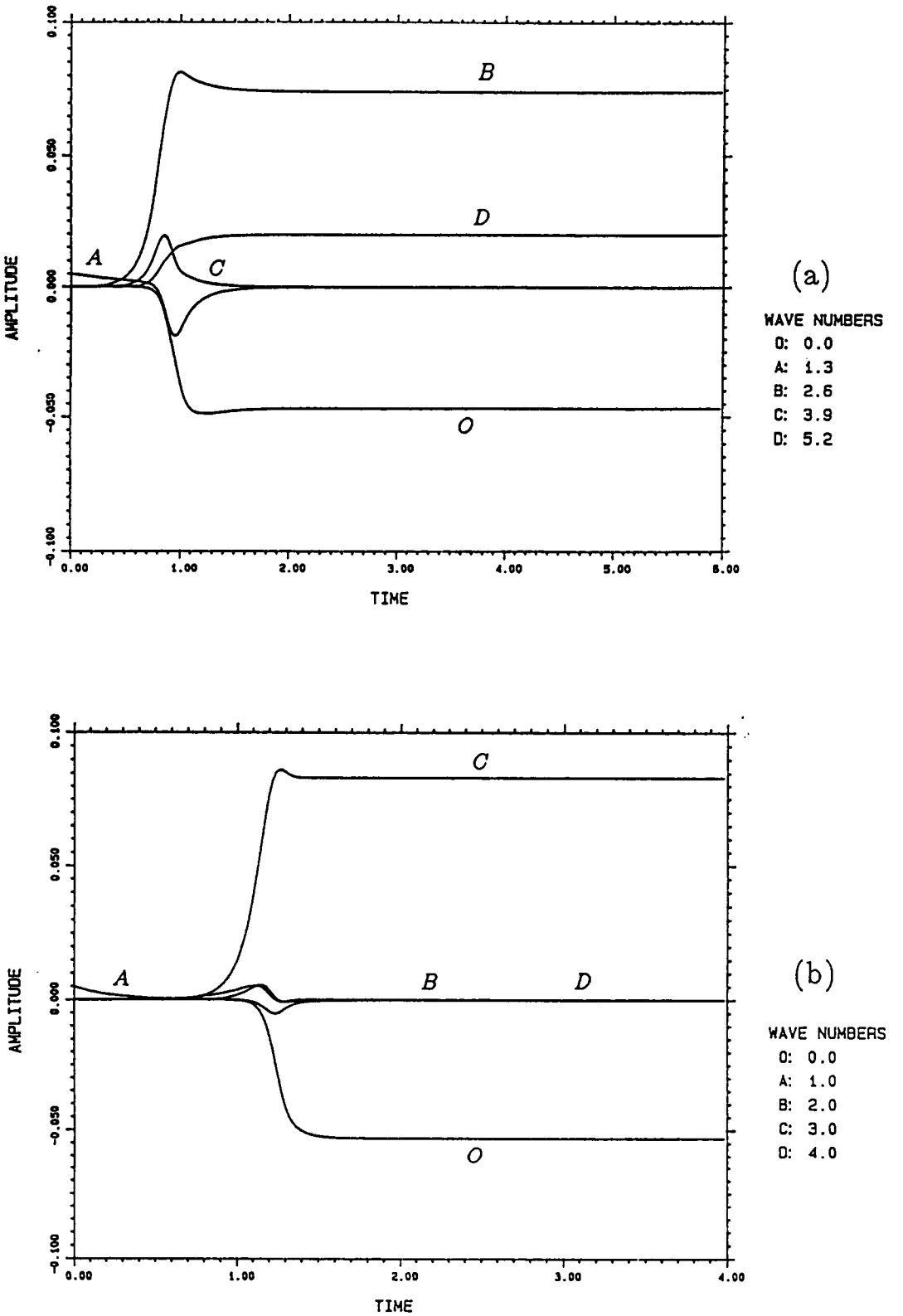

Fig.5.6. Evolution of amplitudes at $T=6000$ for $\eta=0.5$ obtained by numerical method (9 harmonics)
(a). $\beta=1.30$ (b). $\beta=1.00$

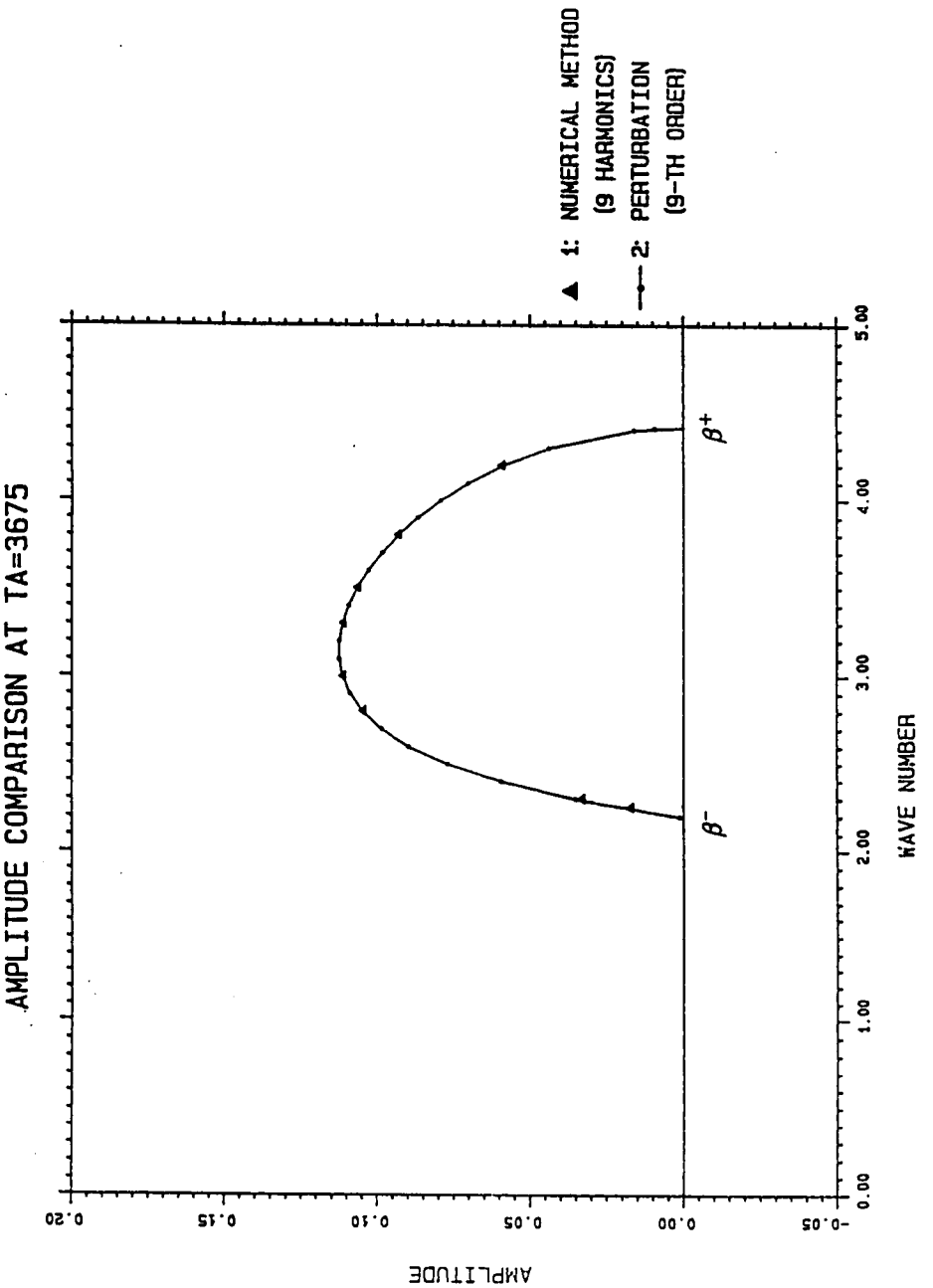

Fig.5.7. Steady state amplitudes of $2V_1$ and A at $T=3675$ for $\eta=0.5$

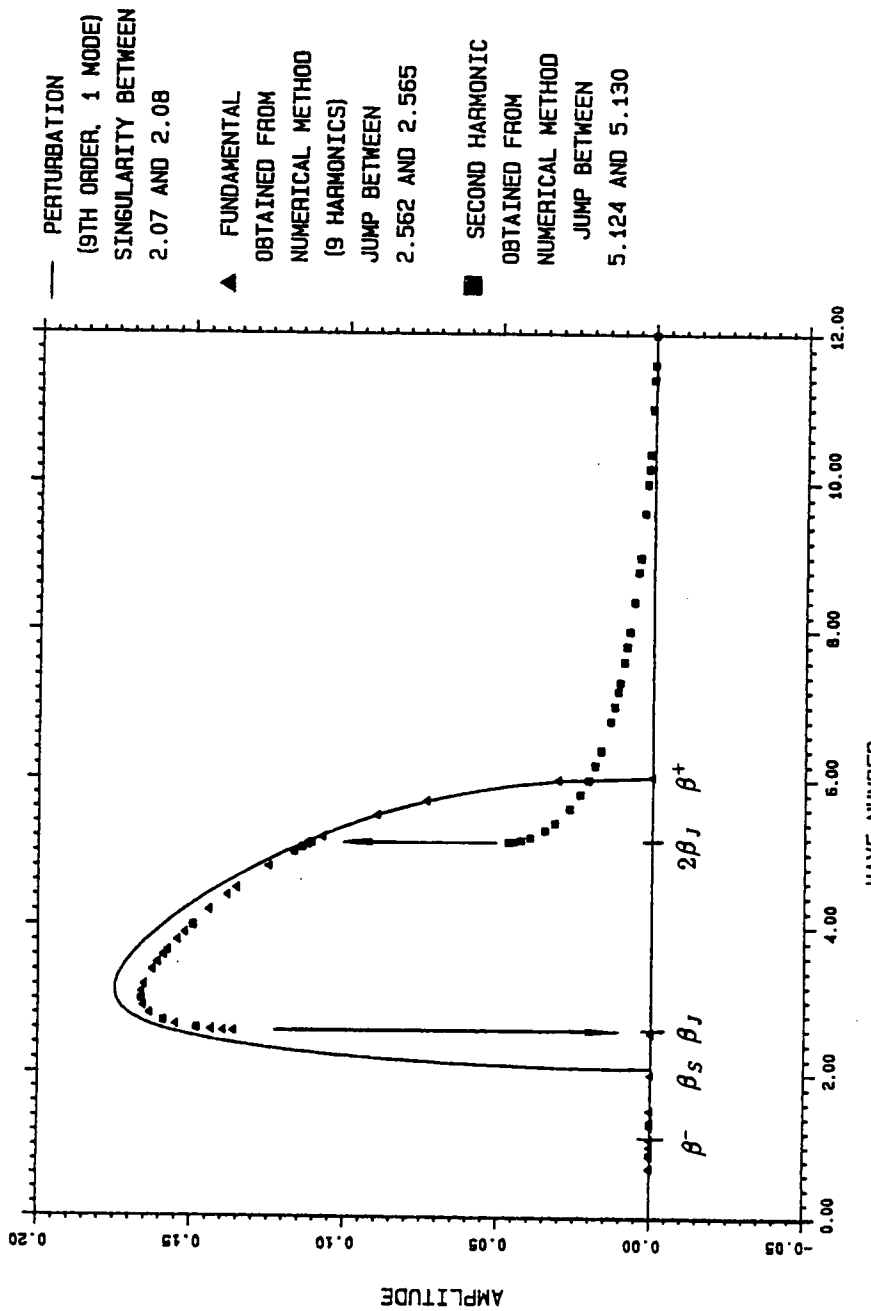

Fig.5.8. Steady state amplitudes of $2V_1$, $2V_2$ and A at T=6000 for η=0.5. Note that V_1 and V_2 are obtained from numerical method (9 harmonics) while A is from single mode perturbation method (9th order)

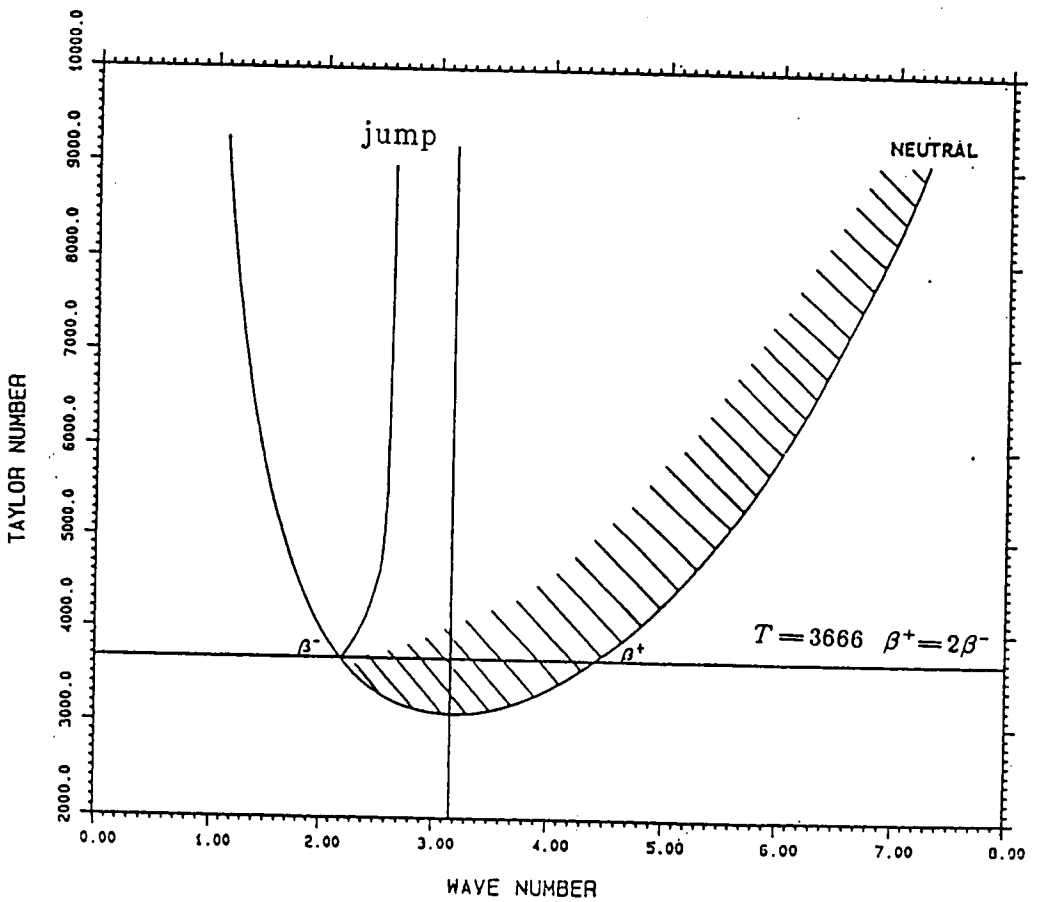

Fig.5.9. The line of occurrence of jump and the shaded domain where the single-mode method gives good results (for $\eta=0.5$)

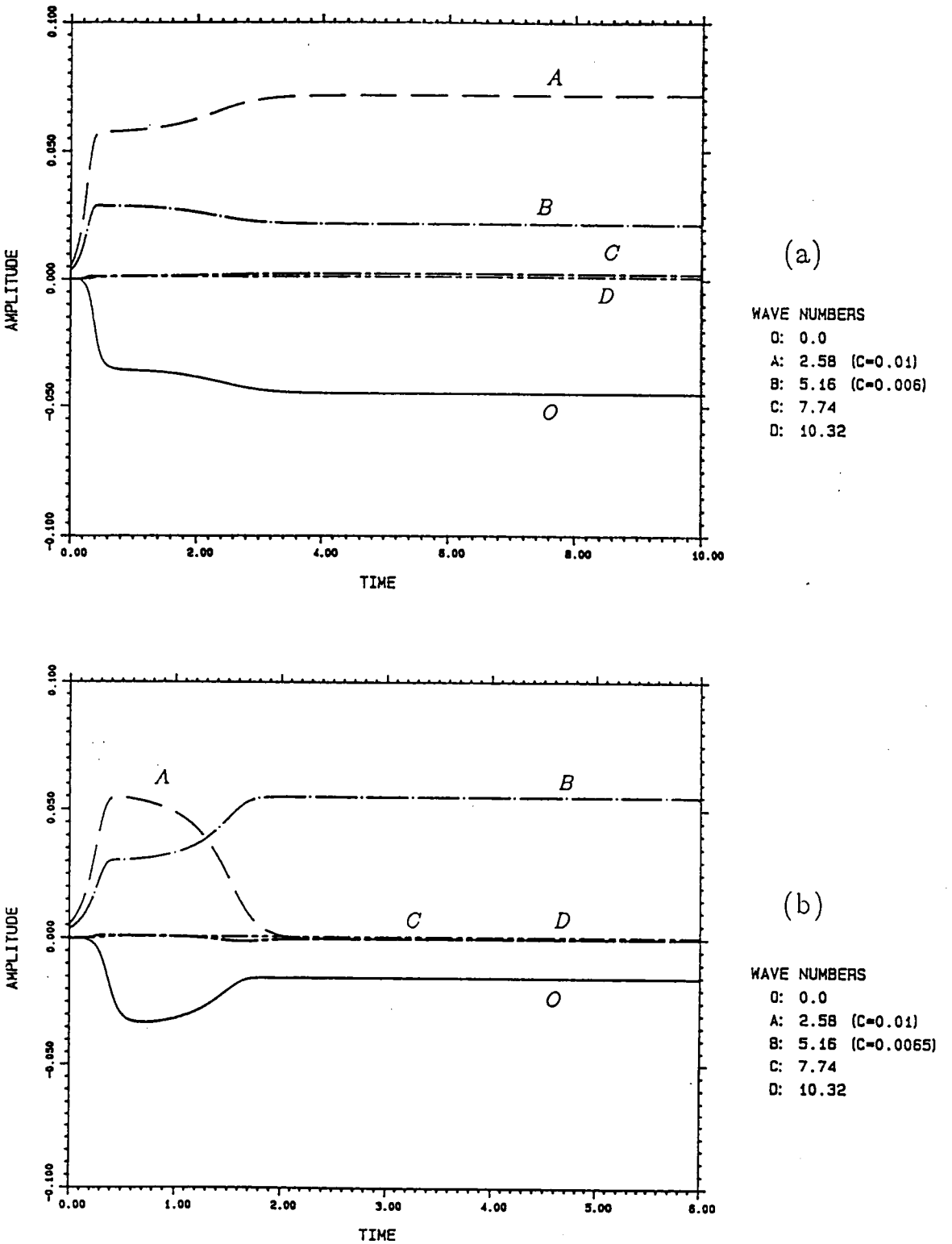

Fig.5.10. Interaction of two waves (β=2.58 and β=5.16) at T=6000 for η=0.5 obtained from numerical method

(a). $V_1(0)$=0.005 $V_2(0)$=0.003

(b). $V_1(0)$=0.005 $V_2(0)$=0.00325

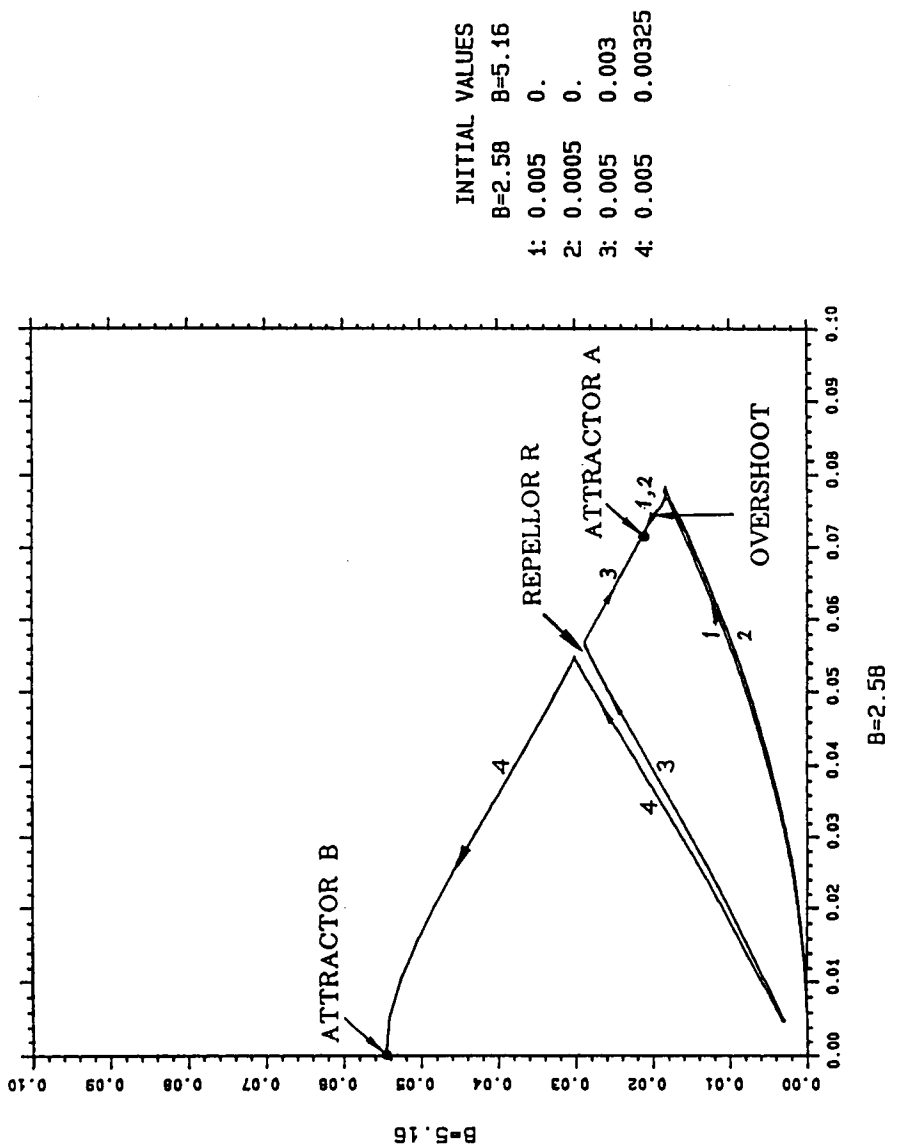

Fig.5.11. Amplitude diagram of interaction of two waves (β=2.58 and β=5.16) at T=6000 for η=0.5

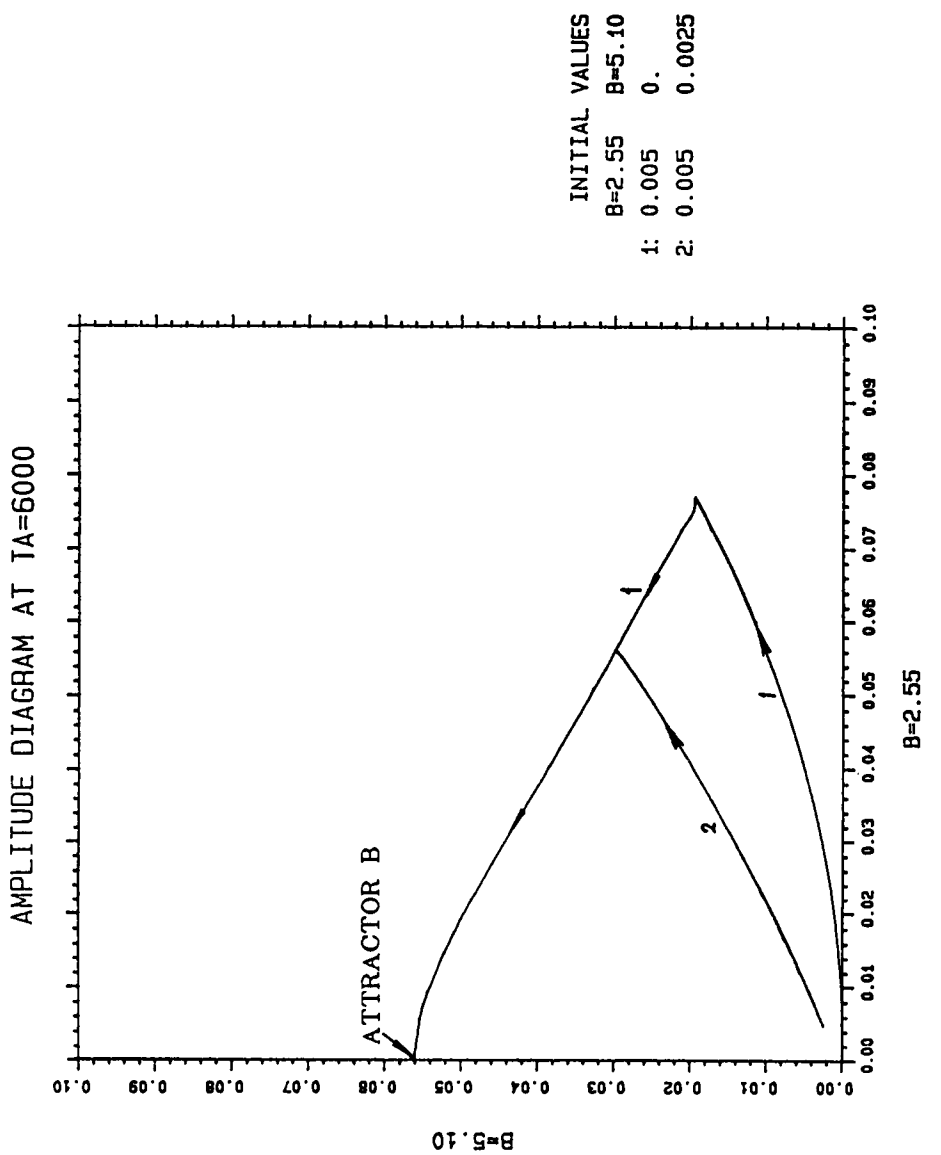

Fig.5.12. Amplitude diagram of interaction of two waves (β=2.55 and β=5.10) at T=6000 for η=0.5

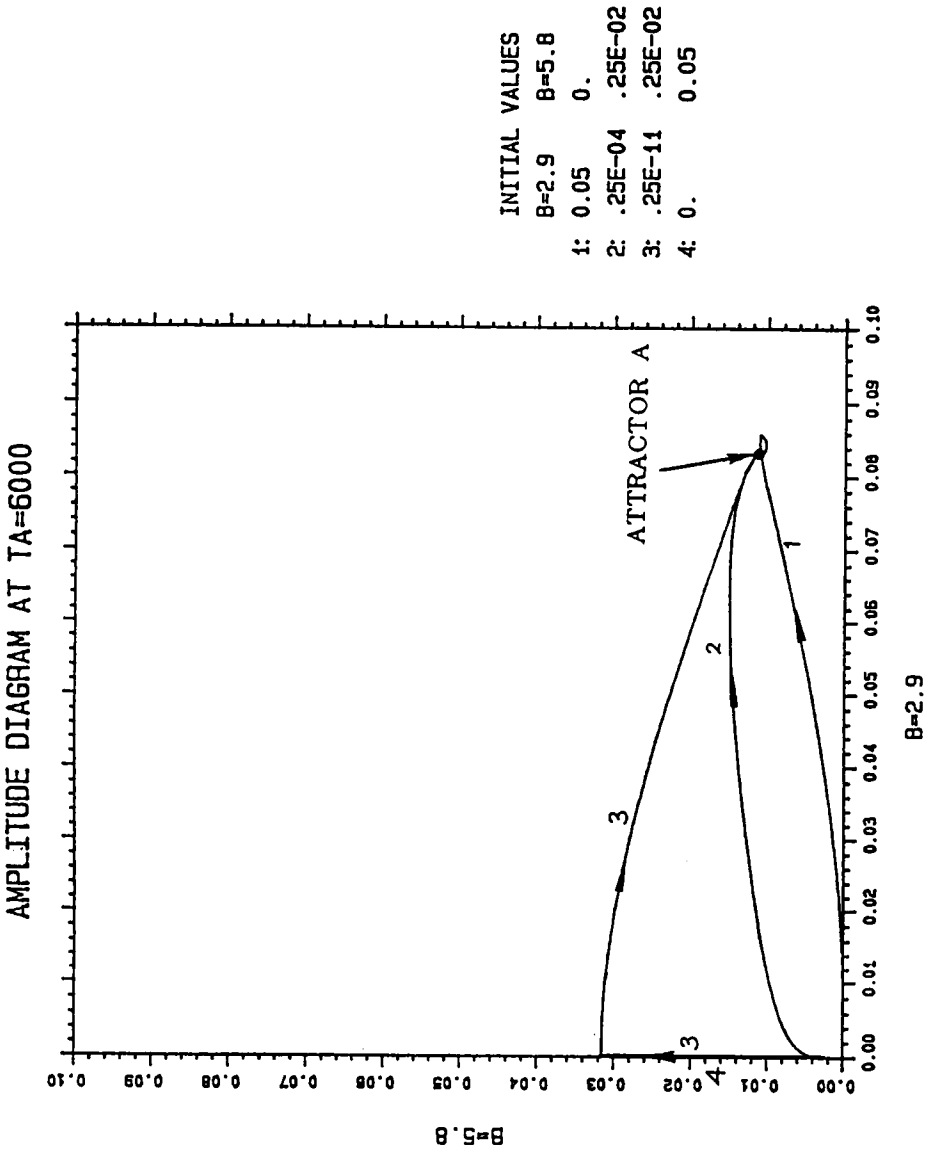

Fig.5.13. Amplitude diagram of interaction of two waves (β=2.90 and β=5.80) at T=6000 for η=0.5

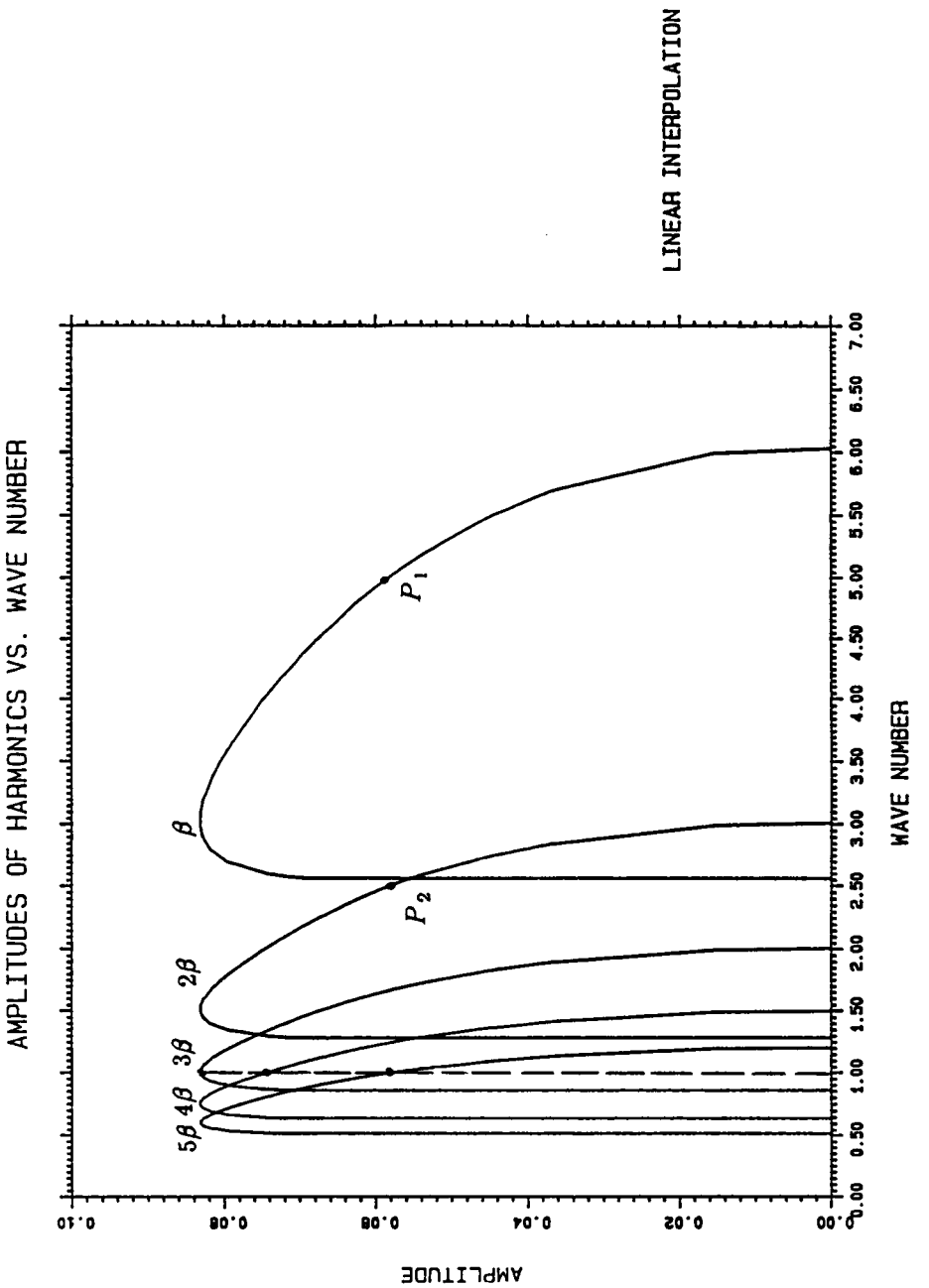

Fig.5.14. Multiple solutions for small wave number ($T=6000$, $\eta=0.5$)

Table 5.1 Comparison of T_k
at β=2.200 and β=2.199

T	β=2.200	β=2.199
T_0	3.6606E+03	3.6620E+03
T_1	1.5803E+07	-1.2589E+07
T_2	1.7791E+14	-9.0773E+13
T_3	4.0090E+21	-1.3078E+21
T_4	1.1292E+29	-2.3552E+28
T_5	3.5623E+36	-4.7507E+35
T_6	1.2041E+44	-1.0267E+43
T_7	4.2636E+51	-2.3245E+50
T_8	1.5612E+59	-5.4421E+57
T_9	5.8632E+66	-1.3068E+65
T_{10}	2.2460E+74	-3.2006E+72

Table 5.2 Singularities of T_1, T_2, T_3, and T_4

β	T_1	T_2	T_3	T_4
2.600	4.1147E+04	1.0307E+06	2.5839E+07	8.5481E+08
2.500	4.6674E+04	1.5356E+06	5.0334E+07	2.4564E+09
2.400	5.8121E+04	3.3048E+06	2.2847E+08	2.5241E+10
2.300	9.2857E+04	1.8350E+07	6.4457E+09	3.1694E+12
2.200	1.5803E+07	1.7791E+14	4.0090E+21	1.1292E+29
2.199	-1.2589E+07	-9.0773E+13	-1.3078E+21	-2.3553E+28
2.100	-4.7111E+04	-1.6322E+07	-6.2478E+09	-3.3040E+12
2.000	-1.1494E+04	-2.4322E+06	2.7813E+07	5.0745E+10

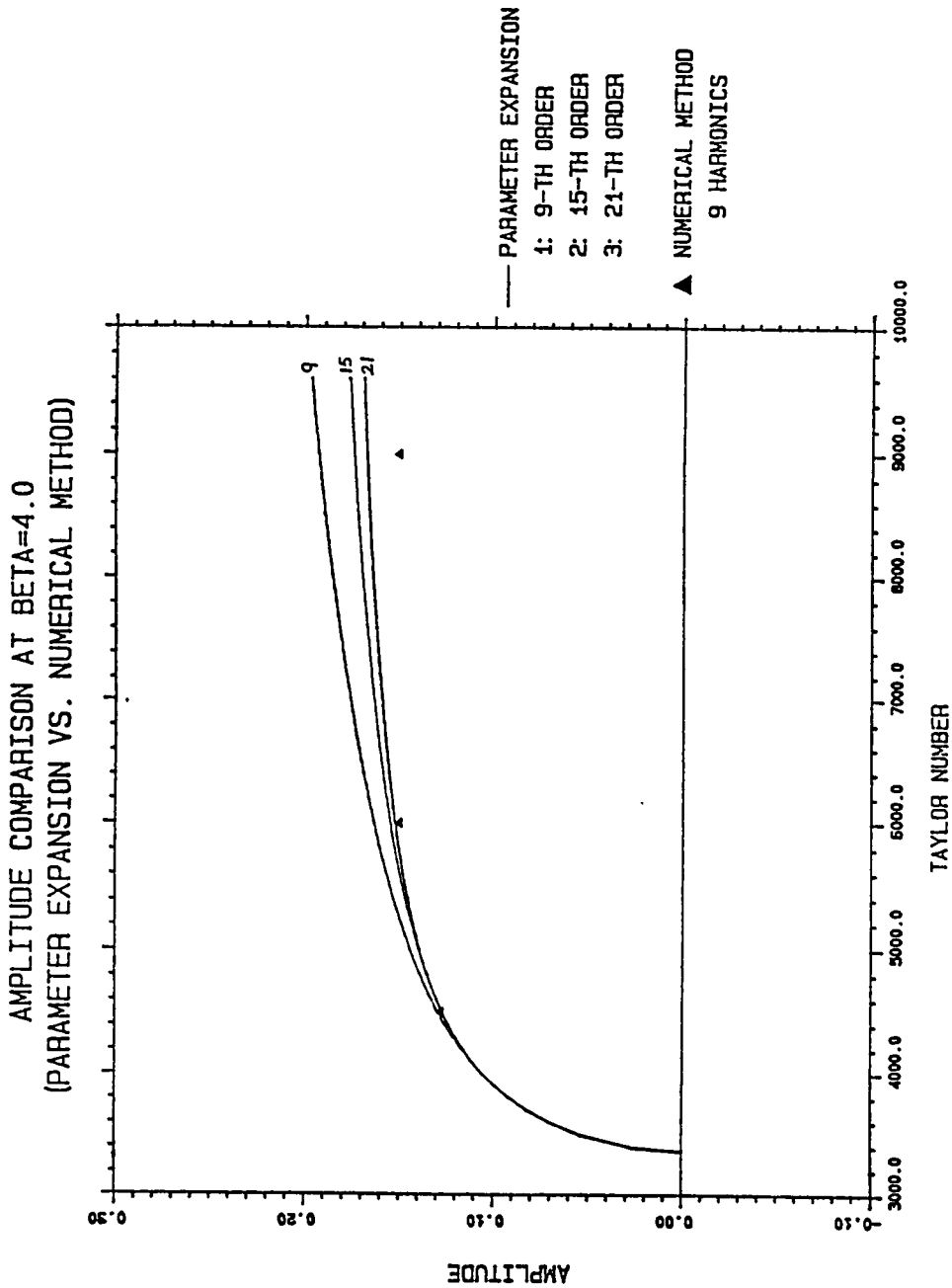

Fig.5.15. Amplitude comparison at β=4.0 between A (obtained from parameter expansion) and $2V_1$ (obtained from numerical method)

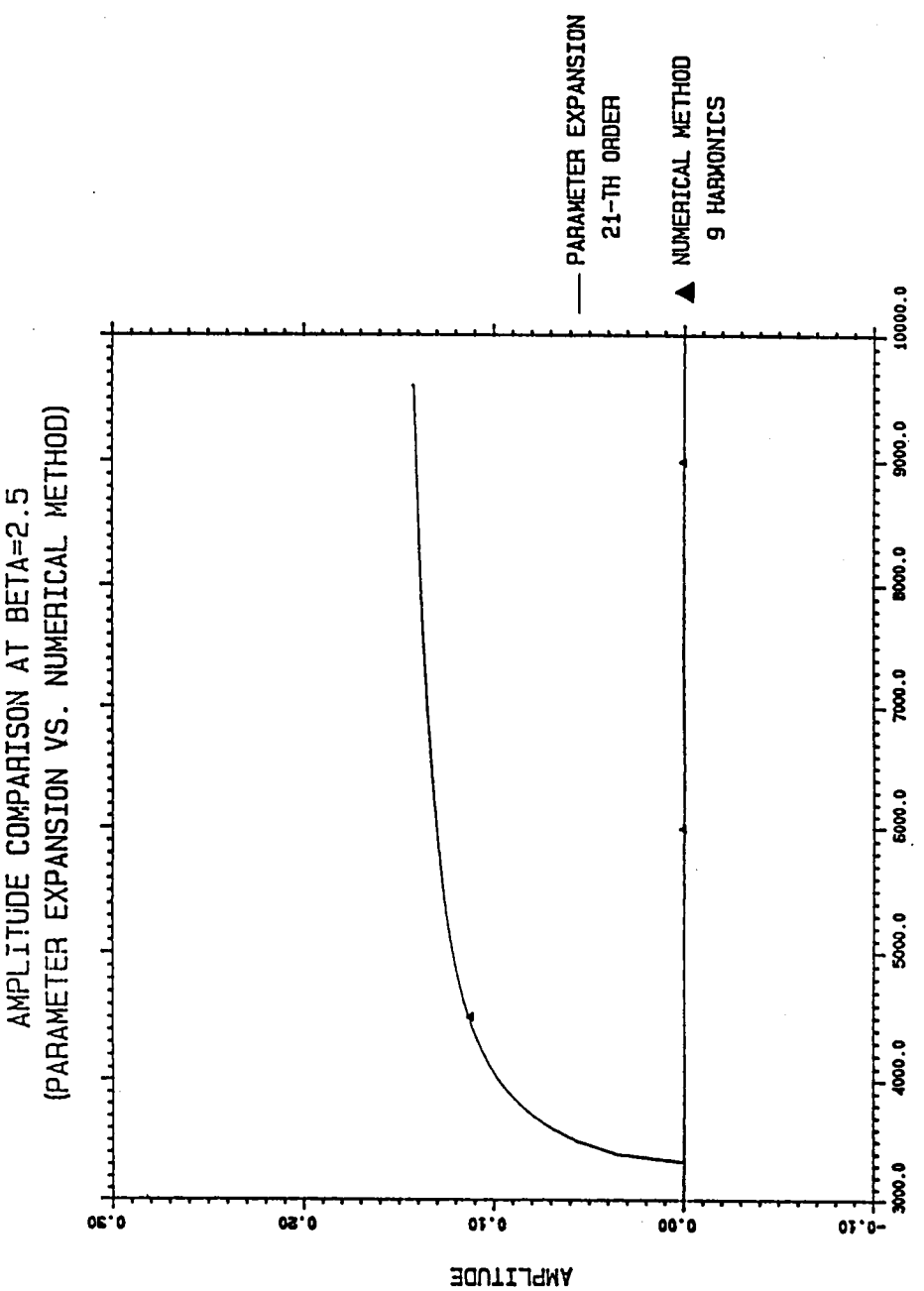

Fig.5.16. Amplitude comparison at β=2.5 between A (obtained from parameter expansion) and $2V_1$ (obtained from numerical method)

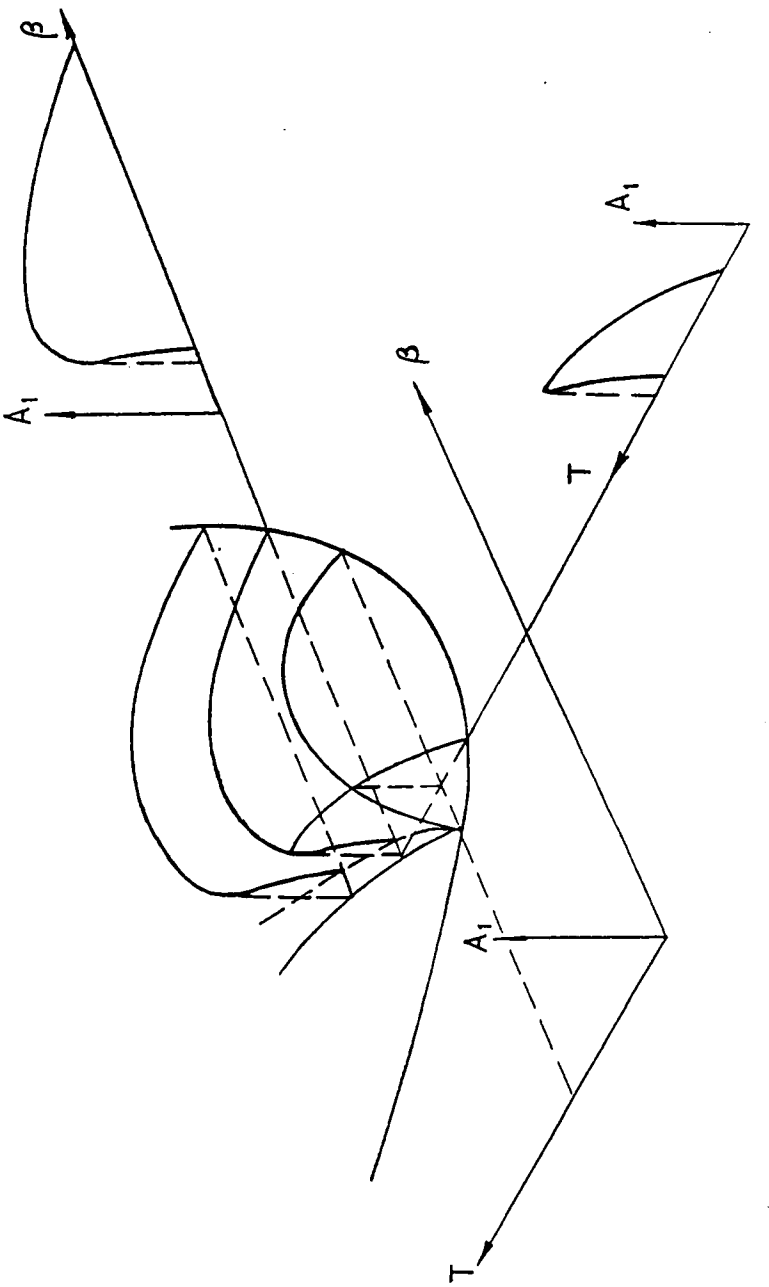

Fig.5.17. Sketch of A_1 for $\eta=0.5$

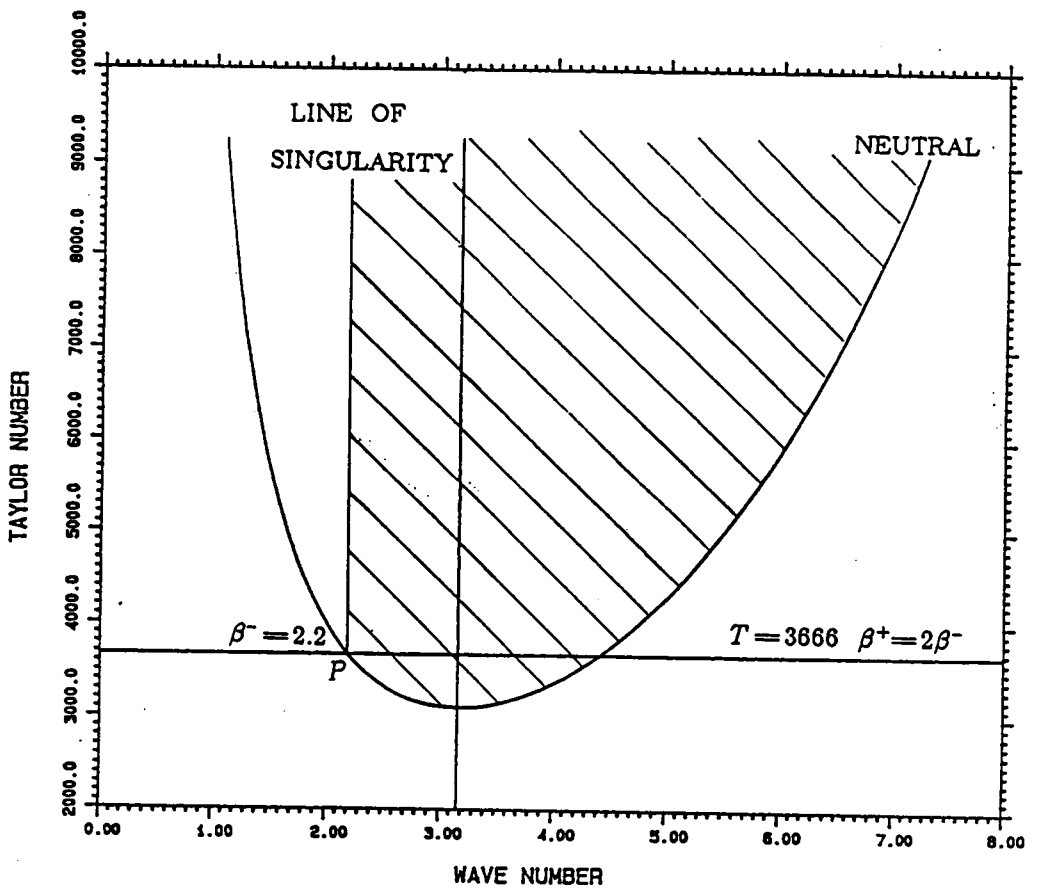

Fig.5.18. Stable and unstable regions of Couette flow (obtained from the parameter expansion method for η=0.5). Note that the shaded region is the unstable region.

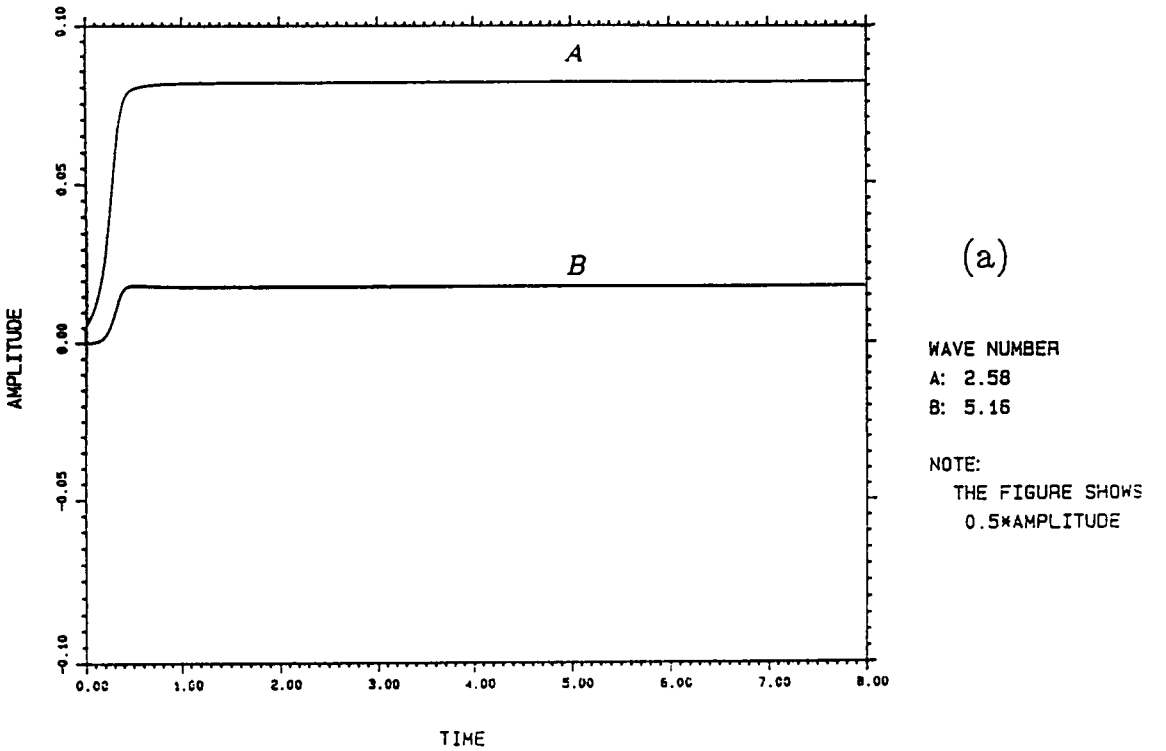

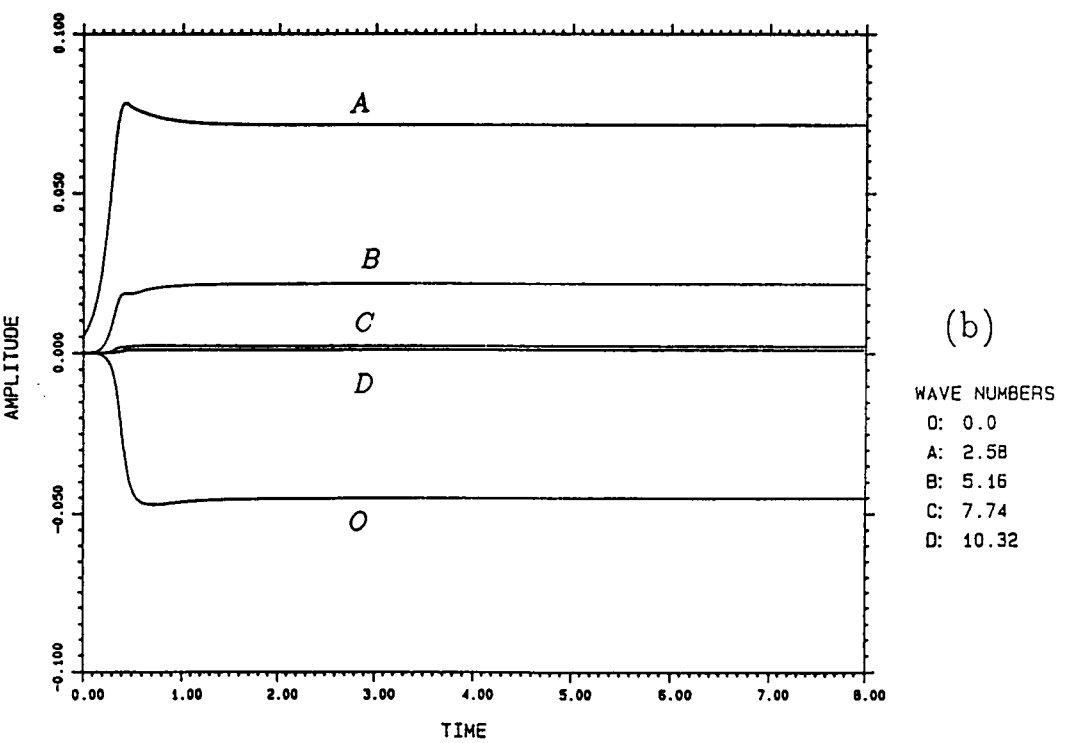

Fig.6.1. Evolution of amplitudes at $T=6000$ for $\eta=0.5$ ($\beta=2.58$, $\beta=5.16$)
(a). two mode perturbation method (9th order)
(b). numerical method (9 harmonics)

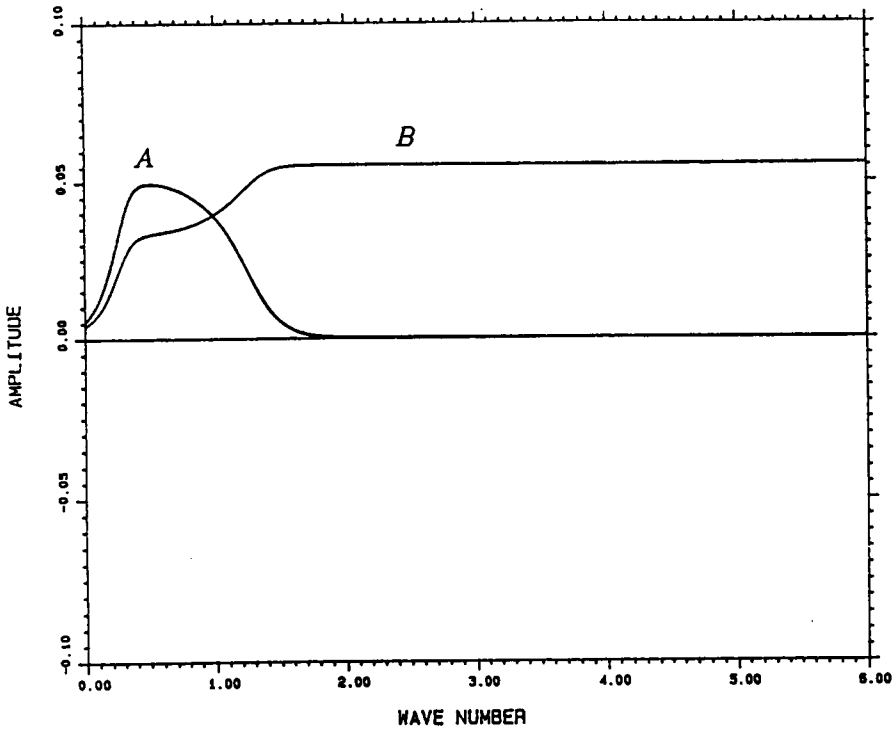

(a)

WAVE NUMBERS
A: 2.58 (AI=0.005)
B: 5.16 (BI=0.00375)

NOTE:
THE FIGURE SHOWS
0.5*AMPLITUDE

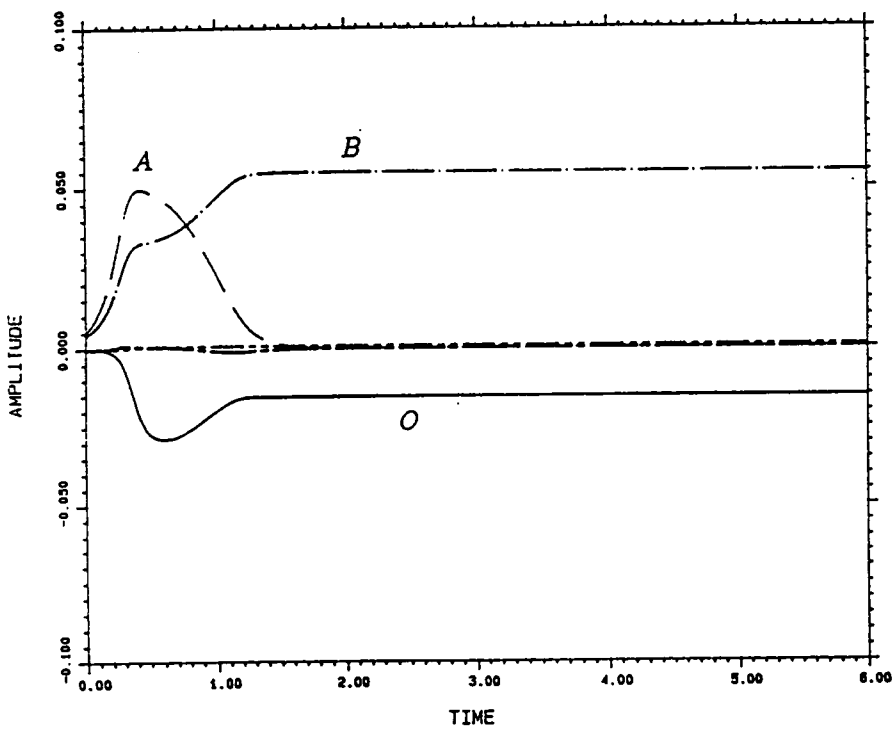

(b)

WAVE NUMBERS
O: 0.0
A: 2.58 (C=0.01)
B: 5.16 (C=0.0075)
C: 7.74
D: 10.32

Fig.6.2. Interaction of two waves (β=2.58, β=5.16) at T=6000 for η=0.5
(a). two-mode perturbation method (9th order): $A(0)$=0.01, $B(0)$=0.0075
(b). numerical method (18 harmonics): $2V_1(0)$=0.01, $2V_2(0)$=0.0075

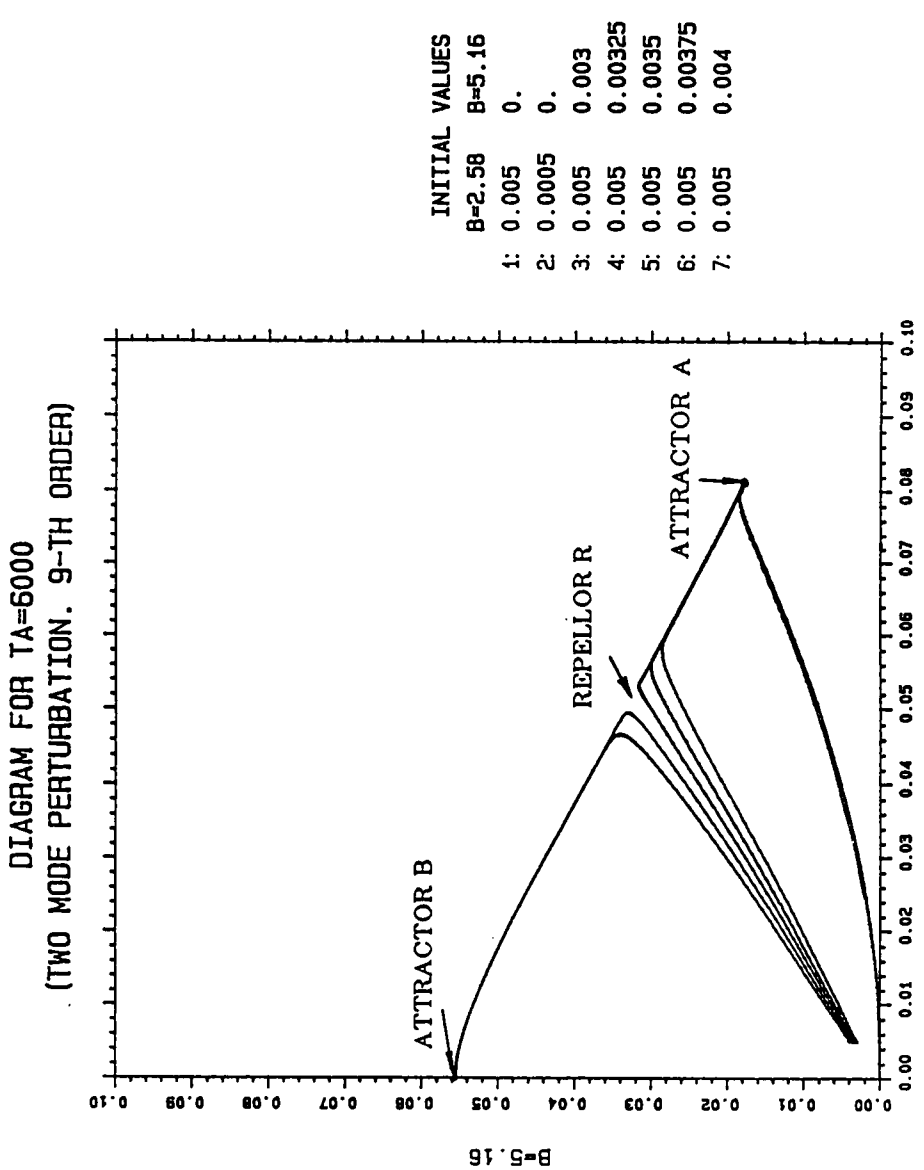

Fig.6.3. Amplitude diagram of interaction of two waves (β=2.58 and β=5.16) at T=6000 for η=0.5 (obtained by two mode method)

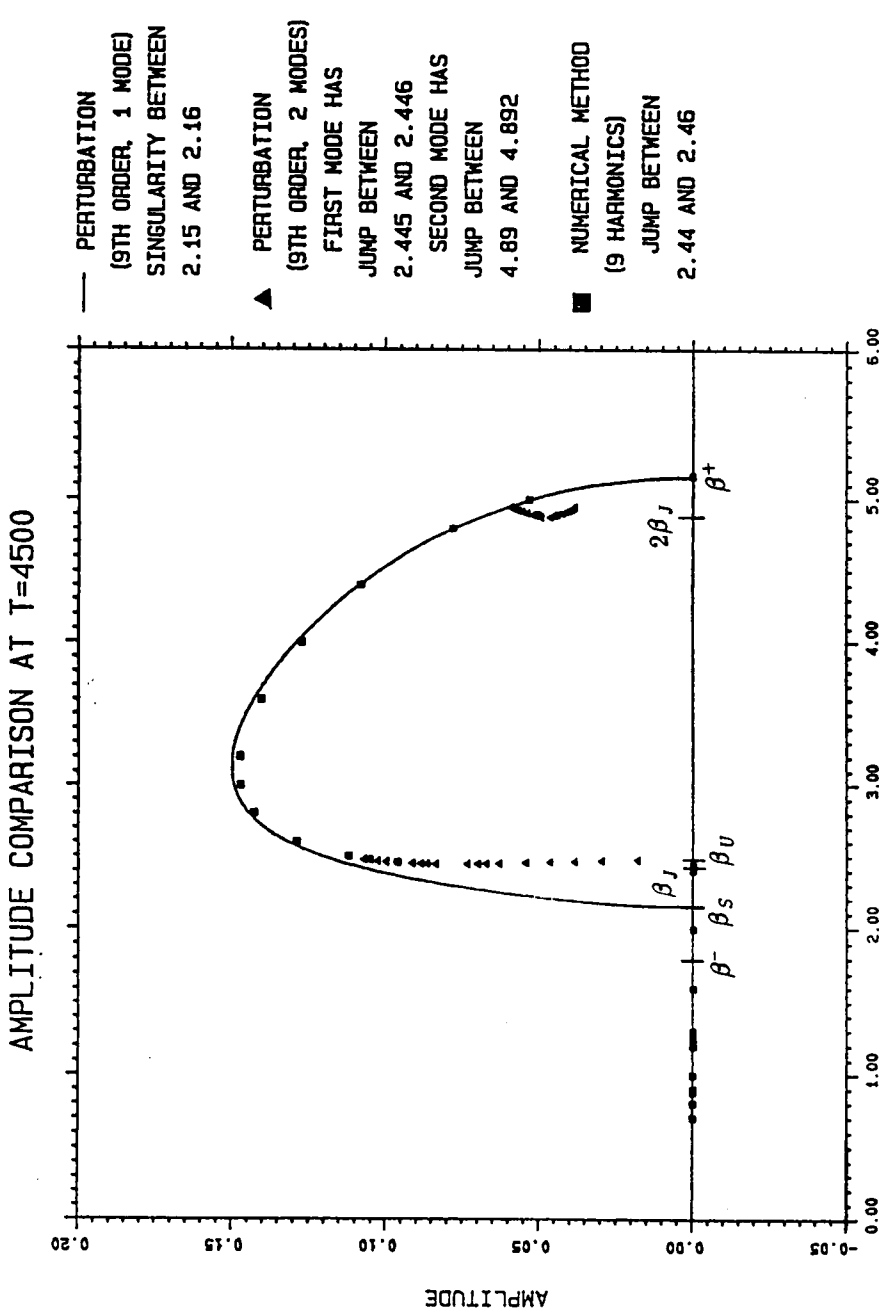

Fig.6.4. Amplitude comparison at $T=4500$ for $\eta=0.5$

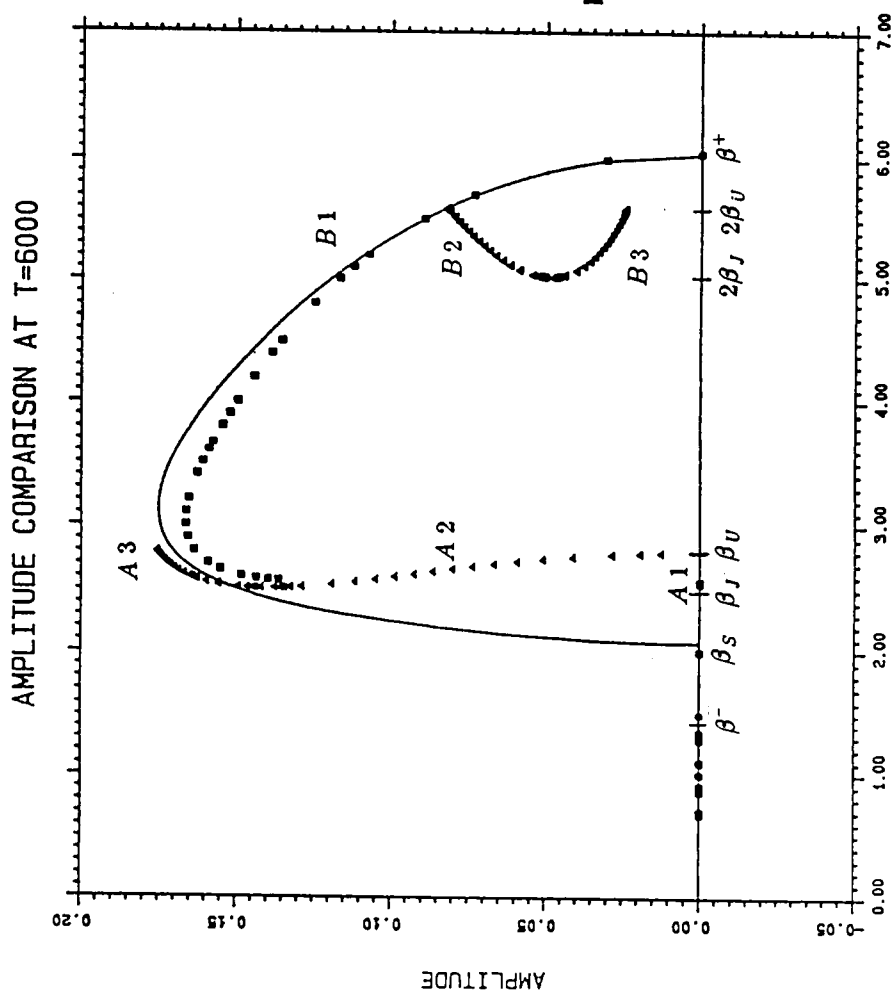

Fig.6.5. Amplitude comparison at $T=6000$ for $\eta=0.5$

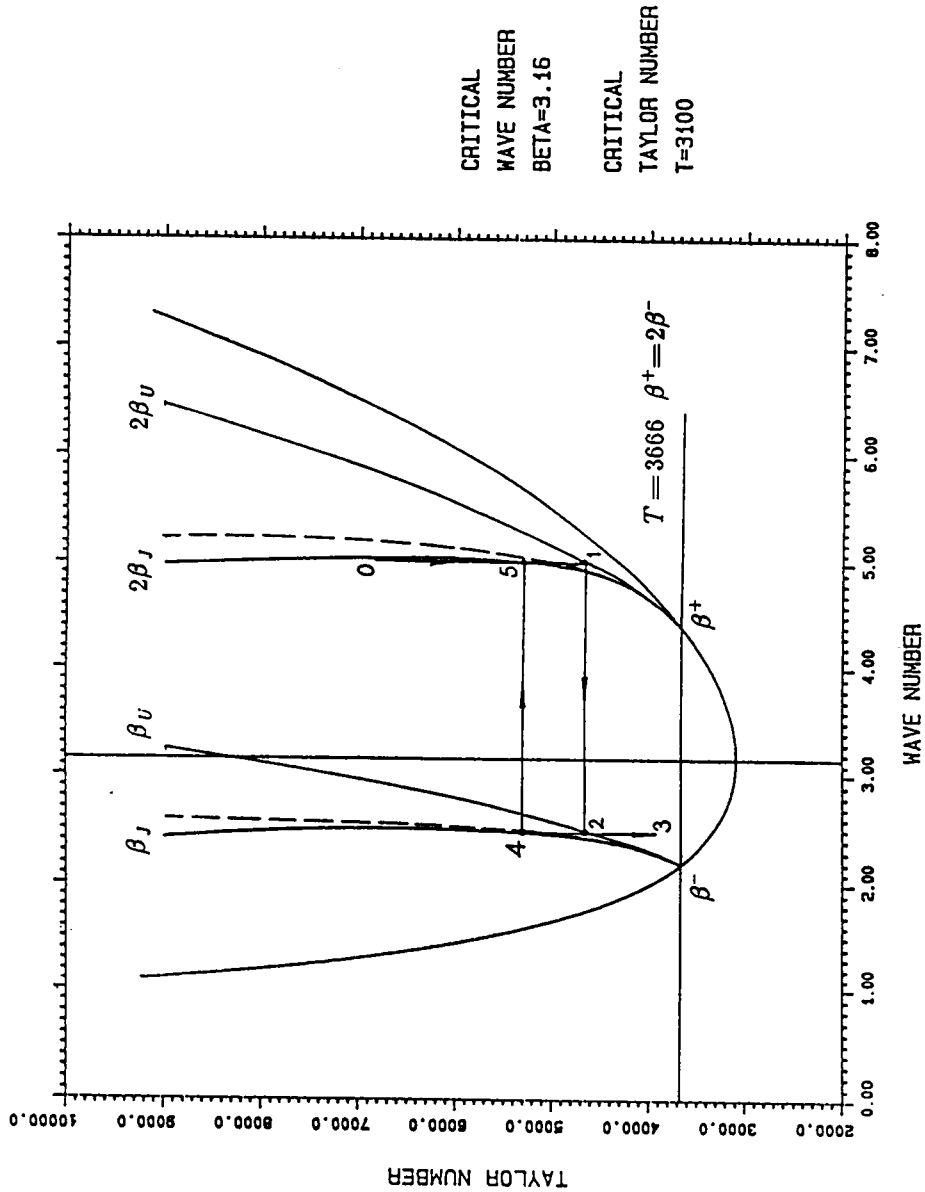

Fig.6.6. Intervals of multiple solutions at $T=6000$ for $\eta=0.5$ and explanation of hysteresis phenomenon (Note that the dashed lines are from the numerical method while the solid lines are from two mode perturbation method)

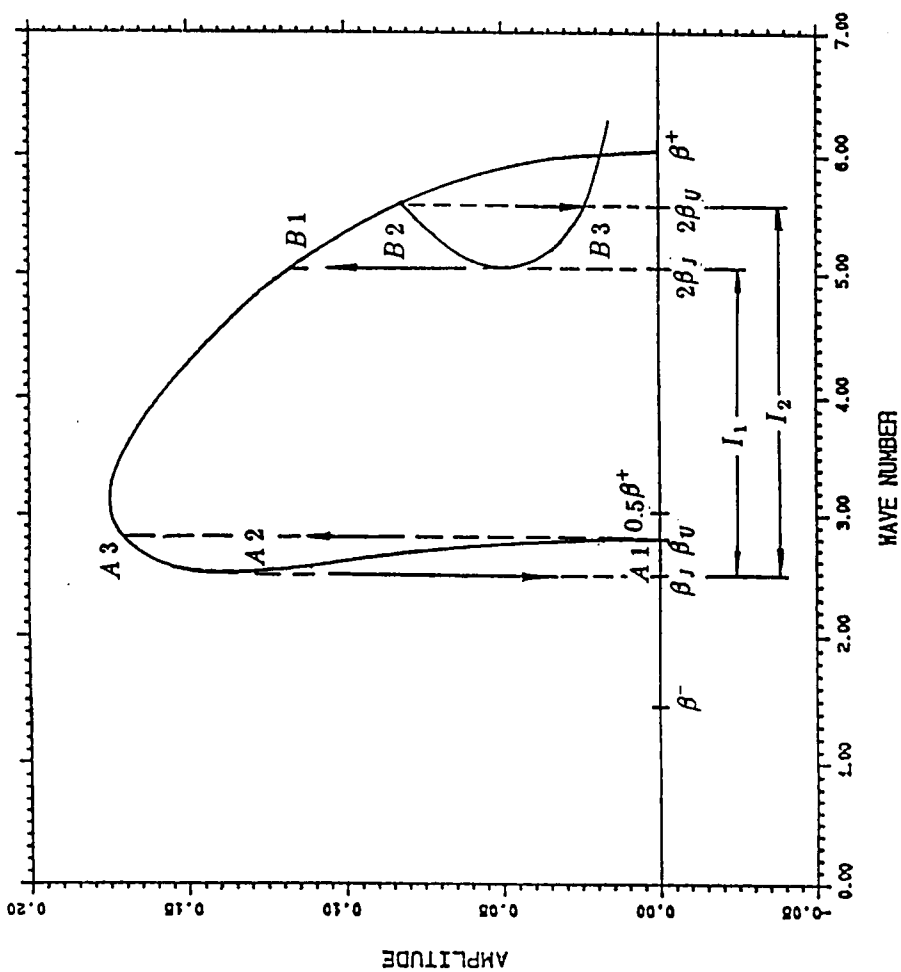

Fig.6.7. Sketch of stable and unstable solutions at $T=6000$ for $\eta=0.5$

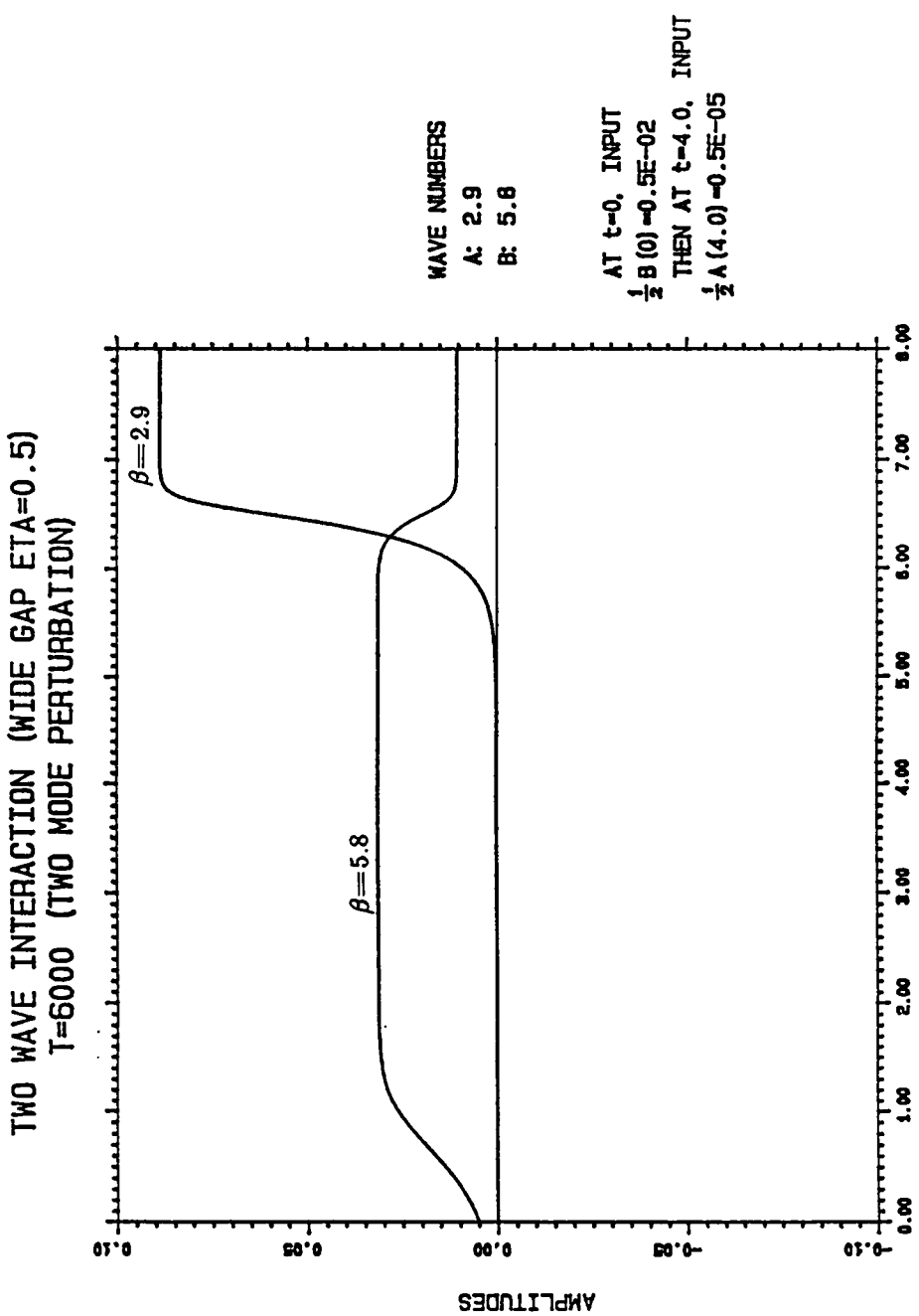

Fig.6.8. Interaction of two waves (β=2.9 and β=5.8) input at different time obtained from two mode perturbation method (T=6000 and η=0.5)

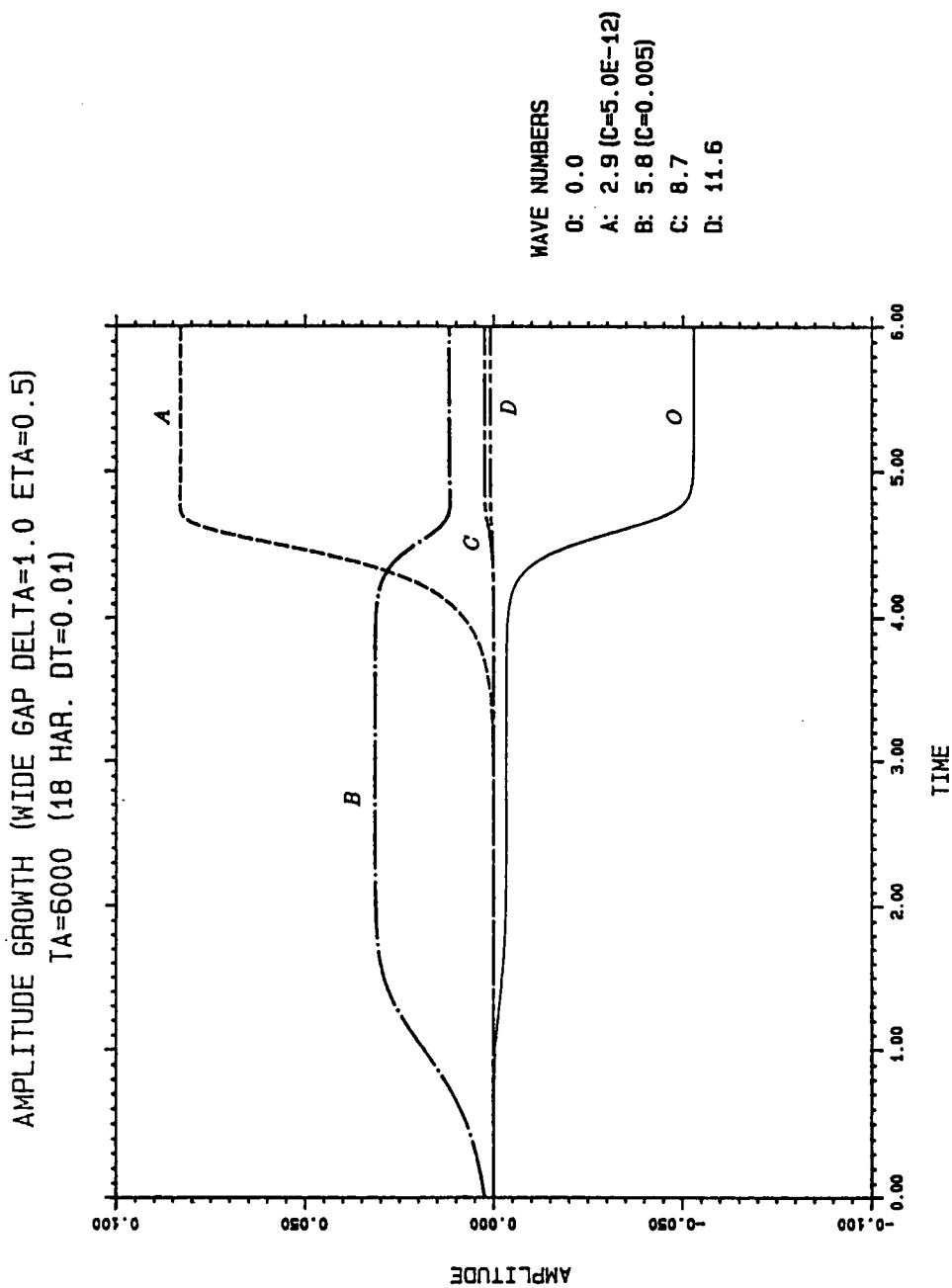

Fig.6.9. Interaction of two waves (β=2.9 and β=5.8) obtained from numerical method (T=6000 and η=0.5)

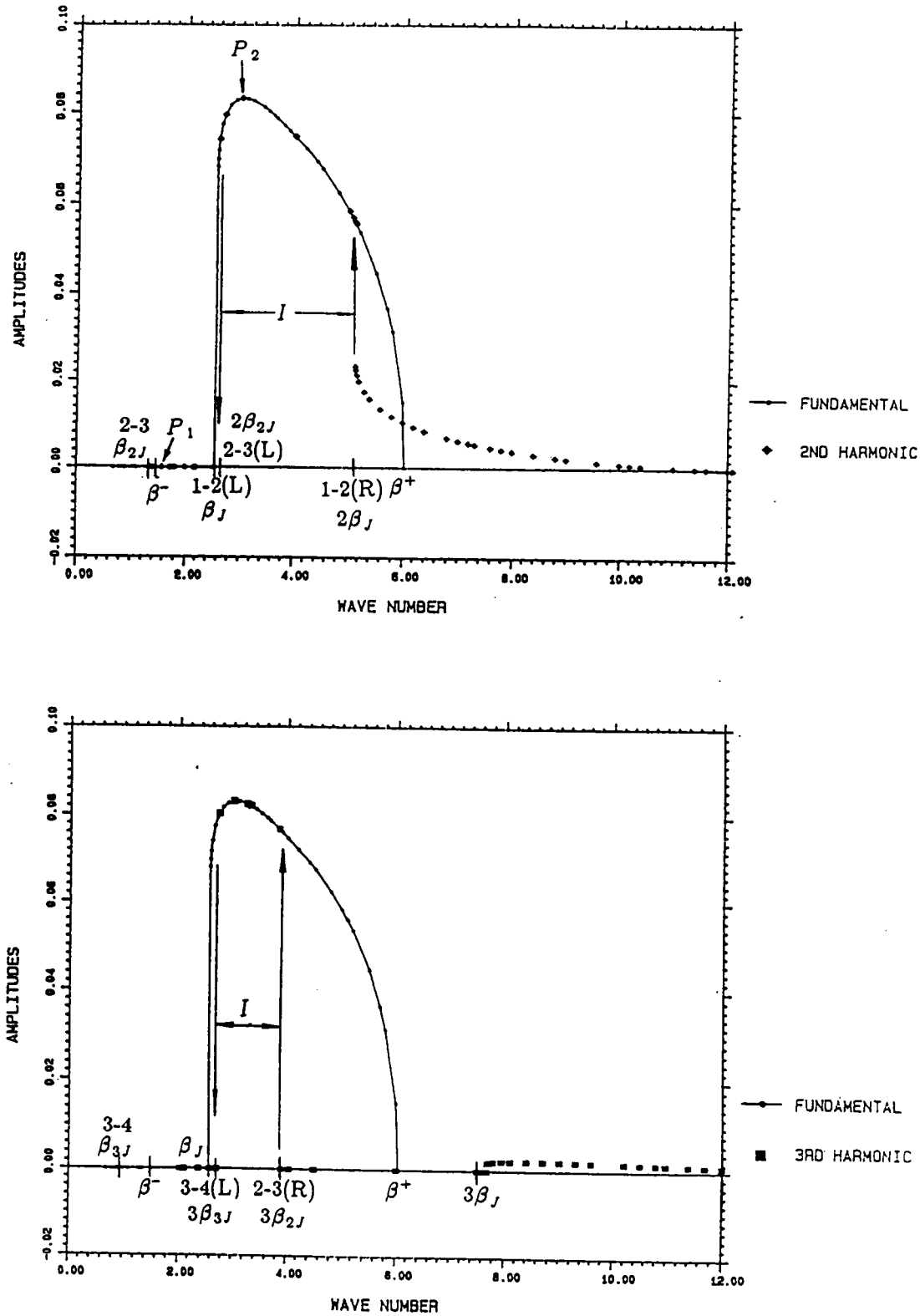

Fig.7.1. Jump phenomenon at $T=6000$ for $\eta=0.5$
(a). jump between β and 2β (b). jump between 2β and 3β

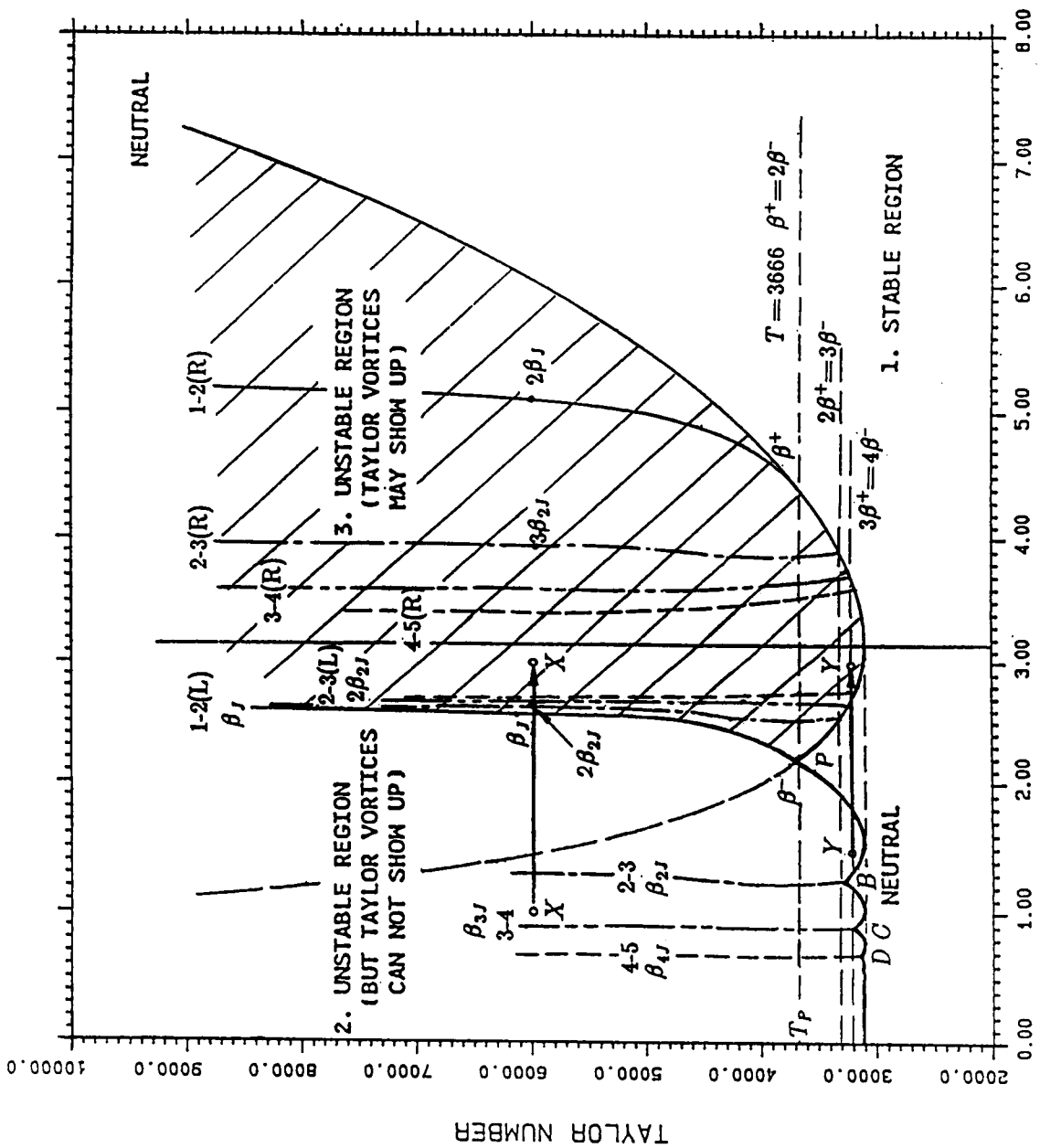

Fig.7.2. Stability diagram of single input disturbance

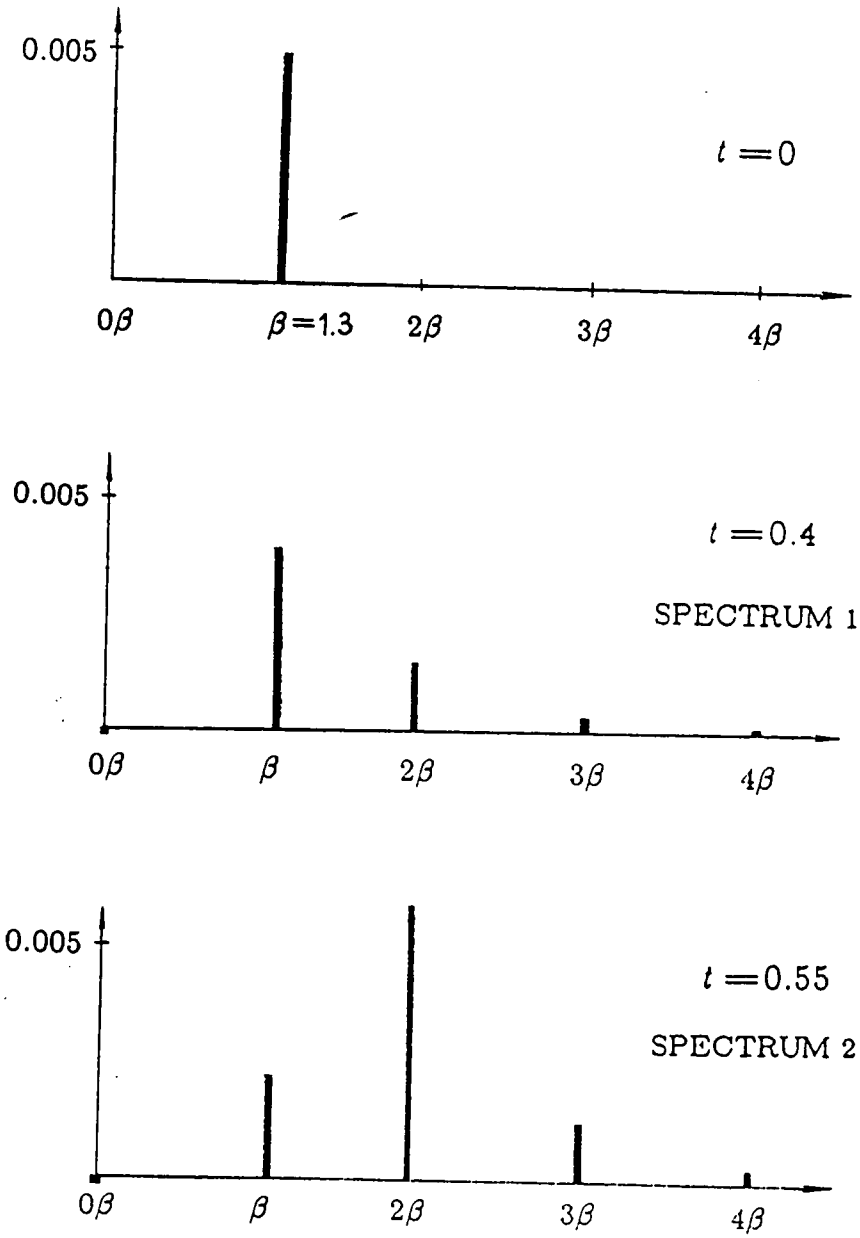

Fig.7.3. Sketch of disturbance spectra at different time

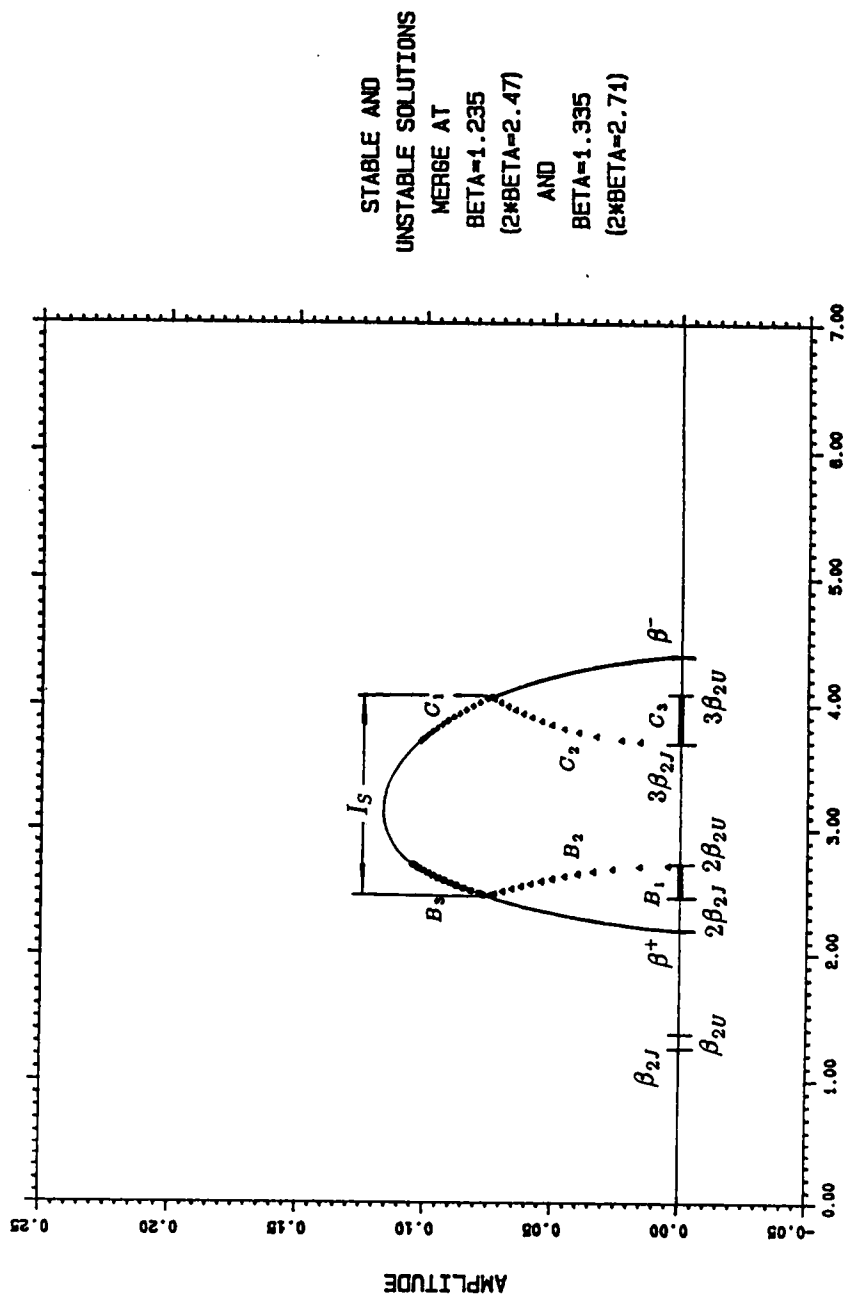

Fig.7.4. Stable and unstable solutions (3rd order) for the interaction between 2β and 3β at $T=3666$ and $\eta=0.5$

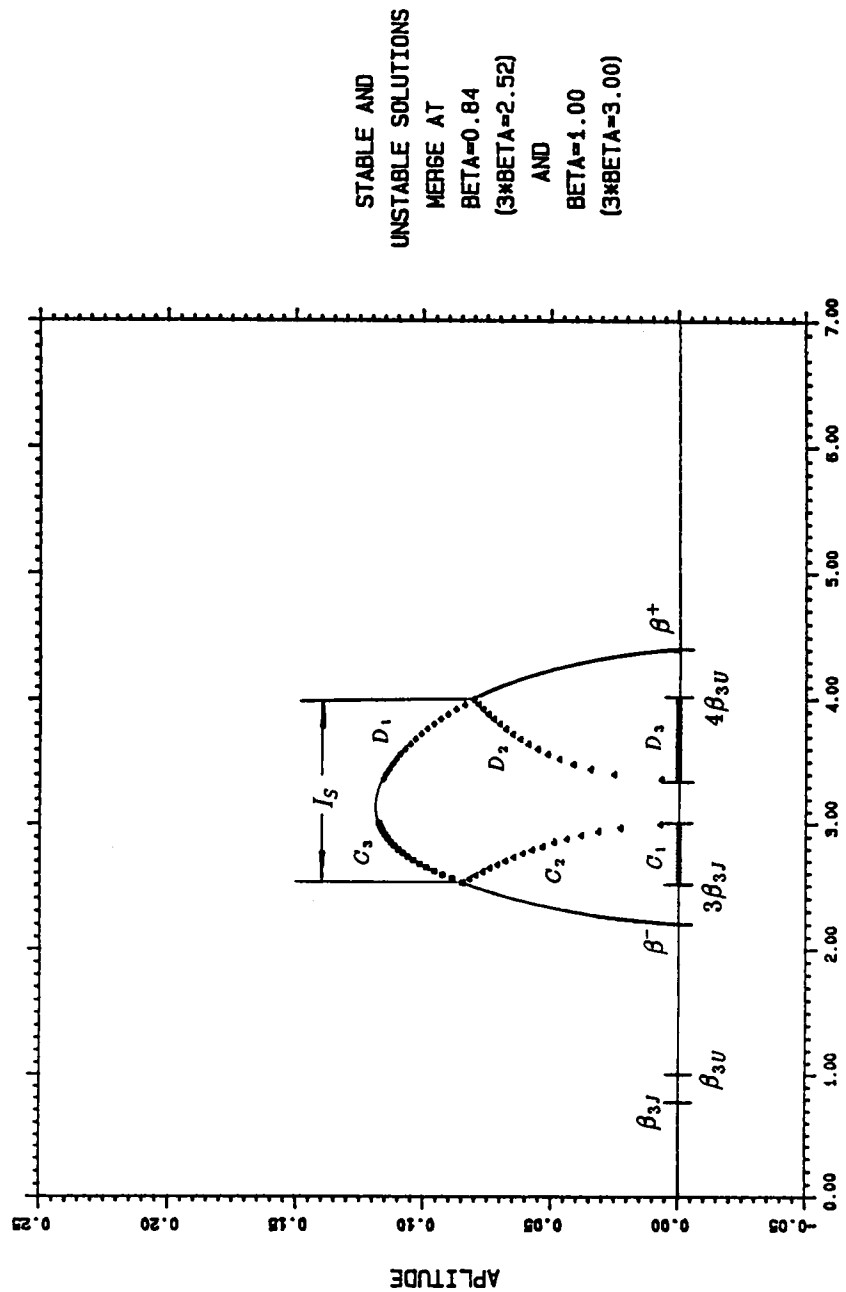

Fig.7.5. Stable and unstable solutions (3rd order) for the interaction between 3β and 4β at $T=3666$ for $\eta=0.5$

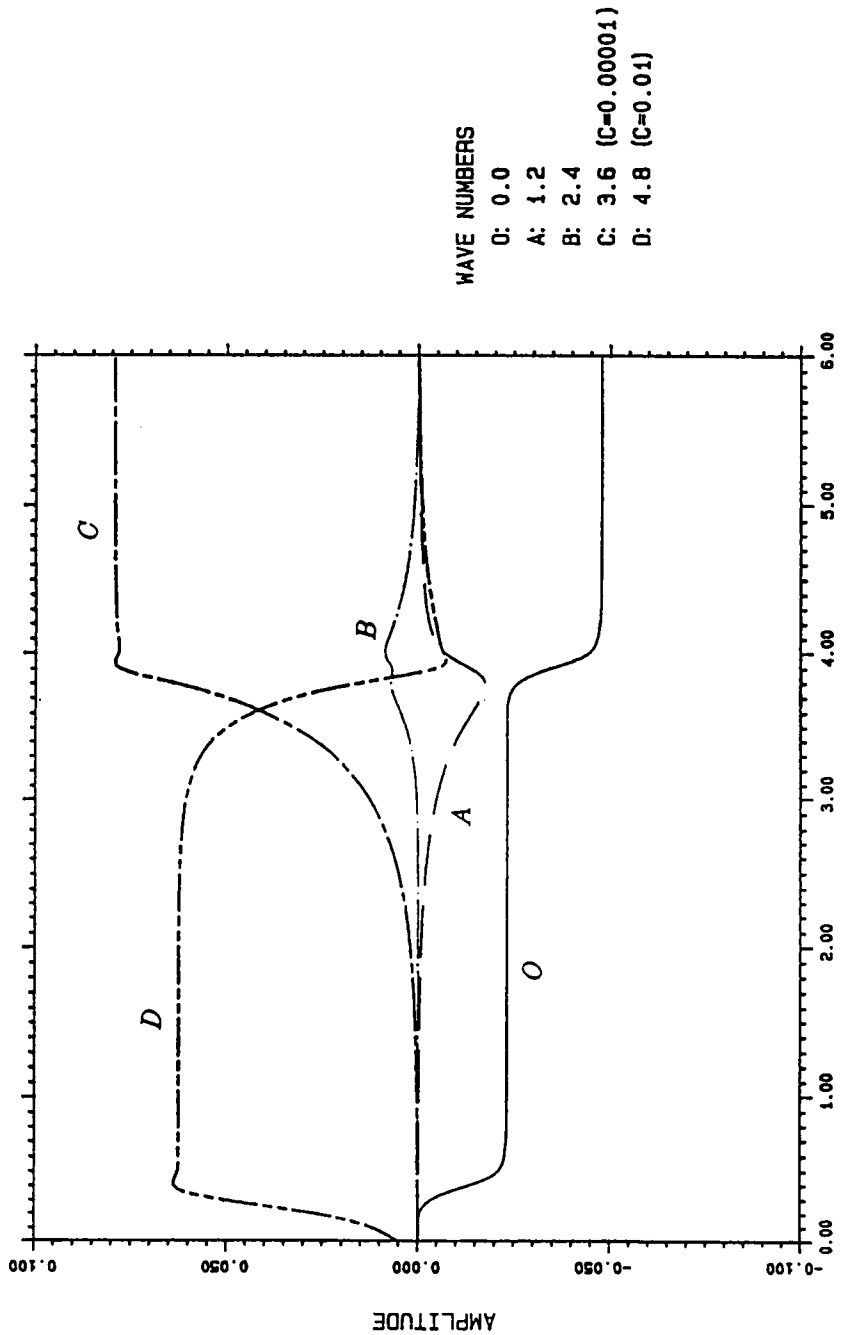

Fig.7.6. Interaction of two waves (β=3.6 and β=4.8) at T=6000 for η=0.5 obtained from numerical method

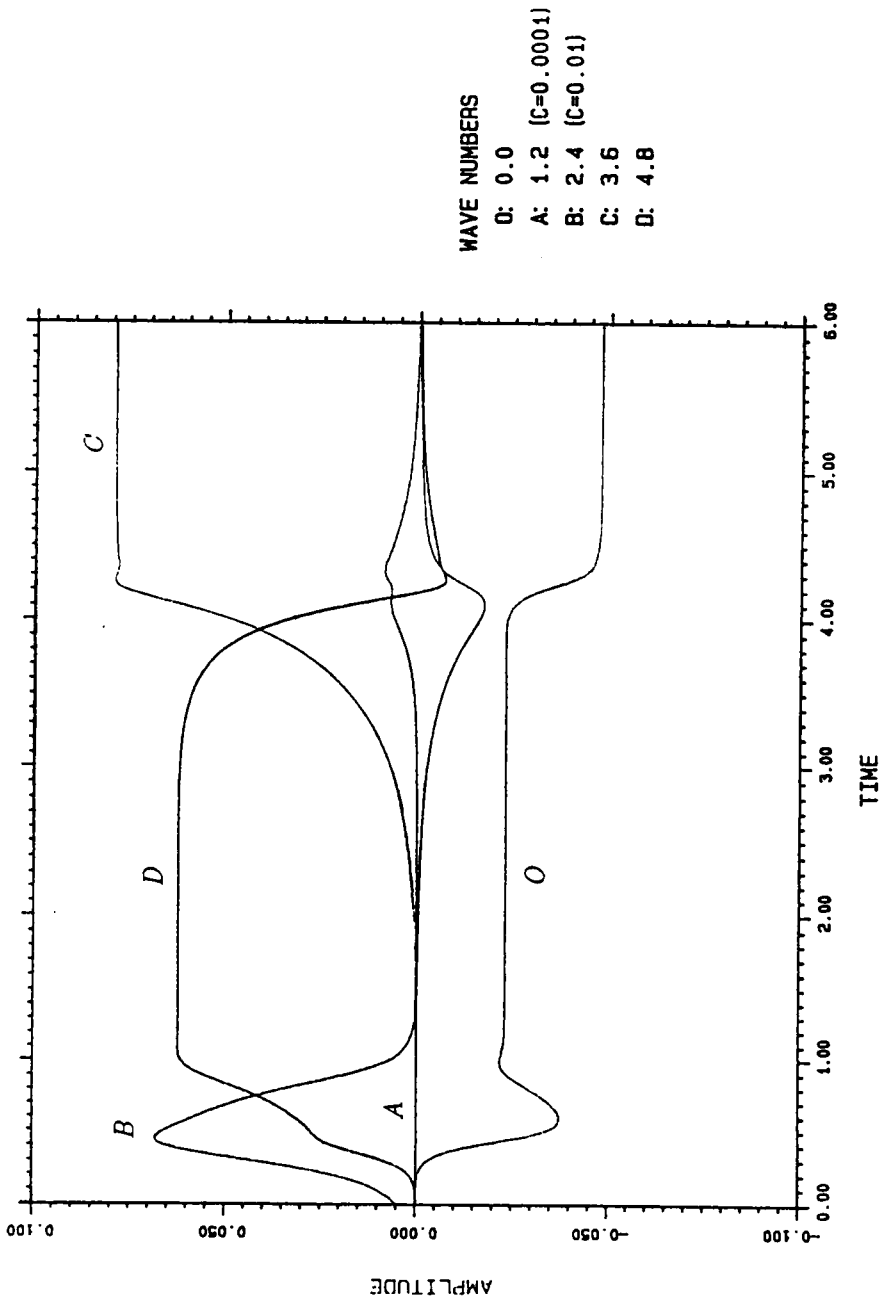

Fig.7.7. Interaction of two waves (β=1.2 and β=2.4) at T=6000 for η=0.5 obtained from numerical method

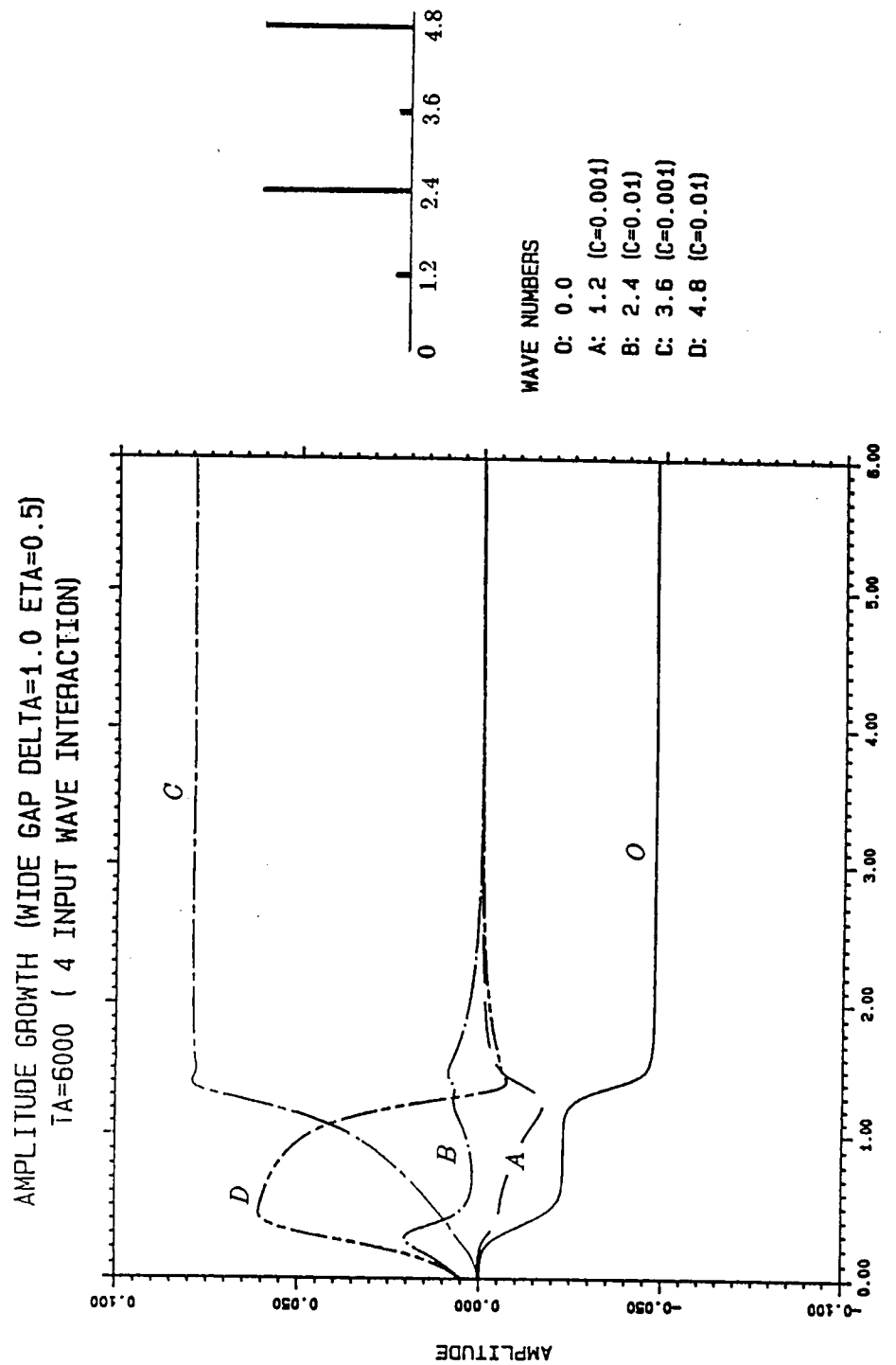

Fig.7.8. Interaction of four waves (β=1.2, β=2.4, β=3.6,β=4.8) at T=6000 for η=0.5 obtained from numerical method

Table 7.1 Initial disturbance spectra for four wave interaction at $T=6000$ and $\eta=0.5$

CASE	$\beta=1.2$	$\beta=2.4$	$\beta=3.6$	$\beta=4.8$
1	0.01	0.01		
2	0.01	0.003		
3	0.01	0.001		
4	0.01	0.03		
5	0.001	0.01		
6	0.0001	0.01		
7	0.01			0.01
8	0.00001			0.01
9	0.0001			0.01
10	0.01	0.01		0.01
11	0.0001	0.01		0.01
12	0.00001	0.01		0.01
13	0.001	0.01	0.001	0.01
14	0.001	0.01	0.002	0.001
15	0.01	0.01	0.01	0.01
16	0.01	0.005	0.002	0.001

Note that all above cases lead to the same steady state with $\beta=3.6$

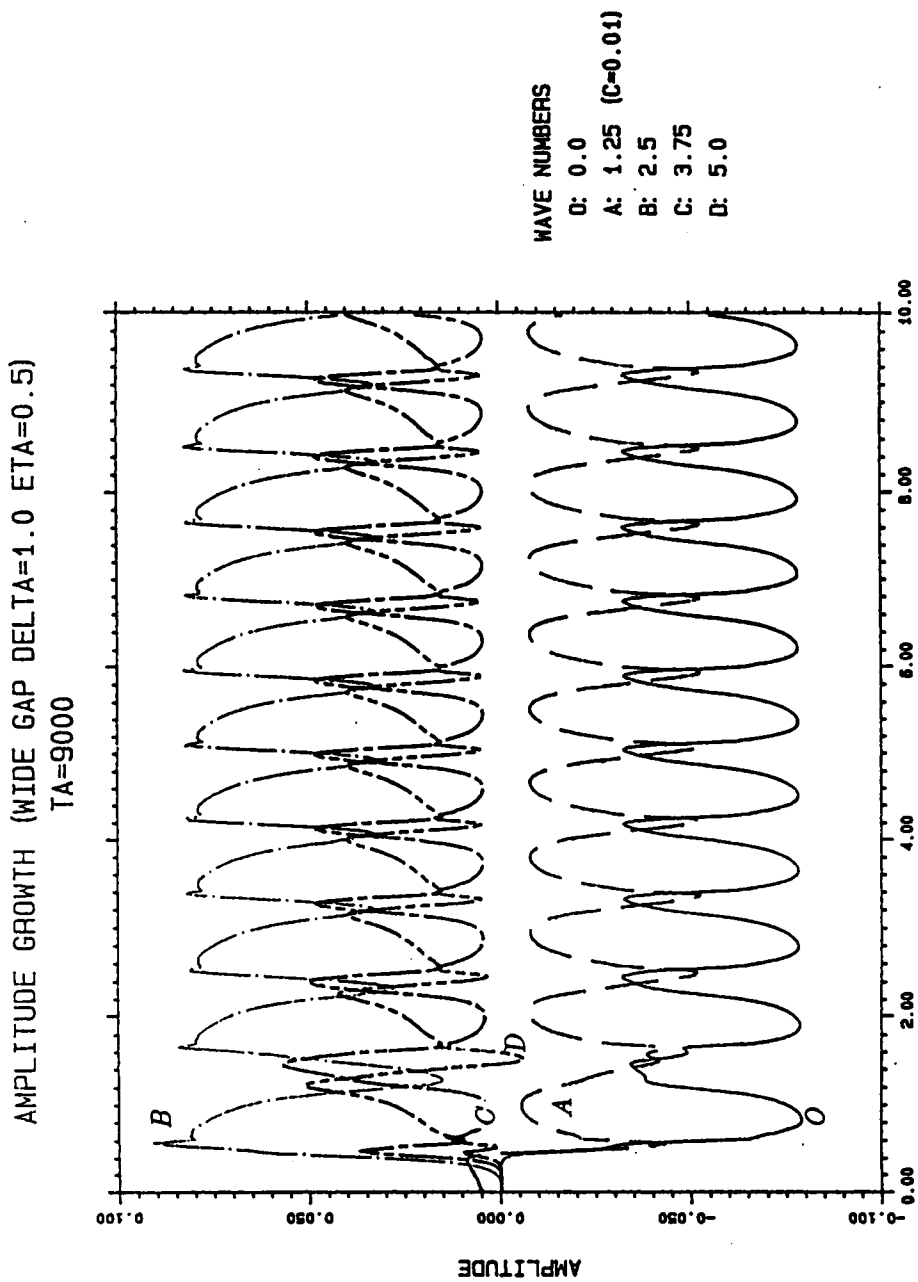

Fig.7.9. Oscillation phenomenon at β=1.25 and T=9000 for η=0.5 (Note that only a small disturbance $V_1(0)$=0.005 is introduced)

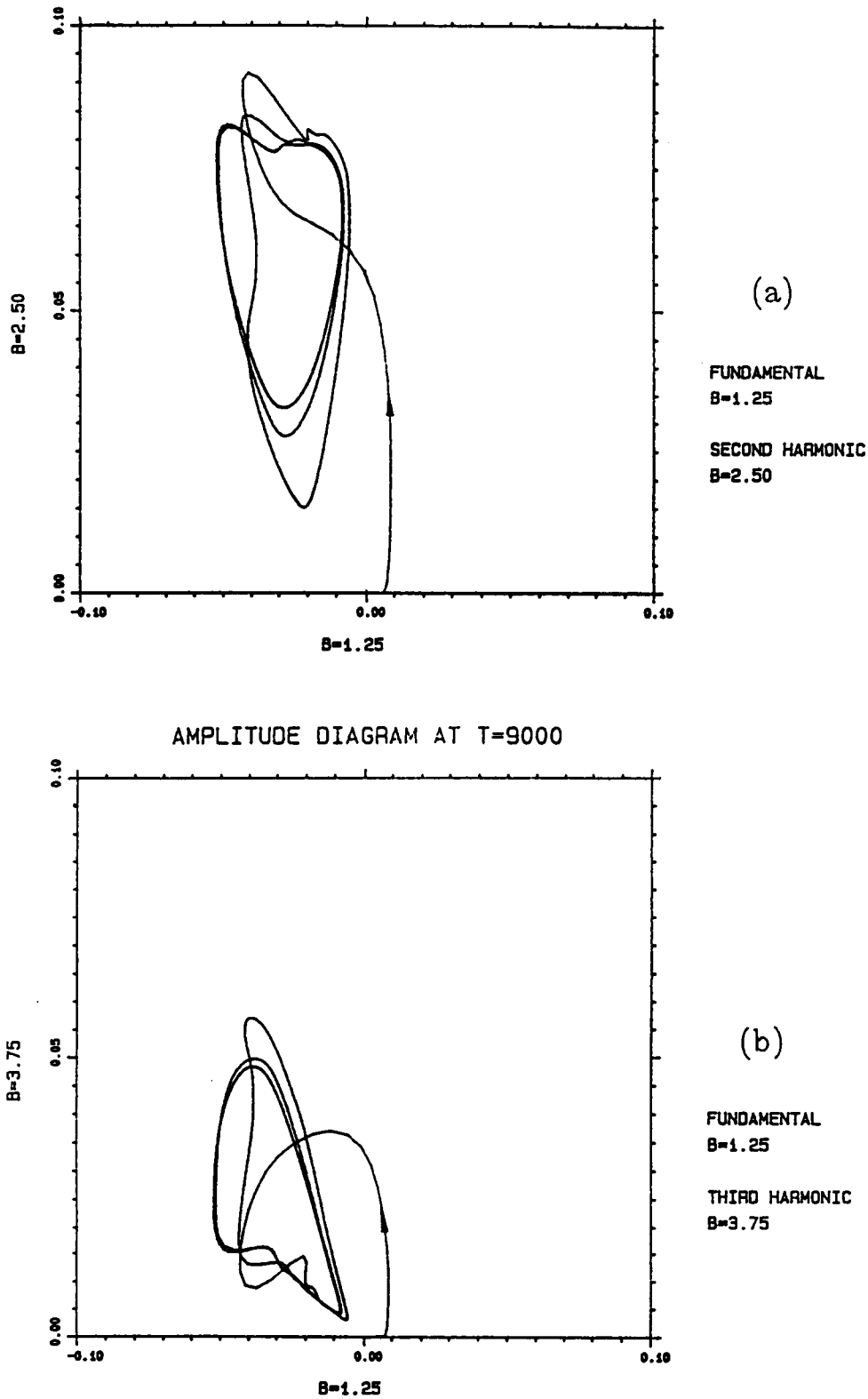

Fig.7.10. Amplitude diagram at $\beta=1.25$ and $T=9000$ for $\eta=0.5$
(a). for $\beta=1.25$ and $2\beta=2.50$
(b). for $\beta=1.25$ and $3\beta=3.75$

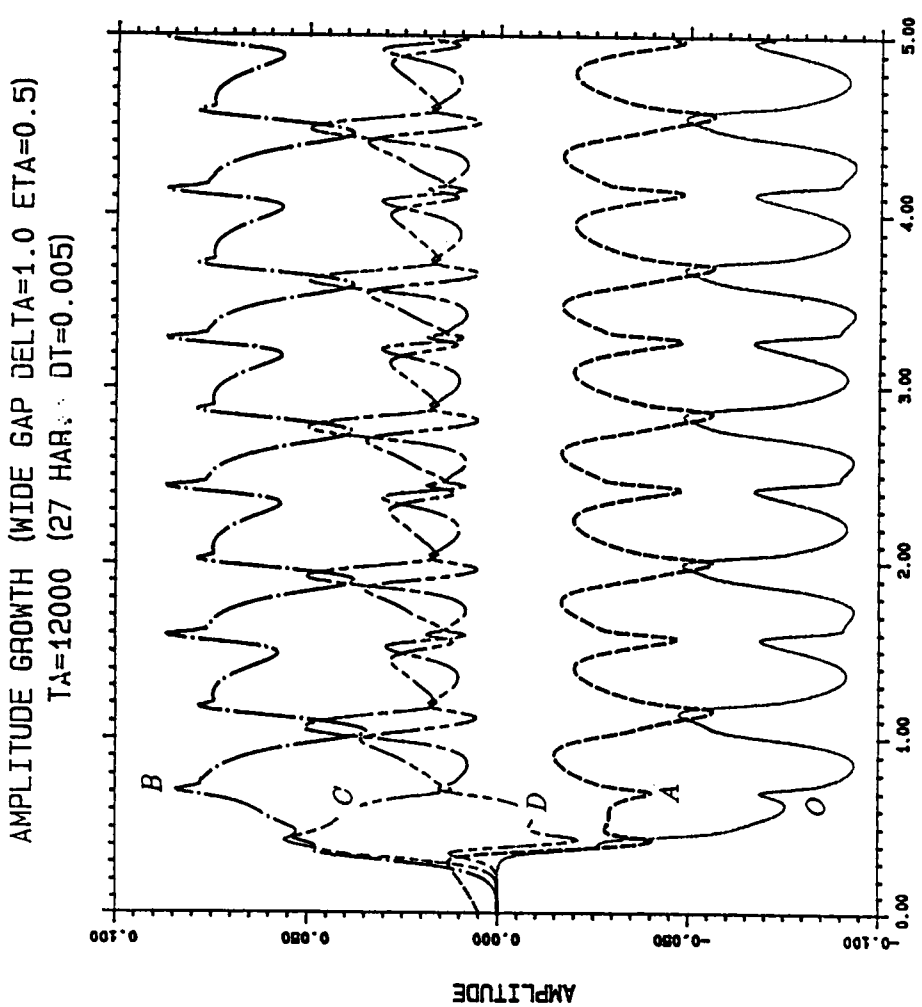

Fig.7.11. Oscillation phenomenon at β=1.16 and T=12000 for η=0.5

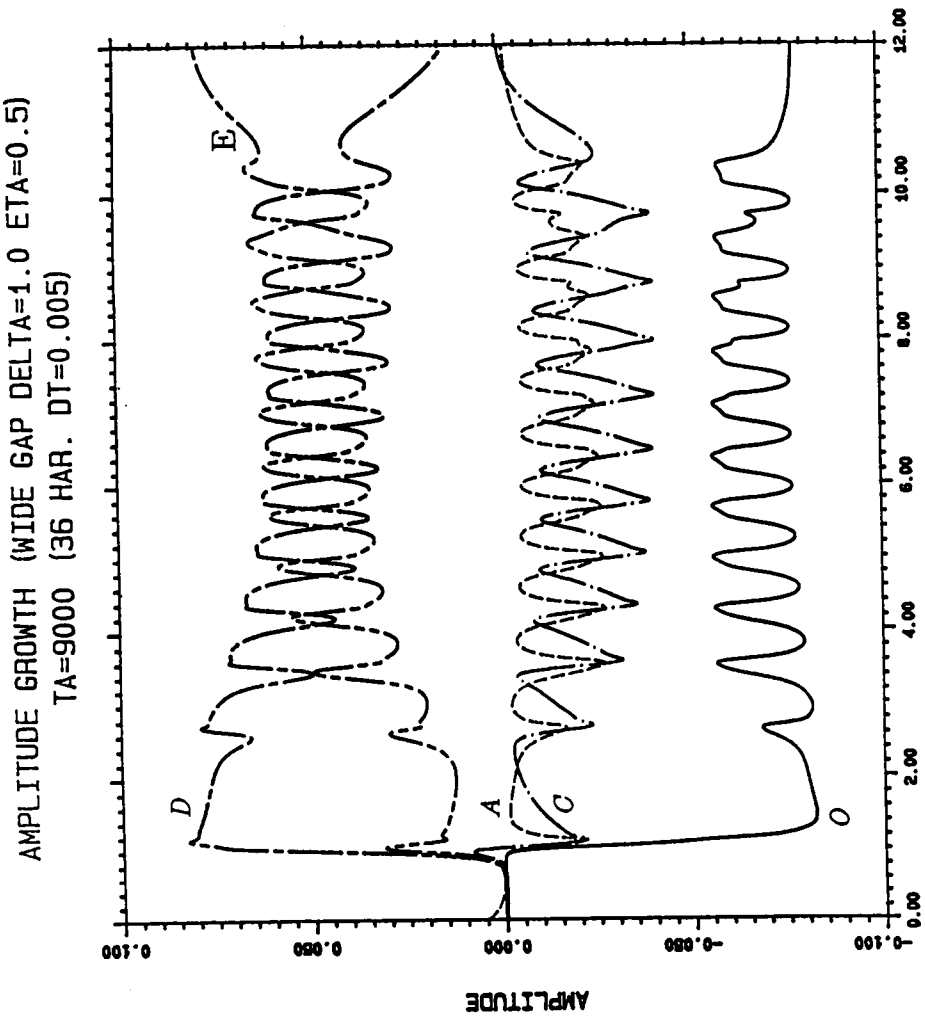

Fig.7.12. Evolution of amplitudes at β=0.675 and T=9000 for η=0.5

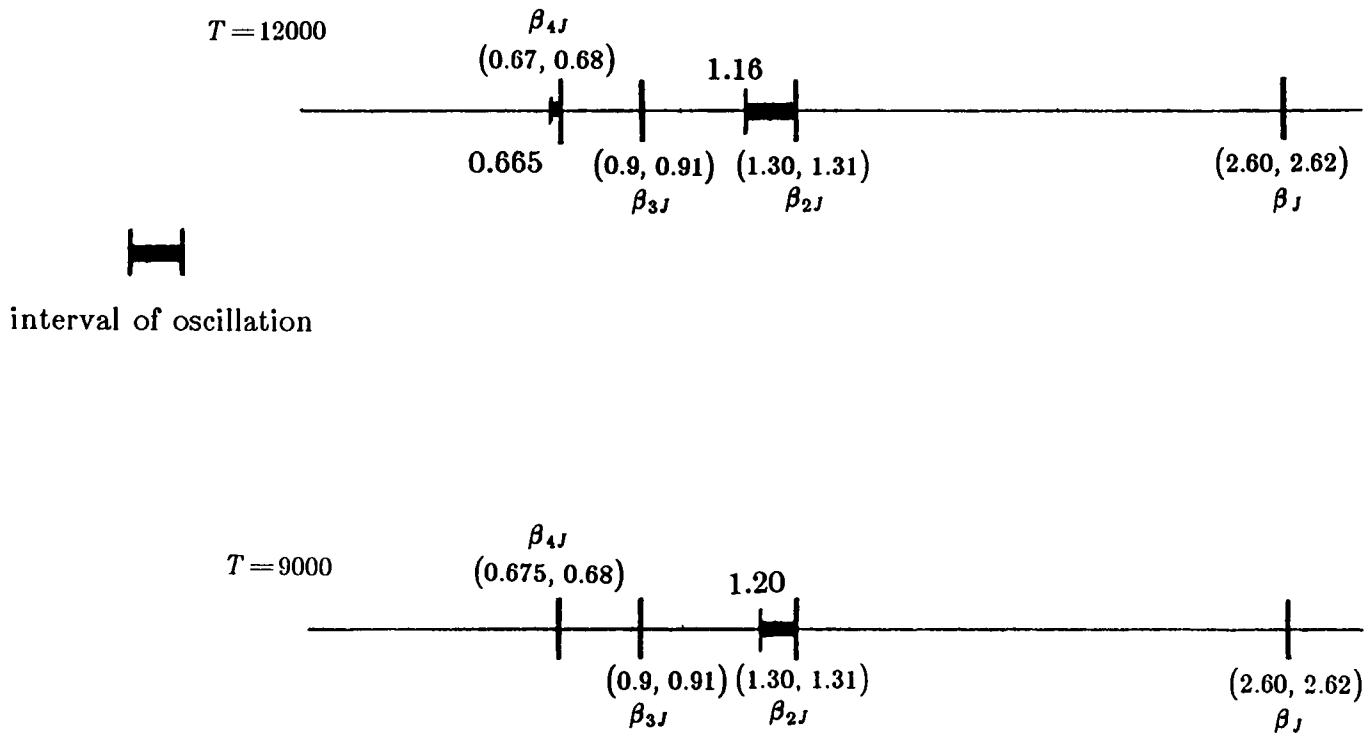

Fig.7.13. A sketch of intervals with oscillation phenomenon at $T=9000$ and $T=12000$ for $\eta=0.5$

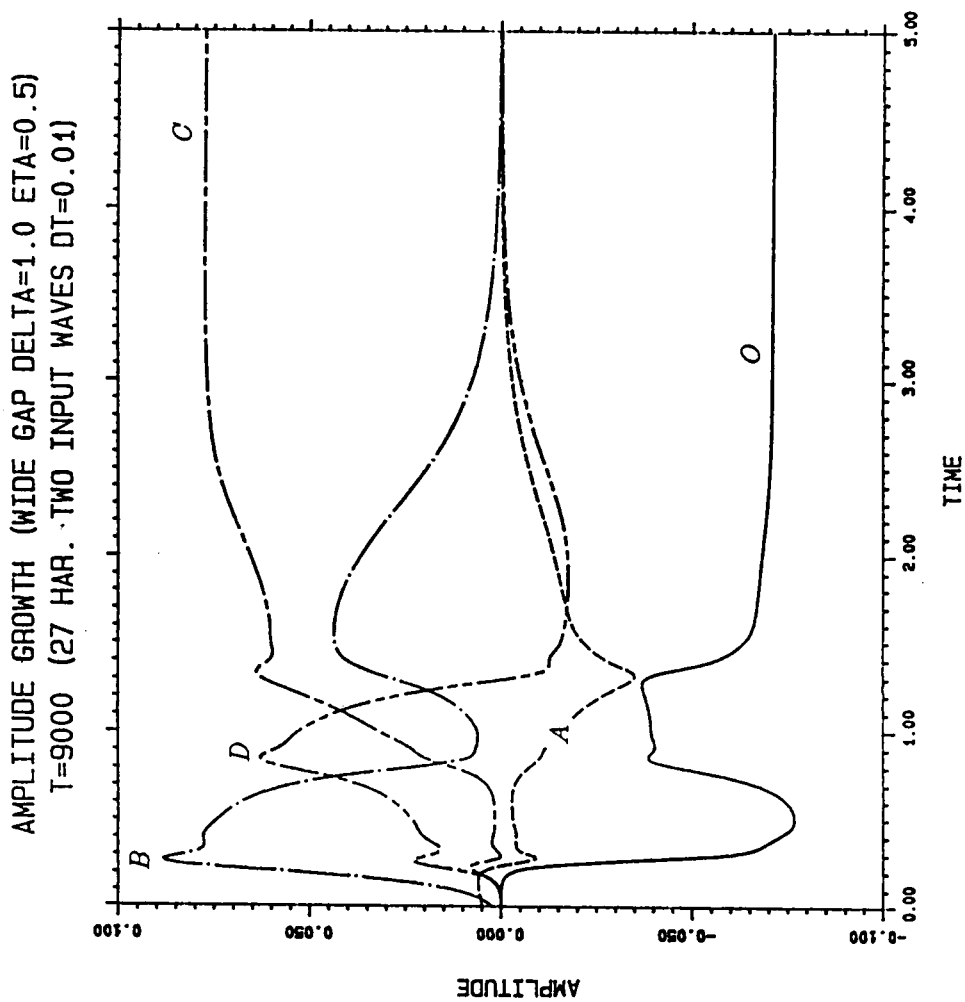

Fig.7.14. Interaction of two waves (β=1.25 and β=2.50) at T=9000 for η=0.5. Note that $V_1(0)$=0.005 and $V_2(0)$=0.0025

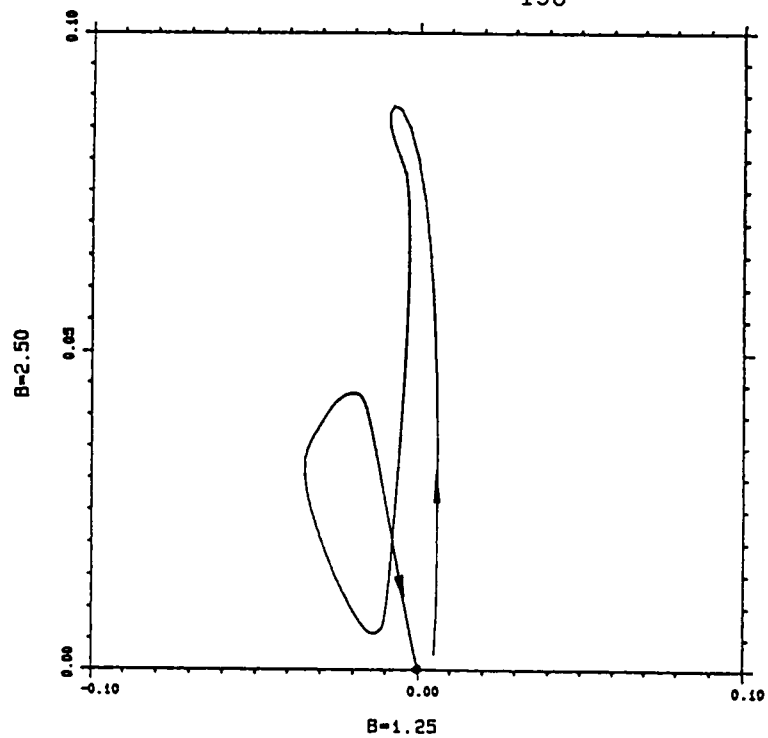

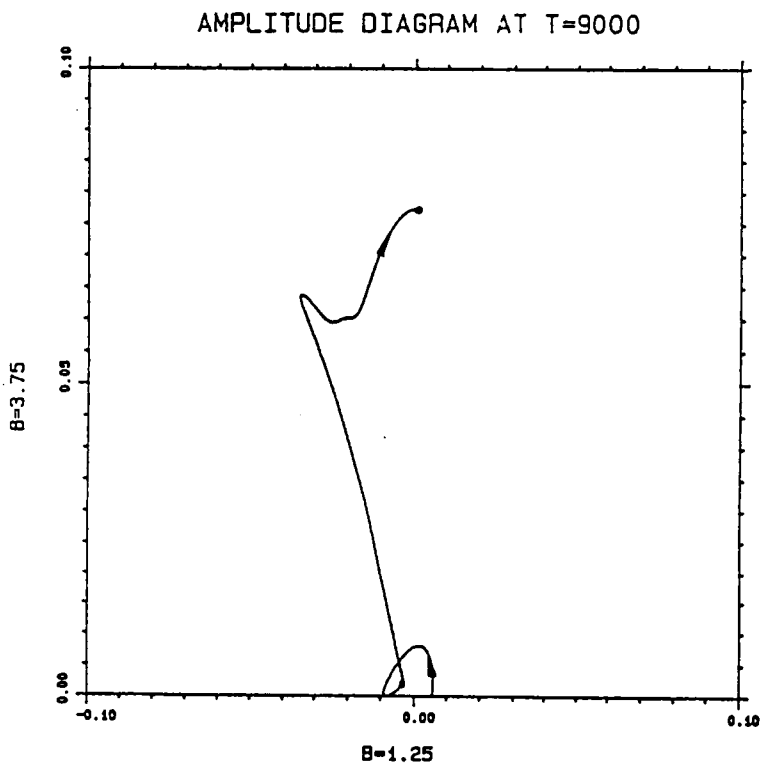

Fig.7.15. Amplitude diagram at $\beta=1.25$ and $T=9000$ for $\eta=0.5$ ($V_1(0)=0.005$ and $V_2(0)=0.0025$)

(a). for $\beta=1.25$ and $2\beta=2.50$

(b). for $\beta=1.25$ and $3\beta=3.75$

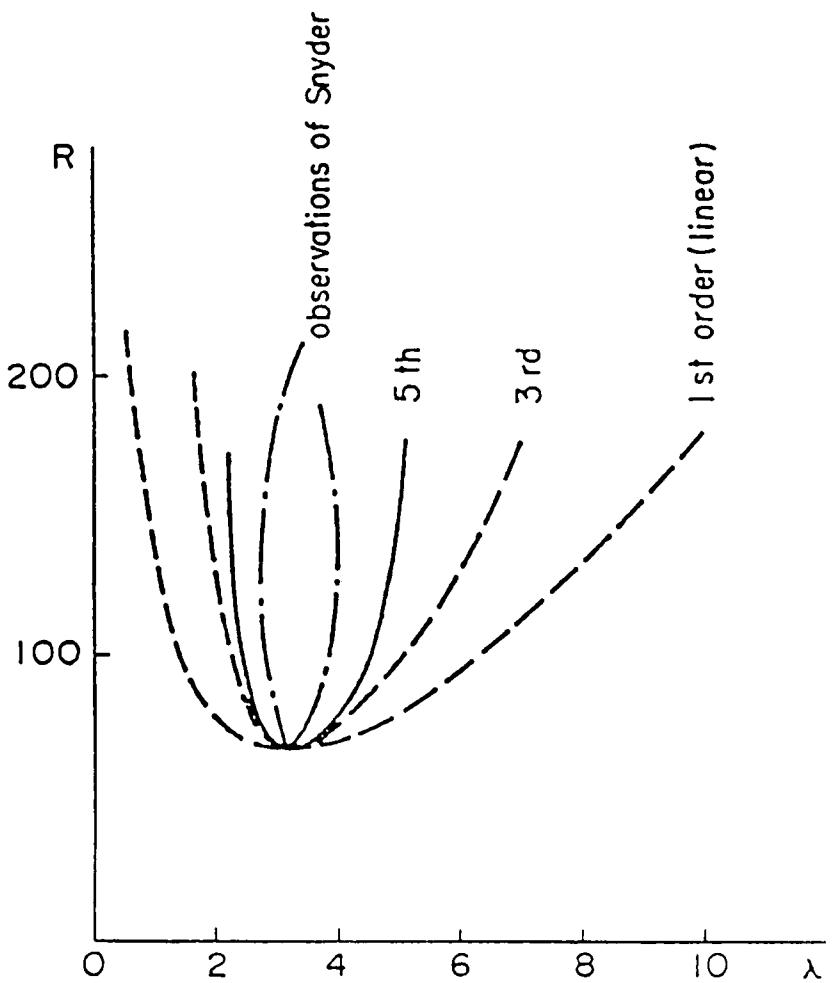

Fig.8.1. Side-band stability curve (up to the 5th order) by Nakaya [19]

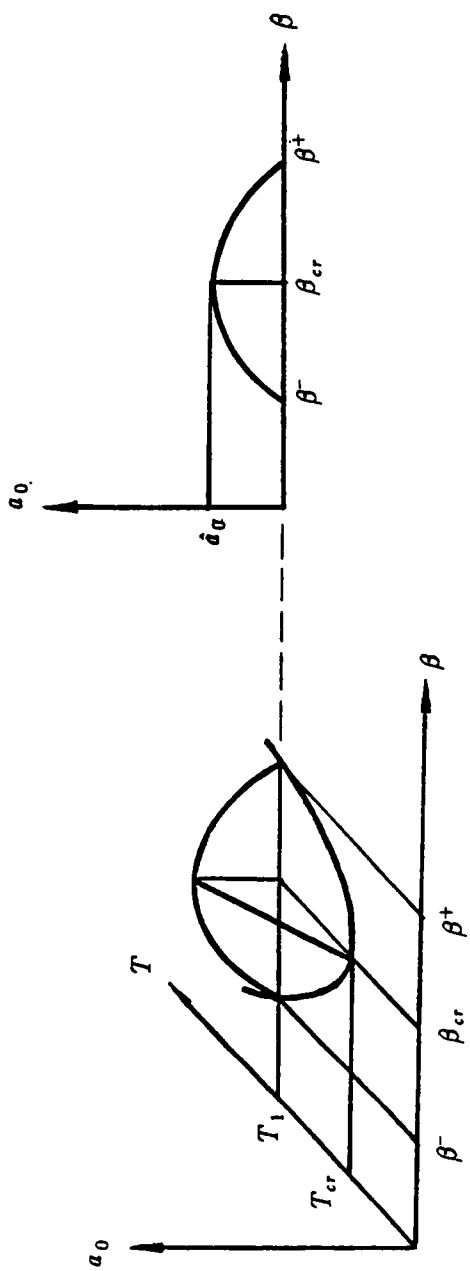

Fig.8.2. Geometric interpretation of approximation (parabola) for the first Landau constant a_0 (linear growth rate)

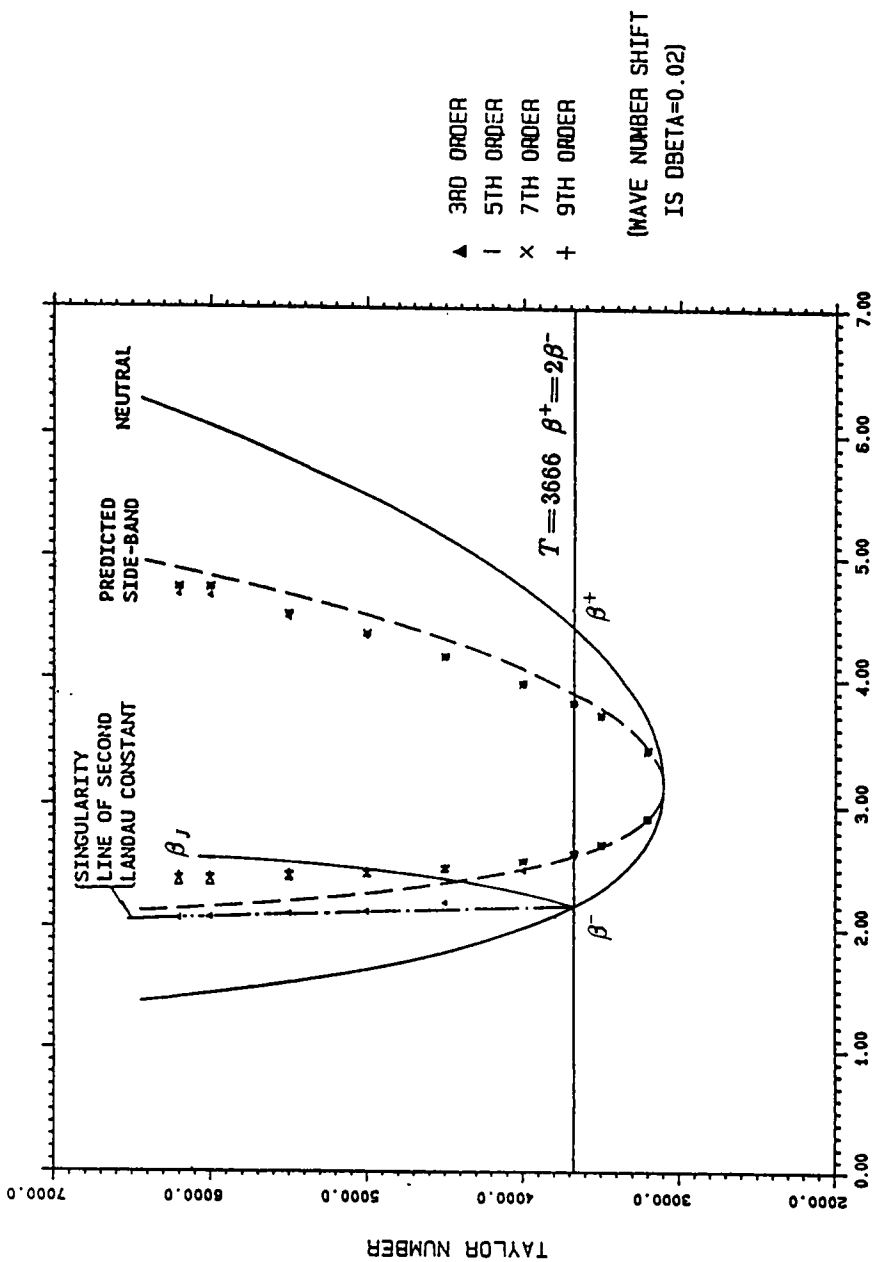

Fig.8.3. Side-band stability curve for wide gap case (η=0.5) by Approach 1

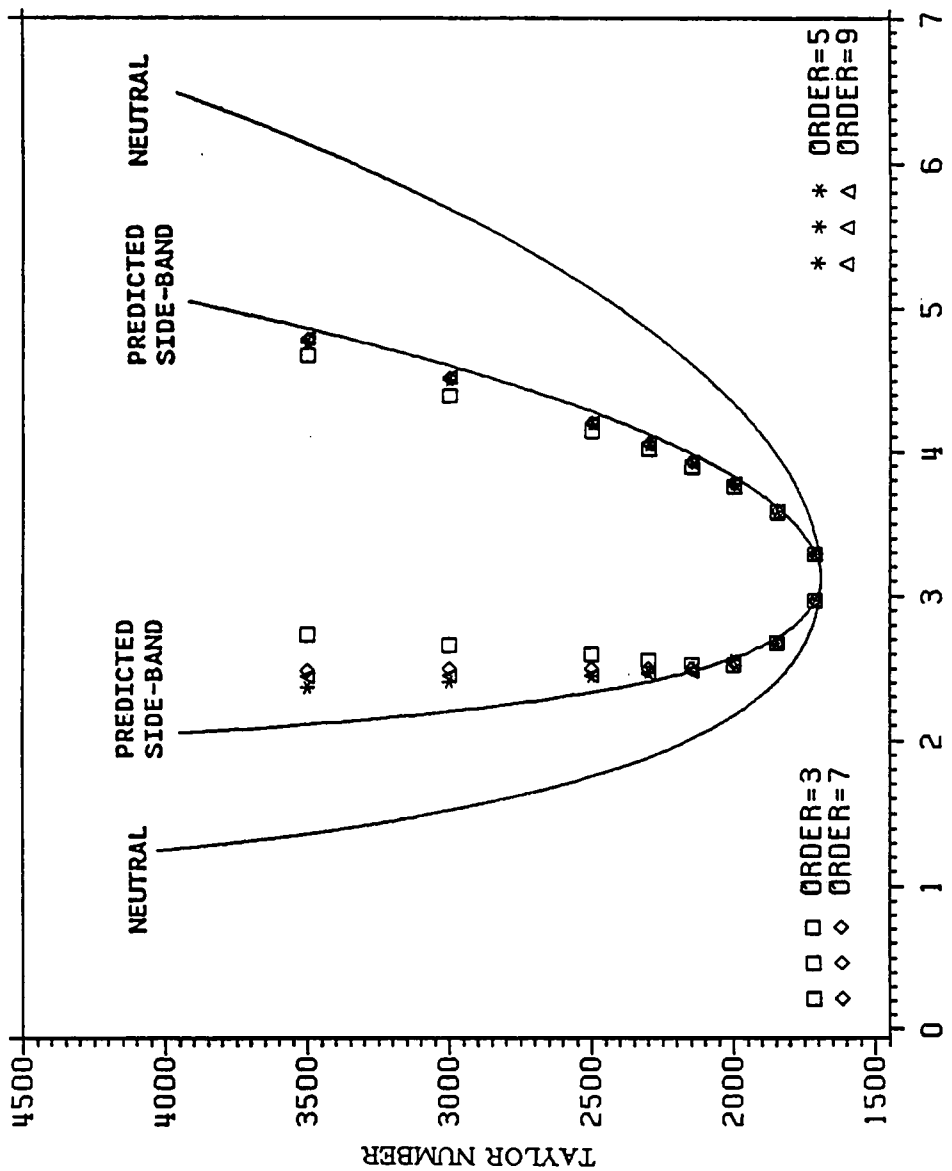

Fig.8.4. Side-band stability curve for small gap case (η=0.9524 i.e., δ=0.05) by Approach 1

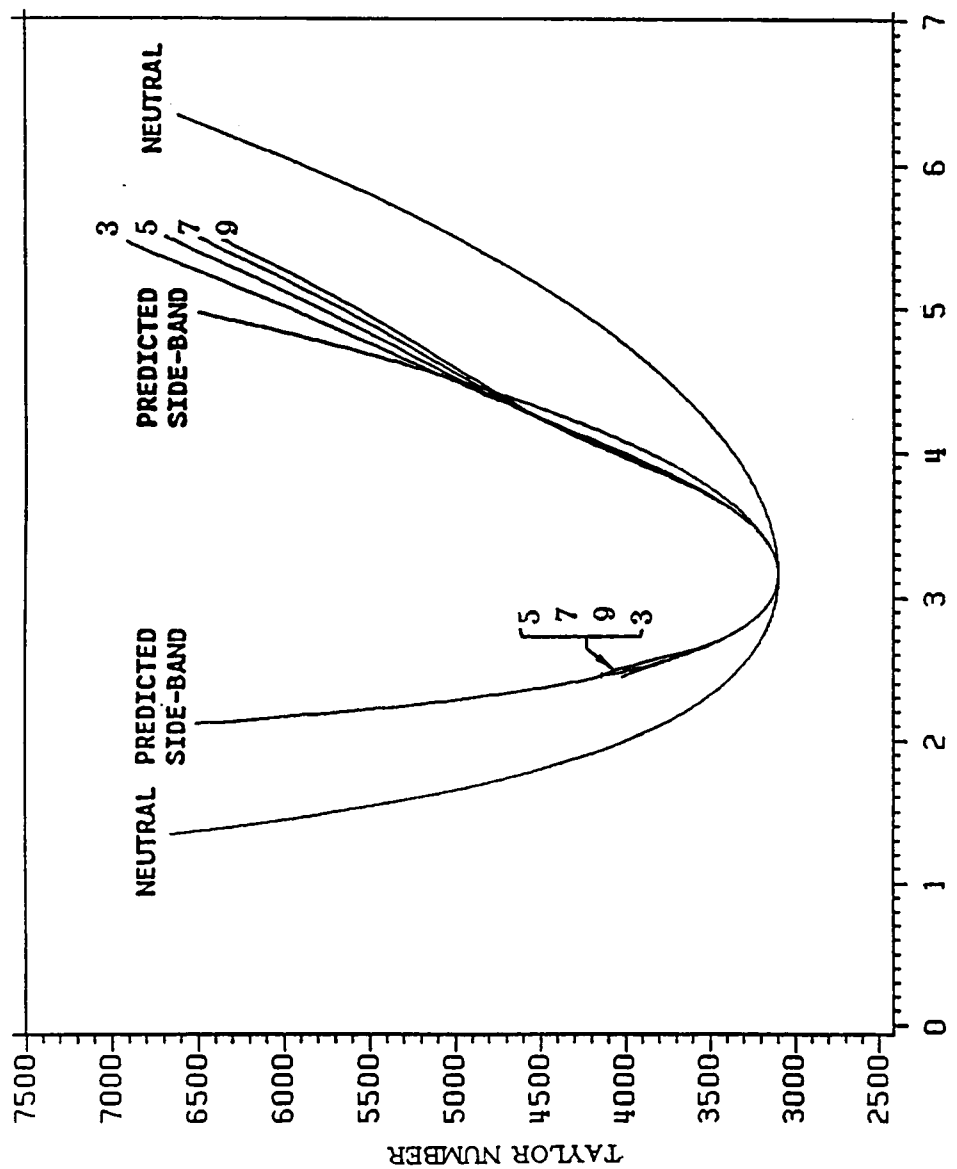

Fig.8.5. Side-band stability curve for wide gap case (η=0.5) by Approach 2

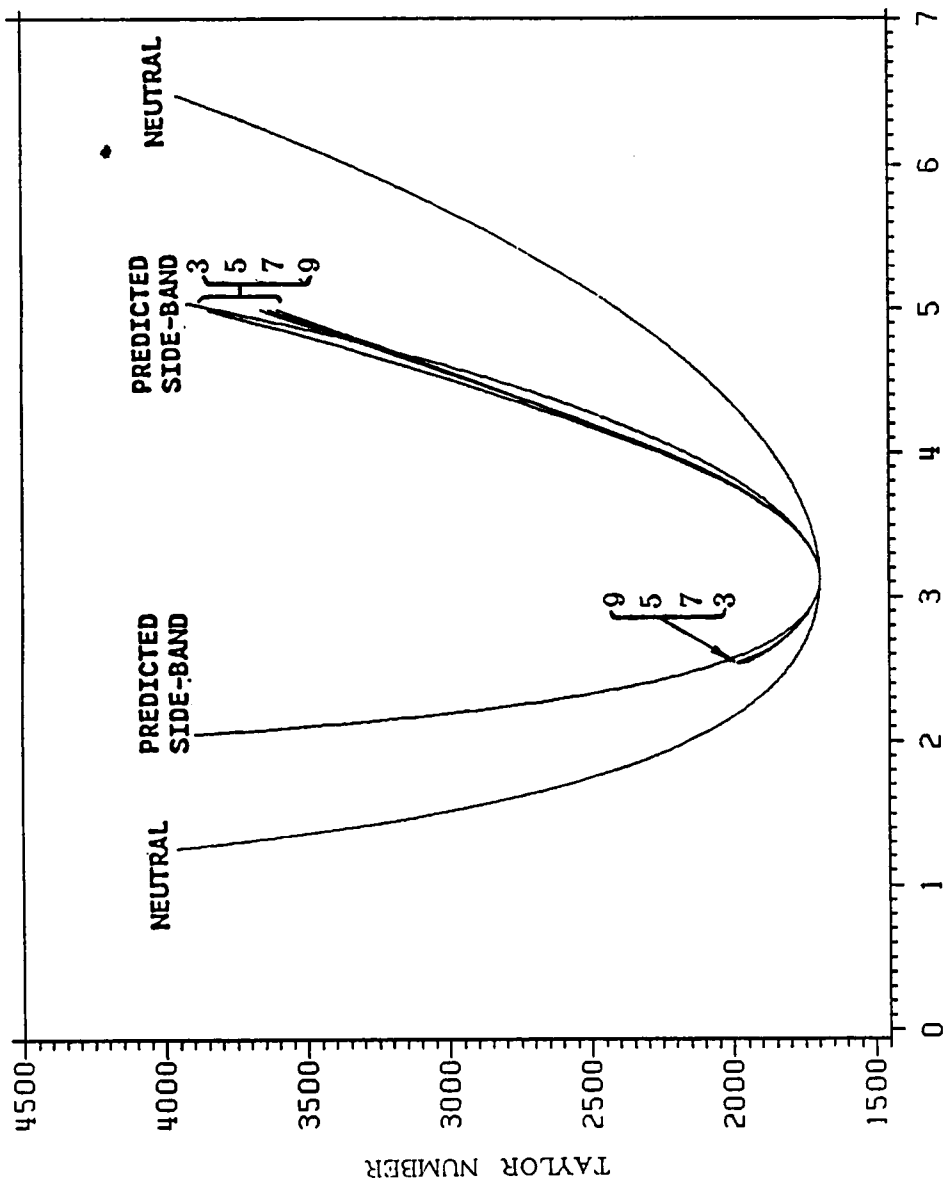

Fig.8.6. Side-band stability curve for small gap case ($\eta = 0.9524$ i.e., $\delta = 0.05$) by Approach 2

Table 8.1 Some values at neutral curve and predicted curve (3rd order) for wide gap case η=0.5

T	β^-	$\overline{\beta}_p^-$	$\overline{\beta}_p^+$	β^+
3200	2.71	2.90	3.45	3.67
3500	2.32	2.67	3.76	4.20
3675	2.20	2.61	3.88	4.41
4000	2.00	2.49	4.08	4.75
4500	1.80	2.37	4.31	5.16
5000	1.65	2.29	4.51	5.50
5500	1.54	2.22	4.68	5.80
6000	1.45	2.17	4.83	6.05
6200	1.41	2.15	4.89	6.15

Table 8.2 Some values of side-band stability curves of different orders for wide gap case η=0.5

T	$\overline{\beta}^-$				$\overline{\beta}^+$			
	(3*rd*)	(5*th*)	(7*th*)	(9*th*)	(3*rd*)	(5*th*)	(7*th*)	(9*th*)
3200	2.90	2.90	2.90	2.90	3.43	3.43	3.43	3.43
3500	2.69	2.69	2.69	2.69	3.70	3.70	3.70	3.70
3675	2.61	2.62	2.62	2.63	3.81	3.81	3.80	3.80
4000	2.48	2.54	2.55	2.56	3.97	3.97	3.96	3.96
4500	2.21	2.47	2.49	2.50	4.17	4.18	4.17	4.17
5000	2.13	2.42	2.45	2.47	4.34	4.36	4.36	4.35
5500	2.11	2.39	2.43	2.45	4.49	4.53	4.52	4.52
6000	2.08	2.35	2.40	2.43	4.67	4.73	4.73	4.73
6200	2.07	2.35	2.40	2.43	4.68	4.73	4.74	4.74

Table 8.3 Some values at neutral curve and predicted curve (3rd order) for small gap case $\eta=0.9524$ ($\delta=0.5$)

T	β^-	$\overline{\beta}_p^-$	$\overline{\beta}_p^+$	β^+
1715	2.85	2.97	3.30	3.42
1850	2.41	2.71	3.62	3.98
2000	2.18	2.58	3.83	4.34
2150	2.01	2.48	3.99	4.62
2300	1.89	2.41	4.13	4.86
2500	1.76	2.34	4.29	5.14
3000	1.52	2.20	4.61	5.69
3500	1.37	2.11	4.87	6.14

Table 8.4 Some values of side-band stability curves of different orders for small gap case $\eta=0.9524$ ($\delta=0.5$)

T	$\overline{\beta}^-$				$\overline{\beta}^+$			
	(3rd)	(5th)	(7th)	(9th)	(3rd)	(5th)	(7th)	(9th)
1715	2.97	2.97	2.97	2.97	3.29	3.29	3.29	3.29
1850	2.68	2.68	2.68	2.68	3.58	3.59	3.59	3.59
2000	2.53	2.56	2.54	2.54	3.76	3.78	3.78	3.78
2150	2.53	2.51	2.50	2.49	3.90	3.93	3.93	3.93
2300	2.56	2.48	2.50	2.47	4.02	4.05	4.06	4.06
2500	2.60	2.45	2.50	2.46	4.15	4.20	4.21	4.21
3000	2.67	2.41	2.50	2.46	4.40	4.51	4.52	4.53
3500	2.74	2.37	2.49	2.45	4.68	4.77	4.79	4.80

Table 8.5 The effect of wave shift on the Taylor numbers of side-band stability curve in Approach 2 (β=3.975 and η=0.5)

$\Delta\beta$	T		
	(3*rd*)	(5*th*)	(7*th*)
0.2	3953	3985	4004
0.1	3965	3998	4017
0.01	3965	3998	4017
0.001	3966	3998	4017
0.0001	3994	4028	4048

REFERENCES

1. R.C. DiPrima, H.L. Swinney: Instabilities and transition in flow between concentric rotating cylinders. (Hydrodynamic instabilities and the transition to turbulence. Second edition. ed. H.L. Swinney & J.P. Gollub). Topics in Applied Physics **45**, 140-180 (Springer-verlag 1985)

2. D. Coles: Transition in circular Couette flow. J. Fluid Mech. **21**, 385-425 (1965)

3. H.A. Snyder: Wave number selection at finite amplitude in rotating Couette flow. J. Fluid Mech. **35**, 273-298 (1969)

4. J.E. Burkhalter, E.L. Koschmieder: Steady supercritical Taylor vortices after sudden starts. Phys. Fluids **17**, 1929-1935 (1974)

5. J.E. Burkhalter: Experimental Investigation of supercritical Taylor vortex flow. Report 30, College of Engineering, Univ. of Texas at Austin (1972)

6. T.B. Benjamin: Bifurcation phenomena in steady flow of a viscous fluid. 1. Theory; 2. Experiment. Proc. R. Soc. London A**359**, 1-43 (1978)

7. T. Mullin: Mutation of steady cellular flows in the Taylor experiment. J. Fluid Mech. **121**, 207-218 (1982)

8. T.B. Benjamin, T. Mullin: Notes on the multiplicity of flows in the Taylor experiment. J. Fluid Mech. **121**, 219-230 (1982).

9. G.P. Neitzel: Numerical computation of time-dependent Taylor vortex flows in finite-length geometries. J. Fluid Mech. **141**, 51-66 (1984)

10. R. Meyer-Spasche, H.B. Keller: Some bifurcation diagrams for Taylor vortex flows. Phys. Fluids **28**, 1248-1252 (1985)

11. L.D. Landau, E.M. Lifshitz: Fluid mechanics. (Pergamon Press 1959)

12. J.T. Stuart: On the non-linear mechanics of hydrodynamic stability. J. Fluid Mech. **4**, 1-21 (1958)

13. J.T. Stuart: On the nonlinear mechanics of wave disturbances in stable and unstable parallel flows. Part 1: The basic behavior in plane Poiseuille flow. J. Fluid Mech. **9**, 353-370 (1960)

14. J. Watson: On the nonlinear mechanics of wave disturbances in stable and unstable parallel flows. Part 2: the development of a solution for plane Poiseuille flow and for plane Couette flow. J. Fluid Mech. **9**, 371-389 (1960)

15. A. Davey: The growth of Taylor vortices in flow between rotating cylinders. J. Fluid Mech. **14**, 336-368 (1962)

16. A. Davey, R.C. DiPrima, J.T. Stuart: On the instability of Taylor vortices. J. Fluid Mech. **31**, 17-52 (1968)

17. W. Eckhaus: Studies in nonlinear stability theory. (Springer-Verlag 1965)

18. S. Kogelman, R.C. DiPrima: Stability of spatially periodic supercritical flows in hydrodynamics. Phys. Fluids **13**, 1-11 (1970)

19. C. Nakaya: Domain of stable periodic vortex flows in a viscous fluid between concentric circular cylinders. J. Phys. Soc. Japan **36**, 1164-1173 (1974)

20. Th. Herbert: Nonlinear stability of parallel flows by high-order amplitude expansions. AIAA J. **18**, 243-248 (1980)

21. Th. Herbert: On perturbation methods in nonlinear stability theory. J. Fluid Mech. **126**, 167-186 (1983)

22. S. Chandrasekhar: Hydrodynamic and hydromagnetic stability. (Oxford University Press, Oxford University Press 1961)

23. P.G. Drazin, W.H. Reid: Hydrodynamic stability. (Cambridge University Press 1981)

24. L. Meirovitch: Computational methods in structural dynamics. (Sijthoff & Noordhoff 1980)

25 D. Gottlieb, S.A. Orszag: Numerical analysis of spectral methods: theory and applications. SIAM, Philadelphia (1977)

26. W.C. Reynolds, M.C. Potter: Finite-amplitude instability of parallel shear flows. J. Fluid Mech. **27**, 465-492 (1967)

27. Th. Herbert: In Seventh International Conference on Numerical Methods in Fluid Dynamics (ed. W.C. Reynolds & R.W. MacCormack). Lecture Notes in Physics, **141**, 200-205. (Springer-Verlag 1981)

28. L.W. Johnson, R.D. Riess: Numerical Analysis (Addison-Wesley 1982).

29. J.D. Lambert: Computational methods in ordinary differential equations. (John Wiley 1973)

30. A. Davey, H.P.F. Nguyen: Finite-amplitude stability of pipe flow. J. Fluid Mech. **45**, 701-720 (1971)

The vita has been removed from the scanned document